

**PHOTOACOUSTIC INVESTIGATION OF CRITICALITY
IN THERMAL AND OPTICAL PROPERTIES OF
SELECTED AMORPHOUS SEMICONDUCTORS**

SHEENU THOMAS

THESIS SUBMITTED TO THE
COCHIN UNIVERSITY OF SCIENCE AND TECHNOLOGY
FOR THE DEGREE OF
DOCTOR OF PHILOSOPHY

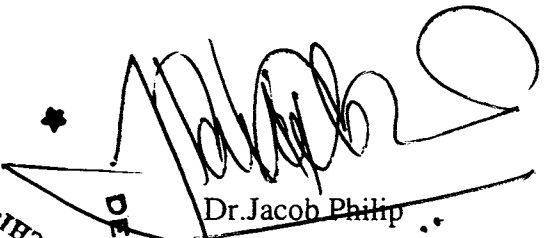
**DEPARTMENT OF INSTRUMENTATION
COCHIN UNIVERSITY OF SCIENCE AND TECHNOLOGY
COCHIN - 682 022**

1998

CERTIFICATE

Certified that the work presented in this thesis is based on the bona fide work done by Ms. Sheenu Thomas under my guidance in the Department of Instrumentation, Cochin University of Science and Technology, and has not been included in any other thesis submitted previously for the award of any degree.

Cochin 682 022
29th May, 1998

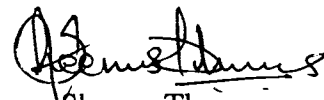

Dr. Jacob Philip
Supervising Guide

DEPARTMENT OF INSTRUMENTATION
Cochin University of Science & Technology
KOCCHI-682 022

DECLARATION

Certified that the work presented in this thesis is based on the original work done by me under the guidance of Dr. Jacob Philip, Professor and Head, Department of Instrumentation, Cochin University of Science and Technology, and has not been included in any other thesis submitted previously for the award of any degree.

Cochin 682 022
29th May, 1998


Sheenu Thomas

PREFACE

Amorphous semiconductors, in general, are bringing a silent revolution to the science and technology of materials. They have been shown to possess unique properties, cheaper and less sophisticated technology requirements and compatibility with existing techniques. The greatest impact of amorphous materials has been a possible shift from selecting suitable materials for specific applications to synthesising appropriate materials with required properties for the applications concerned. The greatest advantage of glassy materials is the composition dependent tunability of properties which enables one to design materials for specific requirements. A wide variety of glasses belonging to the oxide, semiconducting and metallic groups have been synthesised and investigated in laboratories around the world.

Semiconducting glasses containing chalcogen atoms (S, Se or Te) form an important class of amorphous solids. They have very interesting physical properties and can be prepared in the bulk as well as thin film forms. Over the past few decades a great deal of effort has been expended to understand the variation of mechanical, optical, chemical, thermal, and electrical properties of amorphous chalcogenides with composition. The interest in chalcogenide glasses among solid state physicists and electronic engineers are mainly due to their potential technological applications such as materials for threshold switching, memory switching, inorganic photoresist, xerography, IR detection and transmission etc. Since these glasses do not absorb IR radiations, they are suitable for IR optical elements such as cell windows, prisms and as FIR beam condensers, splitters and other accessories. Many of these glasses can be easily formed by melt quenching over a wide range of composition, making them suitable model systems for the systematic studies of composition dependence.

Various models such as the chemically ordered covalent network (COCN) model, topological model based on constraints theory and structural dimensionality considerations are used to explain the features observed in the composition dependence of various properties of chalcogenide glasses. According to the COCN model, heteropolar bonding is maximized,

thereby favouring chemical order, which results in features such as extremum or distinct change in properties at the stoichiometric composition of these glasses. Topological models emphasise the concept of average coordination number Z and interprets the dynamical properties of chalcogenides in terms of Z .

In this thesis we report the results of our investigations on the composition dependence of optical and thermal properties of selected ternary chalcogenide glasses. The Ge-Ga-Se and Ge-In-Se systems, which are easy glass formers, can be prepared by the conventional melt quenching technique over the entire glass forming range covering both the predicted topological and chemical threshold regions. In glasses containing V-VI or IV-VI elements the chemical threshold coincides with the mechanical threshold. But, for these glass systems containing IV-III-VI elements, the chemical threshold occurs at $Z = 2.73$ which is different from the topological thresholds occurring at $Z = 2.4$ or $Z = 2.67$. This makes them ideal systems to study the variations in properties around different thresholds, which in turn helps to test the validity of various models. The third system which we have selected is bismuth doped Ge-Se glasses, which also is an easy glass former prepared by melt quenching technique. This system, unlike most other semiconducting glasses which are p-type and insensitive to impurity doping, show a carrier type reversal from p-type to n-type at a certain Bi doping level. Although several mechanisms have been proposed to account for the influence of Bi doping on electronic properties, no conclusive explanation has been put forth so far. We have carried out measurements on optical band gap (E_g) and thermal diffusivity (α) of bulk chalcogenide glasses using photoacoustic (PA) technique. The E_g values determined using the PA technique have been compared with the values obtained from UV-Vis-NIR absorption spectra. The thesis is presented in seven chapters and a chapterwise organisation of the thesis is briefly outlined in the following paragraphs.

Chapter I, which is an introductory chapter, is divided in to two parts. Part A outlines the details of the PA effect, the theory behind PA effect in solids and its applications in measuring optical and thermal properties of solids. Part B places in perspective the properties

of amorphous semiconductors, various theoretical models that have been proposed to explain properties of amorphous semiconductors and their applications.

Chapter II focuses on the instrumentation techniques employed to carry out our investigations on chalcogenide glasses. The PA spectrometer used for spectral analysis as well as to measure thermal diffusivity of solids is outlined with the help of necessary block diagrams. Also, the details of preparation of bulk amorphous semiconductors and technical details of a temperature controller designed to measure and control the furnace temperature while preparing bulk chalcogenides are discussed.

We have employed a single beam PA phase lag technique for determining the thermal diffusivity of solids, which involves measurement of the phase difference of the PA signal between the front and rear surfaces of illumination of the sample at a single chopping frequency. The principle of this method, its advantages, the cell design, cell calibration and measurement technique are outlined in the third chapter.

In chapters IV and V we present the results of our measurements on the variation of optical energy gap E_g and thermal diffusivity α of Ge-Ga-Se and Ge-In-Se glasses with average coordination number Z using the PA phase lag technique. Thresholds in α observed at $Z = 2.4$ and $Z = 2.67$ are explained in terms of mechanical stiffening of the glass network due to threshold percolation of rigidity based on the Phillips-Thorpe model and a two to three dimensional structural transition as predicted by Tanaka's model respectively, both driven by the average coordination of the atoms in the network. The E_g values obtained using PA technique are compared with the values obtained from UV-Vis-NIR absorption spectra.

Measurement of the composition dependence of thermal diffusivity by the PA phase lag technique on bismuth doped Ge-Se glasses, which are seen to exhibit carrier type reversal from p-type to n-type at around 7 at.% of Bi, reveals a maximum occurring at around the same Bi content. Results obtained and interpretations in terms of a two phase model and constraints theory are described in chapter VI. The E_g values measured using UV-Vis-NIR technique are also given in this chapter.

The last chapter summarises the overall conclusions drawn from the work presented in the previous chapters and the scope for doing further work in this exciting field.

Most of the results presented in this thesis have either been published or communicated for publication in the form of the following papers/symposium proceedings.

1. General purpose high performance temperature controller for elevated temperatures
Int. J. Electronics (UK) **74** 92 (1993) .
2. Thermal diffusivity of solids by photoacoustic cell rotation and phase lag measurement
Rev. Sci. Instruments (USA), **66** 3907 (1995) .
3. Optical band gap, infra-red absorption and thermal diffusivity of Ge-Ga-Se glasses
Phys. Stat. Solidi (b) (Germany) **200**, 359 (1997) .
4. Carrier type reversal in Bi doped Ge-Se glasses manifested in thermal transport measurements
Solid State Commun. (to appear shortly).
5. Investigation of chemical and mechanical thresholds in Ge-In-Se glasses using photoacoustic technique
J. Appl. Phys. (communicated).

Symposium papers presented during the course of work

1. A high precision temperature controller for high temperature applications
National Symposium on Instrumentation (NSI-16), Nov. 26-29 (1991) p.8,
CUSAT, Cochin.
2. Optical band gap of Ge-Ga-Se glasses
Solid State Physics Symposium (DAE) Dec. 27-31 (1994), p.244, Jaipur.
3. Thermal diffusivity of solids by single beam photoacoustic phase lag
measurement
National Symposium on Instrumentation (NSI-20) Sept.25-28 (1995) p.20,
Osmania University, Hyderabad.
4. Carrier type reversal in Bi doped Ge-Se glasses manifested in thermal
transport measurements
Solid State Physics Symposium (DAE) Dec.27-31 (1997), p.44, Cochin.
5. Photoacoustic investigation of chemical and mechanical thresholds in Ge-
In-Se glasses
Solid State Physics Symposium (DAE) Dec.27-31 (1997), p.45, Cochin.

CONTENTS

| | | |
|-------------------------|--|-----------|
| PREFACE | | i |
| ACKNOWLEDGEMENTS | | vi |
| Chapter I | INTRODUCTION | 1 |
| Part A | Photoacoustic study of optical and thermal properties of solids | 1 |
| 1.1 | The photoacoustic effect | 1 |
| 1.2 | Rosencwaig-Gersho theory of PA effect in solids | 3 |
| 1.3 | Optical absorption in solids by PA technique | 15 |
| 1.4 | Measurement of thermal properties of solids | 17 |
| Part B | Recent developments in the study of amorphous semiconductors | 19 |
| 1.5 | The amorphous state of matter | 19 |
| 1.6 | Band models of amorphous semiconductors | 21 |
| 1.7 | Properties of amorphous semiconductors | 25 |
| 1.8 | Chalcogenide glasses | 35 |
| 1.9 | Applications of amorphous semiconductors | 42 |
| | References | 43 |
| Chapter II | INSTRUMENTATION | 50 |
| 2.1 | Introduction | 50 |
| 2.2 | Basic PA spectrometer for spectral studies | 56 |
| 2.3 | Basic PA setup to study thermal diffusivity of solids | 59 |
| 2.4 | Preparation of amorphous materials | 62 |
| 2.5 | A temperature controller for high temperature applications | 65 |
| | References | 73 |

| | | |
|--------------------|---|------------|
| Chapter III | PHOTOACOUSTIC PHASE LAG TECHNIQUE TO DETERMINE THERMAL DIFFUSIVITY OF SOLIDS | 75 |
| 3.1 | Introduction | 75 |
| 3.2 | Principle of the method | 76 |
| 3.3 | PA Phase lag cell design | 81 |
| 3.4 | Calibration of the cell | 83 |
| 3.5 | Conclusions | 87 |
| | References | 89 |
| | | |
| Chapter IV | OPTICAL AND THERMAL PROPERTIES OF Ge-Ga-Se SEMICONDUCTING GLASSES | 90 |
| 4.1 | Introduction | 90 |
| 4.2 | Sample preparation | 92 |
| 4.3 | Composition dependence of E_g using PA and UV-Vis-NIR methods | 92 |
| 4.4 | Thermal diffusivity by PA phase lag method | 99 |
| 4.5 | Discussions based on COCN model and constraints theory | 105 |
| 4.6 | Conclusions | 108 |
| | References | 109 |
| | | |
| Chapter V | COMPOSITION DEPENDENCE OF OPTICAL AND THERMAL PROPERTIES OF Ge-In-Se GLASSES | 111 |
| 5.1 | Introduction | 111 |
| 5.2 | Preparation of samples | 114 |
| 5.3 | Experimental details | 118 |
| 5.4 | Results and discussions | 118 |
| 5.5 | Conclusions | 129 |
| | References | 130 |

| | | |
|--------------------|---|------------|
| Chapter VI | OPTICAL AND THERMAL PROPERTIES OF Bi-DOPED Ge-Se GLASSES | 132 |
| 6.1 | Introduction | 132 |
| 6.2 | Experimental method | 134 |
| 6.3 | Results and discussions | 134 |
| 6.4 | Conclusion | 146 |
| | References | 147 |
| Chapter VII | SUMMARY AND CONCLUSIONS | 149 |

CHAPTER I

INTRODUCTION

This chapter of the thesis embodies a general introduction to the experimental technique used in the work and the materials under investigation. Part A of this chapter outlines principles of the photoacoustic technique, theory of photoacoustic signal generation from solids and applications of the technique with special reference to determination of optical and thermal properties of solids. Part B of this chapter describes the features, models and properties of amorphous semiconductors, particularly chalcogenide glasses which are the materials subjected to investigation in this work.

PART A

PHOTOACOUSTIC STUDY OF OPTICAL AND THERMAL PROPERTIES OF SOLIDS

1.1 The photoacoustic effect

Over the past few decades, photoacoustic technique has emerged as a powerful tool for determining the optical and thermal properties of solids, liquids and gases. Eventhough the photoacoustic [PA] effect, which involves heat flow in the medium, was discovered almost a century ago by Alexander Graham Bell, the exploitation of the potential utility of the technique for spectroscopic studies of solid and liquid samples have been undertaken only a couple of decades ago. The impetus for such an exploitation has come from the need for a spectroscopic technique which would provide reliable information about samples, which are difficult to examine by conventional optical transmission or reflectance spectroscopy in the

UV-visible and near IR regions of the electromagnetic spectrum. Moreover, need was there for a technique which could provide the above information with minimal sample pretreatment. Further stimulus to the adoption of the PA effect for spectroscopy has come from the realisation of its potential for the study of heat flow characteristics of the material. The real power of this technique lies in its ability to determine indirectly and with high sensitivity the periodic component of the surface temperature of the sample which affords possibilities for non-destructive testing, depth profiling, thickness determination and thermal transport measurements.

In photoacoustic spectroscopy of solids or liquids, the sample is enclosed within a cell containing a gas, usually air at atmospheric pressure and is fitted with a window transparent to incident radiation and a sensitive microphone. When radiation in the UV-visible or IR region of the electromagnetic spectrum is allowed to fall on the sample in the cell, energy is absorbed and if the material does not luminesce or degrade photochemically it is converted to kinetic energy (heat) of atoms or molecules. This conversion of absorbed energy takes place rapidly, and the energy absorbed by electronic and vibrational excitations of the sample get degraded through a cascade process to lower electronic and vibrational energy levels within nanoseconds or less. If the incident radiation is interrupted at a particular frequency (intensity modulation), the heat produced in the sample after the energy conversion process also appear at this frequency. This periodic heating of the sample produces a periodic increase in the pressure of the air surrounding the sample which follows the modulation frequency of the incident radiation. As PA effect can be observed only when radiation is absorbed by the sample, variation of the wavelength of incident radiation and measurement of the amplitude of the PA signal at any wavelength will provide a measure of the ability of the material to absorb at that wavelength; or the absorption spectrum of the sample will be obtained. The PAS spectrum therefore closely resembles the electronic and vibrational absorption spectra and is complementary to the reflectance spectrum. The use of this technique for examining the solid and liquid samples have a number of important advantages over conventional optical spectroscopy, which include freedom from light

scattering problems, possibility for the use of optically opaque and weakly absorbing materials etc. Eventhough several techniques like diffuse reflectance [1], internal reflectance spectroscopy [2], Raman scattering [3], etc. have been developed in the above said situations, the applications of these techniques are limited to a relatively small category of materials and wavelength regions. Since PA effect provides a means for measurement of nonradiative transition occurring in the sample followed by an increase in the temperature of the sample, it can be considered as a radiometric technique and can be employed as a calorimetric method of material analysis [4,5,6]. Rosencwaig and others, have employed PAS for the investigation of the absorption spectra of a variety of solid and liquid samples and have proposed theoretical models for the processes involved in the generation of PA signal allowing improved understanding of the technique [7-9]. Adams et al and Lahman [10-11] have demonstrated the use of PAS as a calorimetric tool.

In PA spectroscopy, since a microphone is employed to follow the pressure changes in an enclosed cell caused by the changes in temperature of the sample, this indirect monitoring of sample temperature provides a number of practical advantages over other calorimetric techniques. Since the microphone as a pressure transducer responds only to the periodic variation of gas pressure in the cell, freedom from ambient temperature is also ensured. This acoustic detection proves to be superior to other conventional thermal detection methods as far as sensitivity detector rise time and speed at which measurements can be made are considered.

1.2 Rosencwaig-Gersho (RG) theory of PA effect in solids

Eventhough several theories have been proposed from Parker [12] in 1973 to Mc Donald and Wetsel [13] and Aamodt and Murphy [14] in 1978 to understand photoacoustic effect in solids, the most successful and widely used one is that due to Rosencwaig and Gersho [15]. In the RG theory, the authors assume that the PA effect is produced by the pressure variations of the thickness of a thin layer of gas in contact with the sample and acting as an acoustic piston acting on the rest of the gas column. Most of the

published experimental results agree with the RG theory, which accounts particularly for the saturation of the signal with highly absorbing substances, as Mc Clelland and Kinseley [16] have verified. Wetsel and Mc Donald [17] have used the RG model to determine quantitatively the optical absorption coefficient for a concentrated solution by analysing the variation of the amplitude of the signal as a function of the frequency of modulation of the light. Rosencwaig [18] has successfully checked these theoretical assumptions studying the variations of the phase and amplitude of the PA signal with regard to frequency of modulation for highly absorbing, transparent and intermediary materials.

The RG theory is based on a one dimensional analysis of the production of a PA signal in a cylindrical cell and gives an exact equation for the magnitude and phase of the signal in terms of the thermal, optical and geometrical properties of the cell, the sample and the ambient gas. The PA signal is seen to depend on the generation of an acoustic pressure disturbance at the sample-gas interface and is governed by thermal diffusion equations. In order to discuss the salient features of the theory a simple cylindrical PA cell is considered as shown in Fig.(1.1). The PA cell has diameter D and length L , which is assumed to be small compared to the wavelength of the generated acoustic signal. The sample is considered to be in the form of a disc of diameter D and thickness l and it is mounted on a backing material of thickness l'' . The length of the gas column in the cell is l' . The assumptions that the backing material and the gas are non-absorbing are also made.

A sinusoidally chopped monochromatic light beam of wavelength is incident on the solid with intensity,

$$I = 1/2 I_0 (1 + \text{Cos } \omega x) \quad (1.1)$$

where I_0 is the incident monochromatic light flux and $\omega = 2\pi f$ is the angular frequency of modulation. If β denotes the optical absorption coefficient of the solid sample for the incident wavelength, the heat density produced at any point x due to light absorbed at this point in the solid is then given by

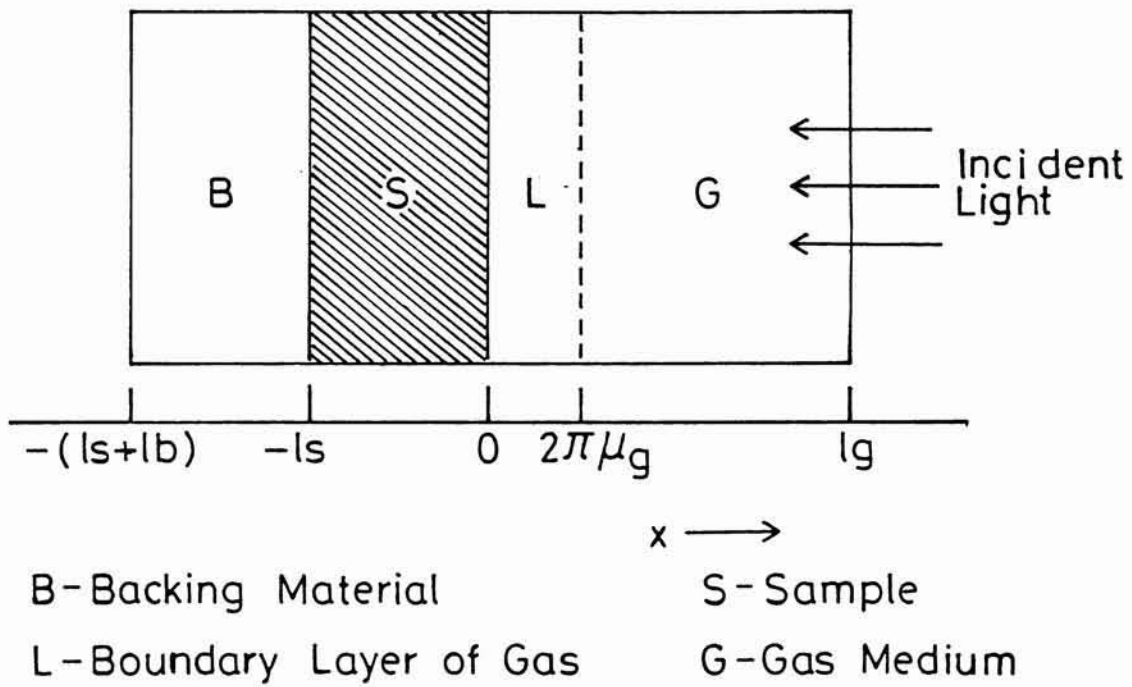


Fig. 1.1 Cross-sectional view of a simple cylindrical PA cell.

$$1/2 \beta I_0 e^{\beta x} (1 + \cos \omega t) \quad (1.2)$$

where x takes on negative values since the solid extends from $x = 0$ to $x = -l$, with the light incident at $x = 0$. The air column extends from $x = 0$ to $x = l'$ and the backing from $x = -l$ to $x = -(l+l'')$. The thermal diffusion equation in the solid where the distance x changes from zero at the surface to negative values inside the solid, taking into account the distributed heat source, can be written as

$$\partial^2 \theta / \partial x^2 = (1/\alpha) \partial \theta / \partial t - A e^{\beta x} (1 + e^{i\omega t}) \quad \text{for } -l \leq x \leq 0 \quad (1.3)$$

$$\text{where } A = \beta I_0 \eta / 2K \quad (1.4)$$

The various terms in the above equations defined are as follows:

θ is the temperature and η is the efficiency at which the absorbed light at wavelength λ is converted to heat by nonradiative deexcitation processes.

| | |
|------------------------------|---|
| I_0 | intensity of light |
| K | thermal conductivity ($\text{cal cm}^{-1} \text{s}^{-1} \text{K}^{-1}$) |
| ρ | density (g cm^{-3}) |
| C | specific heat capacity ($\text{cal g}^{-1} \text{K}^{-1}$) |
| $\alpha = K/\rho C$ | thermal diffusivity ($\text{cm}^2 \text{s}^{-1}$) |
| $a = (\omega/2\alpha)^{1/2}$ | thermal diffusion coefficient (cm^{-1}) |
| $\mu = 1/a$ | thermal diffusion length (cm) |

In the following discussions the sample parameters are represented by unprimed symbols and the gas and backing material parameters by singly primed symbols and doubly primed letters respectively. Assumption is made that the value of η is unity which is a

reasonable assumption for most solids at room temperature. Similar thermal diffusion equations for the backing material and the gas medium respectively are given by

$$\partial^2 \theta / \partial x^2 = (1/\alpha'') \partial \theta / \partial t \text{ for } (-l''-l) \leq x \leq -l \quad (1.5)$$

$$\partial^2 \theta / \partial x^2 = (1/\alpha') \partial \theta / \partial t \text{ for } 0 \leq x \leq l' \quad (1.6)$$

The real part of the solution of equations 1.3, 1.5 and 1.6 represent the temperature variations in the cell relative to the ambient temperature as a function of position and time.

The actual temperature field in the cell is given by

$$\theta(x,t) = \text{Re } \theta(x,t) + \phi_0 \quad (1.7)$$

where ϕ_0 is the ambient temperature. On applying the boundary conditions to the a.c. and d.c. components of the time dependent spatial temperature variations, we obtain the time dependent and independent temperature distribution in the cell. Hence to completely specify the solutions of equations 1.3, 1.5 and 1.6, the appropriate boundary conditions are obtained from the temperature and heat flux continuity at the boundaries $x = 0$ and $x = -l$ and from the constraint that the temperatures at the cell walls $x = +l$ and $x = -l-l''$ are at ambient

The general solution for $\theta(x,t)$ in the cell neglecting transients can be written as

$$\begin{aligned} & (1/l'') (x + l + l'') W_0 + W e^{\sigma(x+l)} e^{i\omega t}; & (-l''-l) \leq x \leq -l \\ \theta(x,t) = & b_1 + b_2 x + b_3 e^{\beta x} + (U e^{\sigma x} + V e^{-\sigma x} - E e^{\beta x}) e^{i\omega t}; & -l \leq x \leq 0 \\ & (1-x/l') F + \theta_0 e^{-\sigma x} e^{i\omega t}; & 0 \leq x \leq l' \end{aligned} \quad (1.8)$$

where W , U , V , E and are complex valued constants; b_1 , b_2 , b_3 , and F are real valued constants and $\sigma = (1+i)a$ with $a = (\omega/2\alpha)^{1/2}$. In particular it should be noted that the complex amplitudes of the periodic temperatures at the sample-gas boundary ($x=0$) and sample-

backing boundary ($x=l$) are given by θ_0 and W respectively. The d.c. solutions in the backing and gas medium make use of the assumption that the temperature is zero at the ends of the cell. W_0 and F denote the d.c. components of the temperature at the sample surfaces $x = -l$ and $x = 0$ respectively. The quantities E and b_3 are determined by the forcing functions in equation (1.3) and are given by

$$b_3 = -A/\beta^2 \quad (1.9)$$

$$E = B/(\beta^2 - \sigma^2) = \beta I_0/2K(\beta^2 - \sigma^2) \quad (1.10).$$

Since for all frequencies ω of interest the thermal diffusion length is small compared to the length of the material in both the gas and the backing, the growing exponential components of the gas and backing material are omitted. This means $\mu'' < l''$ and $\mu' < l'$ and the sinusoidal components of these solutions are sufficiently damped so that they are effectively zero at the cell wall. Therefore, in order to satisfy the temperature constraints at the cell walls, the growing exponential components of the solutions would have coefficients that are essentially zero.

Hence by evaluating the temperature distribution (1.8) in the cell in terms of the optical, thermal and geometric parameters of the system, the explicit solution of the complex amplitude of the periodic temperature θ_0 at the solid-gas boundary is given by

$$\theta_0 = \frac{\beta I_0}{2K(\beta^2 - \sigma^2)} \left[\frac{(r-1)(b-1)e^{\sigma l} - (r+1)(b-1)e^{-\sigma l} + 2(b-r)e^{-\beta l}}{(g+1)(b+1)e^{\sigma l} - (g-1)(b-1)e^{-\sigma l}} \right] \quad (1.11)$$

$$\text{where } b = K'' a'' / Ka \quad (1.12)$$

$$g = K' a' / Ka \quad (1.13)$$

$$r = (1-i) \beta / 2a \quad (1.14)$$

The acoustic signal which arises due to the periodic heat flow from the solid to the surrounding gas produces a periodic temperature variation in the gas as given by the sinusoidal (a.c.) component of the solution (1.8).

$$\theta_{ac}(x,t) = \theta_0 e^{-\sigma x} e^{i\omega t} \quad (1.15).$$

The real part of the a.c. component gives the actual physical temperature variation in the gas

$$T_{ac}(x,t) = e^{-a'x} (\theta_1 \text{Cos}\{\omega t - a'x\} - \theta_2 \text{Sin}\{\omega t - a'x\}) \quad (1.16)$$

where θ_1 and θ_2 are the real and imaginary parts of θ which determine the in-phase and quadrature components. The time dependent temperature variation attenuates rapidly to zero at a distance $2\pi / a' = 2\pi \mu'$ where μ' is the thermal diffusion length in the gas. The boundary layer of thickness $2\pi\mu'$ responds thermally to temperature acting as an acoustic piston for the gas column.

The spatially averaged temperature of the gas within this boundary layer as a function of time can be determined by evaluating

$$\bar{\theta}(t) = \frac{1}{2\pi\mu'} \int_0^{2\pi\mu'} \theta_{ac}(x,t) dx \quad (1.17)$$

The displacement of the boundary layer $\delta x(t)$ can be determined by using the ideal gas law as

$$\delta x(t) = 2\pi\mu' \theta(t) / T_0 = (\theta_0 \mu' \sqrt{2} / T_0) e^{i(\omega t - x/4)} \quad (1.18)$$

where T_0 is the sum of the ambient and d.c. temperature at the surface; $T_0 = \phi_0 + F_0$. Assuming that the rest of the gas responds to the action of the acoustic piston adiabatically, the acoustic pressure in the cell due to the displacement can be derived from the adiabatic gas law,

$$PV^\gamma = \text{constant.}$$

where P is the pressure, V is the gas volume in the cell and γ is the ratio of specific heats. Thus the incremental pressure

$$\delta P(t) = (-\gamma P_0 / V_0) \delta V = (\gamma P_0 / P) \delta x(t) \quad (1.19)$$

where P_0 and V_0 are the ambient pressure and volume respectively and δV is the incremental volume. Thus, from equation 1.18 one can write

$$\delta P(t) = Q e^{i(\omega t - \pi/4)}$$

$$\text{where } Q = \gamma P_0 \theta_0 / \sqrt{2} l' a' T_0 \quad (1.20)$$

Thus the actual physical pressure variation $\Delta P(t)$ is given by

$$\Delta P(t) = Q_1 \cos(\omega t - \pi/4) - Q_2 \sin(\omega t - \pi/4) \quad (1.21)$$

$$\text{or } \Delta P(t) = q \cos(\omega t - \psi - \pi/4) \quad (1.22)$$

where Q_1 and Q_2 are the real and imaginary parts of Q ; and q and ψ are the magnitude and phase of Q ; i.e.

$$Q = Q_1 + iQ_2 = q e^{-i\psi} \quad (1.23)$$

Thus Q specifies the complex envelope of the sinusoidal pressure variation

$$Q = \frac{\beta I_0 \gamma P_0}{2\sqrt{2T_0 K l' a' (\beta^2 - \sigma^2)}} \left[\frac{(r-1)(b-1)e^{\sigma l} - (r+1)(b-1)e^{-\sigma l} + 2(b-r)e^{-\beta l}}{(g+1)(b+1)e^{\sigma l} - (g-1)(b-1)e^{-\sigma l}} \right] \quad (1.24)$$

where $b = K''a'' / Ka$; $g = K'a' / Ka$, $r = (1-i)\beta / 2a$ and $\sigma = (1+i)a$. Thus equation (1.24) may be evaluated for the magnitude and phase of the acoustic pressure wave produced in the cell by photoacoustic effect. Equation (1.24) can be simplified for the following special cases.

Special cases:

Physical interpretation of the full expression of $P(t)$ is a complicated and tedious process. By examining the following special cases, when the expression for Q becomes relatively simple, significant physical insight can be gained. These cases are grouped according to the optical opaqueness of the solid as determined by the relation of the optical absorption length $l_\beta = 1/\beta$ to the thickness l of the solid. For each category of optical opaqueness, three cases are considered, according to the relative magnitude of the thermal diffusion length μ , as compared to the physical length l and optical absorption length l_β . For all the cases discussed below, assumptions are made that $g < b$ and that $b \sim 1$, or $K'a' < K''a''$ and $K''a'' \approx Ka$.

Y and l_β which always appears in the expression for Q as a constant factor are defined as follows.

$$Y = \gamma P_o I_0 / 2\sqrt{2T_o l'}$$

$$l_\beta = 1/\beta$$

Case 1: Optically transparent solids [$l_\beta > l$]

In this case, light is absorbed throughout the length of the sample and some light is transmitted through the sample.

Case 1a: Thermally thin solids [$\mu \gg l; \mu > l_\beta$]

Setting $e^{-\beta l} \approx 1 - \beta l$, $e^{\pm \sigma l} \approx 1$ and $|r| > 1$ in equation (1.24) we obtain

$$Q \approx \frac{(1-i)\beta l}{2a'} \begin{bmatrix} \mu'' \\ - \\ K'' \end{bmatrix} Y \quad (1.27)$$

Thus the acoustic signal is proportional to βl and since μ''/a' is proportional to $1/\omega$, the acoustic signal has an ω^{-1} dependence. Here the thermal properties of the backing material come into play in the expression for Q .

Case 1b: Thermally thin solids ($\mu > l; \mu < l_\beta$)

Setting $e^{-\beta l} \approx -\beta l$; $e^{\pm \sigma l} \approx 1 \pm \sigma l$ and $|r| < 1$ in equation (1.24) we get

$$Q \approx \frac{(1-i)\beta l}{2a'} \begin{bmatrix} \mu'' \\ - \\ K'' \end{bmatrix} Y \quad (1.28)$$

which is identical to equation (1.27), where acoustic signal is proportional to βl and varies as ω^{-1} and depends on the thermal properties of the backing material.

Case 1c: Thermally thick solids ($\mu < l; \mu \ll l_\beta$)

Setting $e^{-\beta l} \approx -\beta l$; $e^{-\sigma l} \approx 0$ and $|r| \ll 1$ in equation (1.24) we get

$$Q \approx \frac{-i\beta\mu}{2a'} \begin{bmatrix} \mu \\ - \\ K \end{bmatrix} Y \quad (1.29)$$

Here the acoustic signal is proportional to $\beta\mu$. rather than βl ; i.e. only the light absorbed within the first thermal diffusion length contribute to the signal, eventhough light is being absorbed throughout the length l of the solid. Also, since $\mu < l$ and Q varies as $\omega^{-3/2}$, the thermal properties of the backing material are replaced by those of the sample.

The above mentioned cases demonstrate a unique capability of PA technique to obtain a depth profile of optical absorption within the sample which opens up exciting possibilities for studying layered and amorphous materials and in determining overlayer and thin film thicknesses.

Case 2: Optically opaque solids ($l_p \ll l$)

In this case, most of the light is absorbed within a distance that is small compared to l . and no light is transmitted.

Case 2a: Thermally thin solids ($\mu \gg l$; $\mu \gg l_p$)

In equation (1.24), setting $e^{-\beta l} \approx 0$; $e^{+\sigma l} \approx 1$ and $|r| \gg 1$ we get

$$Q \approx \frac{(1-i)}{2a'} \begin{bmatrix} \mu'' \\ - \\ K'' \end{bmatrix} Y \quad (1.30)$$

Here the acoustic signal is independent of β and we have photoacoustic opaqueness as well as optical opaqueness as in the case of a very black absorber. The signal is quite strong and varies as ω^{-1} and depends on the thermal properties of the backing material.

Case 2b: Thermally thick solids ($\mu < l$; $\mu > l_\beta$)

Setting $e^{-\beta l} \approx 0$; $e^{-\sigma l} \approx 0$ and $|r| > 1$ in equation (1.24) we obtain

$$Q \approx \frac{(1-i)}{2a'} \left[\frac{\mu}{K} \right] Y \quad (1.31)$$

Here again the acoustic signal is independent of β , varying as ω^{-1} and the thermal properties of the backing are replaced by those of the sample.

Case 2c: Thermally thick solids [$\mu \ll l$; $\mu < l_\beta$]

In equation (1.24) if $e^{-\beta l} \approx 0$; $e^{-\sigma l} \approx 0$ and $|r| < 1$ we get

$$Q \approx \frac{-i\beta\mu}{2a'} \left[\frac{\mu}{K} \right] Y \quad (1.32)$$

This case is an interesting and important one; because eventhough the solid is an opaque one, as long as $\beta\mu < 1$ (i.e. $\mu < l_\beta$), the solid is not photoacoustically opaque since only the light absorbed within the first thermal diffusion length μ contributes to the PA signal. Here the signal depends on the thermal properties of the sample and varies as $\omega^{-3/2}$.

One of the predictions of the RG theory of PA effect in solids is that the PA signal is always linearly proportional to the power of the incident photon beam which holds true for any sample and cell geometry. Also for photoacoustically opaque sample ($\mu > l$) the PA spectrum is simply the power spectrum of the light source. This was verified in 1973 by Rosencwaig [19] and by Adams [20] in 1979. One of the most important aspects of RG theory is that if one has a full knowledge of the thermal and geometrical parameters of the sample, then one can obtain absolute values for the optical absorption coefficient by measuring the dependence of the PA signal on modulation frequency. RG theory indicates

that the PA effect is primarily dependent on the relationship between the length parameters of the sample such as thickness of the sample l , the optical absorption length $l_{\beta} = 1/\beta$ and thermal diffusion length $\mu = (2\alpha/\omega)^{1/2}$. But it is seen that there is a deviation from the theory in the ω versus chopping frequency at very low frequencies, which has been accounted for by Mc.Donald and Wetsel [6] as due to the effect of thermally induced mechanical vibrations of the sample, which has not been included in the RG theory.

1.3 Optical absorption in solids by PA technique

Photoacoustic spectroscopy is gradually finding its own place in the gamut of optical techniques available to materials research and analytical chemistry. When the surface of a solid material is not highly reflective PAS can provide optical data about the bulk itself. The advantage of PAS over traditional optical techniques is that the PA signal is sensitive only to the heat deposited in the sample; light which is reflected or scattered from the sample surface do not affect the signal. For this reason it is possible, to obtain optical absorption spectra of opaque or translucent materials such as powders, gels, biological tissues etc, which do not readily lend themselves to optical transmission techniques. In the case of insulators, PA spectra give direct information about the optical absorption bands in the material. PAS has also been employed to characterise thin-film antireflecting coatings. In the case of semiconductors, both direct and indirect band transitions have been verified by several workers [21-25]. In addition, PAS can be used at cryogenic temperatures and at higher resolutions using lasers to study excitonic and other fine structures in crystalline, powder or amorphous semiconductors and thus to investigate the effects of impurities, dopants and electromagnetic fields. It can be used to study metals if the reflectivity is first diminished by grinding or through the use of powders. In the case of semiconductors, a main advantage of PAS over conventional reflection spectroscopy is that highly reflecting surfaces are not needed and in fact are undesirable for bulk studies. Also, since unclear surfaces do not cause problems, the elaborate high vacuum equipment necessary for conventional reflectance

studies are not really needed for PAS. Organic liquid crystals are another class of materials which are highly light scattering and optical absorption spectroscopy on these states cannot be readily performed. PAS on these can be used to obtain information about the intermolecular interactions in these samples [22]. PA spectroscopy is different from all other forms of spectroscopy in that the energy deposited in the sample is measured directly. Several advantages result from this feature and photoacoustic spectroscopy often complements normal absorption and fluorescence spectroscopy. Applications of PA spectroscopy naturally divide into two categories; those utilising chopped cw excitation sources and those utilising pulsed light sources. Attributes of chopped cw sources are their inherent spectral purity and high average powers. Applications include high resolution spectroscopy, the detection of forbidden transitions such as singlet to triplet electronic transitions or vibrational overtone absorptions. Pulsed excitation sources have a high peak light intensity or power which is advantageous for enhanced nonlinear photoprocess. This include two photon visible UV absorption spectroscopy, stimulated Raman spectroscopy and infrared multiphoton absorption. Pulsed acoustic techniques also provide time domain discrimination allowing real time monitoring of photoinduced relaxation processes. When PA application requires light frequencies out of the more conventional laser regions, pulsed sources can be used to generate new wavelengths via stimulated Raman shifting and a variety of nonlinear frequency mixing techniques. PA spectroscopy typically involves the measurement of the PA signal amplitude divided by the excitation energy as the excitation wavelength is scanned. This normalized PA spectrum is proportional to the linear absorption spectrum of the sample in certain cases. The wavelength dependent excitation energy can be measured by monitoring the PA spectrum of a reference “flat” absorber. Conventional absorption techniques like extinction or reflection measurements are “gross” methods, i.e. incident and transmitted intensities are measured to obtain the difference, which includes absorption plus all scattering losses. These gross methods cannot be readily used to monitor absorption coefficient less than 10^3 cm^{-1} . Better sensitivities are possible with PA method which is with zero background, which means that detected signal is zero if there is no absorption. PA

measurement is convenient since little sample preparation is needed. Furthermore, PA measurements are applicable to diverse types of samples, since non-radiative thermal relaxations occur very generally, may be only partial in certain highly fluorescent or chemically active systems, while ion attachment, diffusion and recombination phenomena may impose serious limitations on other detection schemes involving ionisation or luminescence.

Applications of PAS also include PA imaging which is concerned with the detection of subsurface thermoelastic property variations in a sample. PA imaging, mainly concerned with the property variations in the thickness directions, is usually called "PA depth profiling". On the other hand, if lateral resolution is required, the technique is called "PA microscopy" [26]. PAS is also used as a non-destructive technique to examine biological cells [27,28] and for the measurement of absolute quantum efficiencies [29] and absolute absorption coefficients [30,31]. Determination of absolute quantum efficiency is based on the measurement of the PA signal at two exciting wavelengths and calculating the ratio of these two signals. These unique features of PAS ensure a continued growth in popularity describing new applications to which it has been put.

1.4 Measurement of thermal properties of solids

The PA effect turns out to be an effective method for determining thermal parameters of various materials when PA signal is measured as a function of chopping frequency. Front surface illumination can lead to an accurate determination of both thermal effusivity and diffusivity from which conductivity and specific heat can be extracted [32,33]. Being a photothermal technique, the detected signal is strongly dependent upon the interplay of the sample optical absorption coefficient for the incident radiation, efficiency of conversion of light into heat, as well as how heat diffuses through the sample which means that it is complementary to other photoinduced energy conversion processes. The fact that PA signal depends on how heat diffuses through the sample allows one to perform both thermal characterisation of the sample and thermal imaging. PA measurements of diffusivity and

effusivity of their optical coatings investigated proves the ability of this technique to directly measure thin film thermal properties [34,35]. PA measurements performed on selected metallic and dielectric thin film substrates yield spatial information about microstructures. By using the depth profiling option of this measuring technique, thermal properties of films can be determined. Thermal waves induced at the sample surface penetrate into the sample and the penetration depth depends on the frequency of light modulation. The thermal diffusion length μ , characterises the depth which can be reached by the thermal wave. In a homogeneous sample

$$\mu = (K / \pi f C \rho)^{1/2} \quad (1.33)$$

where

K = thermal conductivity

f = chopping frequency

C = heat capacity, and

ρ = density

It is therefore possible in the case of a film-substrate system to measure the thermal properties of the film and substrate in one single run in a non-destructive way [36]. PA method also has the capability of giving spatial information regarding thermal properties [37-40]. Florian et al [41] were the first who observed first order phase transitions in a sample by PA method. In contradiction to this, Korpiun and Tilgner[42] observed a characteristic change in amplitude and phase angle of PA signal by approaching the transition from low to higher temperatures as well as from high to lower temperatures. PA effect is now a well established non-stationary method to study phase transitions. Several papers have appeared in literature utilising PA technique to bring out features of phase transitions in solids [43-47].

PART B

RECENT DEVELOPMENTS IN THE STUDY OF AMORPHOUS SEMICONDUCTORS

1.5 The amorphous state of matter

In the scientific study of amorphous materials there has been an explosion of interest recently as more and more new materials are produced in the amorphous form, some of them having considerable technological promises. Amorphous materials do not possess the long range translational periodicity characteristic of a crystal. A glass is an amorphous material which exhibits a glass transition at a definite temperature. The glass transition is the phenomenon in which a solid amorphous phase exhibits a more or less abrupt change in derivative thermodynamic properties, like heat capacity and thermal expansivity, from crystal like to liquid-like values with change of temperature. Glassy or vitreous solids, which form a special subset of amorphous materials are not completely disordered on the atomic scale. Short range order similar to that present in crystalline materials are present in disordered materials. Disorder in materials can be manifested in many ways as vibrational spin and orientational disorder (all referred to a periodic lattice) and topological disorder, which is the type of disorder associated with the structure of glassy and amorphous solids in which the structure cannot be defined in terms of a periodic lattice. Determination of atomic structure of these materials is unfortunately a nontrivial task because the structure can only be defined essentially in terms of a unit cell containing an infinitely large number of atoms. As there is no long range periodic symmetry, a statistical description is unavoidable. The structure of an amorphous solid can therefore never be determined unambiguously, and this uncertainty is compounded by the fact that the structure of a non-crystalline material is both at microscopic and macroscopic levels, often depending on the method of preparation. It is thus useful for a structural modelling which develops the structure by the repetition of one or more basic

molecular units in a way that cannot be identified topologically with any known crystalline structure. But the atomic order within a molecular unit might be similar within small bond angle distortions in both crystalline and amorphous phases. This reveals the importance of short range in describing the structural behaviour of non-periodic networks. The most important aspects of SRO (short range order) are the number and type of immediate neighbours and their spatial arrangement about a given reference atom. Given the SRO (in the range of 2-5 Å), with three parameters viz., the number of bonds, the bond length and the bond angle having well defined values in a narrow range, it is possible to construct a model for amorphous structure. The lack of periodicity in them are reflected in X-ray, electron and neutron diffraction experiments.

It is customary to classify amorphous semiconductors into two broad groups, mainly depending on the nature of chemical bonds. This classification, also used for crystalline solids, is based on an old idea of Ioffe that the fundamental electronic properties of the solid state are primarily determined by the nature of the chemical bond between nearest neighbours. In this view, two groups can be distinguished which include ionic and covalent materials. The ionic materials are those based on the glass forming oxides such as SiO₂, P₂O₅ and B₂O₃. The covalent amorphous semiconductors are generally further divided into two groups. The first class contain materials with tetrahedral co-ordination such as the elements Si, Ge and the III-V compounds. These materials can only be prepared in the amorphous phase by thin film deposition. The second group contains the chalcogenide glasses which are based on the chalcogen elements S, Se or Te and to which other elements like Si, Ge, As etc. can be added. The features of amorphous semiconductors are the general insensitivity of properties to the incorporation of impurities, pinning of the Fermi level near the mid-gap, the general similarity of the overall distribution of the density of states in the valence and conduction bands to that in the corresponding crystalline phase, the breakdown of the *k* conservation, selection rules for optical excitation of electronic and vibrational states, a Hall effect anomalous in sign and magnitude and an a.c. conductivity that increases with frequency.

1.6 Band Models for Amorphous Semiconductors

In recent years, exciting advances have been made in understanding how disorder in amorphous semiconductors influence the band structure and hence their electrical properties. The various models suggested for the energy distribution or the density of states is mainly concerned with the important question of the existence of localised states in the tails of valence band and conduction band and of a mobility edge separating the extended states from localised states. A type of conduction unique to amorphous semiconductors is variable range hopping in localised states close to the Fermi level. The nature of electronic transport in these materials have arisen much interest in the recent past due to reports of the discovery of non-destructive, fast electrical switching in thin films of multi-component chalcogenide glasses. There appears to be widespread argument that if SRO is the same in amorphous state as in the crystalline one, some basic features of the electronic structure can be preserved. In order to account for the translational disorder accompanied by a possible compositional disorder in multicomponent systems, modifications have been proposed for the band structure of amorphous solid. These are the well known Cohen-Fritzsche-Ovshinsky (CFO) and Davis-Mott models. Introducing the basic idea of the presence of localised states in the band extremities, these models have been widely used to interpret experimental data on electrical and optical properties. In contrast to the CFO and Davis-Mott ideas, a different approach to the understanding of electrical properties of amorphous semiconductors has been put forward by Emin[48]. He suggested that the charge carriers in some amorphous materials might be small polarons. It is generally accepted that hopping of small polarons is the mechanism responsible for electrical transport in oxide glasses. Experimental data on electrical transport properties can only be properly interpreted if a model for electronic structure is available. For semiconductors the main features of energy distribution of the density of electronic states $N(E)$ of crystalline solids are the sharp structure of the valence band and conduction band and the abrupt terminations at the valence band maximum and the conduction band minimum. The sharp edges in the density of states produce a well defined forbidden energy gap. Within the band the states are extended, which means that the wave functions occupy the entire

volume. The specific features of the band structure are the consequence of the perfect short range and long range order of the crystal. In an amorphous solid the long range order is destroyed, whereas the short range order i.e. the interatomic distance and the valence angle, is only slightly changed. The concept of density of states is also applicable to non-crystalline solids. Based on Anderson's theory, Mott argued that the spatial fluctuations in the potential caused by configurational disorder in amorphous materials may lead to formation of localised states, which do not occupy all the different energies in the band, but form a tail above and below the normal band. Mott postulated further that there should be sharp boundary between the energy ranges of extended and localised states. The states are called localised in the sense that an electron placed in a region will not diffuse at zero temperature to other regions with corresponding potential fluctuation. Several models have been proposed for the band structure of amorphous semiconductors, which have been the same to the extent that they all used the concept of localised states in the band tails.

1.6 a. The Cohen-Fritzsche-Ovshinsky (CFO) Model

The CFO model, shown in the Fig.(1.2a) assumes that the tail states extend across the gap in a structureless distribution. This gradual decrease of the localised states destroy the sharpness of the conduction band and valence band edges. The CFO model was specifically proposed for multi component chalcogenide glasses used in switching devices. In chalcogenide alloys, the disorder is sufficiently great that the tails of valence band and conduction band overlap, leading to appreciable density of states in the middle of the gap. A consequence of band overlapping is that there are states in the valence band, ordinarily filled, that have higher energies than states in the conduction band that are ordinarily unfilled. This model therefore ensures self compensation and pins the Fermi level close to the middle of the gap; a feature required to explain the electrical properties of these materials. One of the

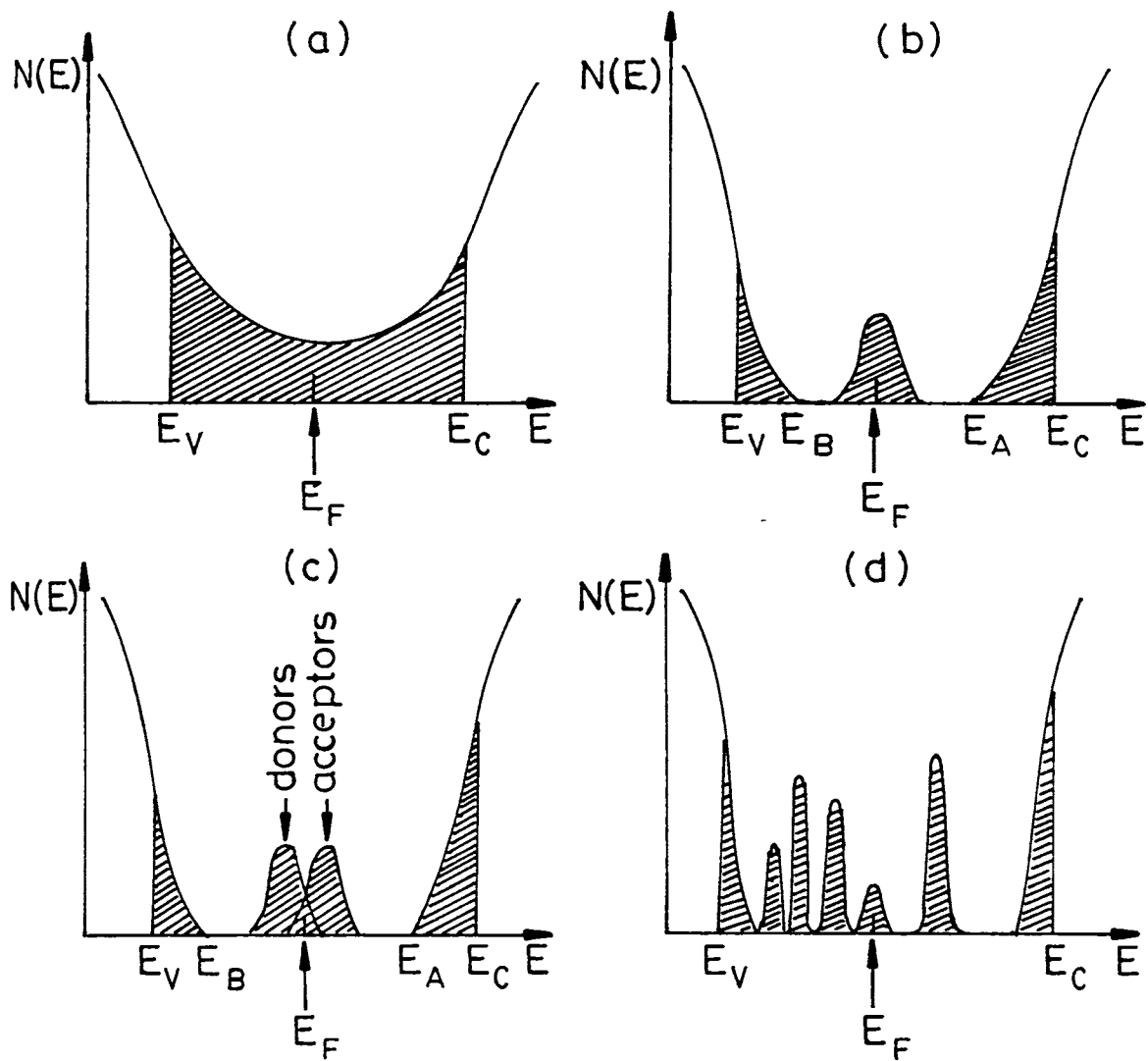


Fig. 1.2 Schematic density of states diagram for amorphous semiconductors
 (a) The CFO model (b) Davis- Mott model showing a band of compensated levels near the middle of the gap (c) modified Davis-Mott model
 (d) the "real" glass with defect states.

major objections against the CFO model has been the high transparency of amorphous chalcogenides below a well defined absorption edge.

1.6 b. Davis - Mott model.

According to Davis and Mott [48] the tails of localised states should be rather narrow and should extend a few tenths of an electron volt into the forbidden gap. They proposed furthermore the existence of a band of compensated levels near the middle of the gap, originating from the defects in the random network like dangling bonds, vacancies etc. Fig.(1.2b) sketches the Davis-Mott model, where E_V and E_r represent the energies which separate the ranges where the states are localised and extended. The centre band may be split into a donor band and an acceptor band, which will also pin the Fermi level (Fig.1.2c). Mott suggested that at the transition from extended to localised states the mobility drops by several orders of magnitude producing a mobility edge. The interval between the energies E_c and E_V acts as a pseudo-gap and is defined as the mobility gap. In recent years, experimental evidences, mainly coming from luminescence, photoconductivity and drift mobility measurements, have been found for the existence of various localised gap states associated with defect centers, which are split off from the tail states and are located at well defined energies in the gap. The position of the Fermi level is largely determined by the charge distribution in the gap states. The interpretation of electrical transport data is closely interwoven with the energy distribution of the density of states. On the basis of Davis-Mott model, there can be three processes leading to conduction in amorphous semiconductors. Their relative contribution to the total conductivity will predominate at different temperature regions. At very low temperatures conduction can occur by thermally assisted tunnelling between states at the Fermi level. At higher temperatures charge carriers are excited to localised states in the band tails, carriers in these localised states can take part in the electric charge transport only by hopping. At still higher temperatures carriers are excited across the mobility edge into the extended states. From this it follows that electrical conductivity

measurements over a wide temperature range are needed to understand the electronic structure of amorphous semiconductors.

1.6 c. Small polaron model

The role of lattice distortion in the presence of an extra charge carrier in an amorphous solid has been discussed by Emin [48]. He suggested that the charge carriers in some amorphous semiconductors may enter a self-trapped (small polaron) state as a result of the polarisation of the surrounding atomic lattice. He argued that the presence of disorder in a non-crystalline solid tends to slowing down of a carrier which may lead to a localisation of the carrier. If the carrier stays at an atomic site sufficiently long enough for atomic rearrangement to take place, it may induce displacements of the atoms in its immediate vicinity, causing small polaron formation. Since the small polaron is local in nature, the absence of long range order in noncrystalline solids may be expected to have no significant influence on its motion. Fermi was able to analyse experimental data on d.c. conductivity, thermopower and Hall mobility obtained on some chalcogenide glasses in the framework of small polaron theory.

1.7 Properties of amorphous semiconductors

Disorder induced potential fluctuations in amorphous semiconductors associated with bond length, bond angle etc. result in the tailing of conduction and valence bands. Experimental results obtained from structural, electrical, optical and thermal properties give evidence for density of states in their mobility gap.

1.7 a. Structural properties

The essential structural difference between a crystal and an amorphous solid is the latter's loss of long-range order. The structure of amorphous semiconductors is developed by the repetition of one or more basic molecular units that cannot be identified topologically with any known crystalline structure or with any infinite periodic array. There have been

many discussions on the types of structural models that can be used to explain amorphous solids [49]. An amorphous solid is one in which three dimensional periodicity is absent. The arrangement of atoms will not be entirely random as in a gas. The binding forces between atoms are very similar to those in a crystal and although long range order is excluded, S.R.O. of a few lattice constant will generally be present. A complete theoretical description of the properties of an amorphous solid would need a complete knowledge of the structure. Even within the restraints imposed by forces between individual atoms and the tendency towards S.R.O., there are infinite numbers of allowed structures for an amorphous material. Techniques used for a more detailed microscopic investigation include electron and X-ray diffraction, infrared absorption and Raman spectroscopy. Diffraction pattern from an amorphous solid consists of broad halves or rings. Given short range order, with three parameters viz., the number of bonds Z , the bond length a and bond angle θ , having well determined values in a narrow range, it is possible to construct a model for the structure which do not have any long range crystalline periodicity. Such models are called random network models. Zachariasen was the first to propose a continuous random model for inorganic covalent glasses [50]. Random network model that applies to tetrahedrally bonded amorphous semiconductors have been constructed by Polk [51]. Models for a network of three fold co-ordination have been constructed by Greaves and Davis [52] and for two-fold co-ordinated atoms by Long et al [53]. Structure of stoichiometric melt-quenched network glasses show that they are not all that random. The sharp first diffraction peak suggests medium range order (M.R.O.) of the scale $15\text{-}30\text{\AA}$ as observed in GeSe_2 and As_2Se_3 glasses [54]. On the basis of results from Raman [55] and Mossbauer [56] experiments; new structural models based on the formation of molecular clusters have been proposed for these systems [57-58].

The experimental methods used to determine the structure fall under four major categories, namely diffraction methods [59], vibrational spectroscopy [60], photoemission spectroscopy [61], and hyperfine interactions [62]. Diffraction technique mainly depends on X-ray diffraction experiments. In the RDF, amorphous semiconductors give evidence of

S.R.O. EXAFS is an important technique which can determine the local atomic arrangement about each type of atom separately. Vibrational spectra obtained by IR absorption or reflectance and Raman scattering are very useful for structural studies. Information about the ring statistics of networks can be obtained from X-ray and UV photoemission techniques.

The local bonding chemistry, which is very useful in structural investigations, can be studied by hyperfine interaction methods. These include nuclear quadrupole resonance, NMR, Mossbauer effect etc. Structural changes in an amorphous solid as a function of temperature can be detected by differential thermal analysis [63]. Materials which can be transformed into the semiconducting amorphous state generally contain elements of the groups III, IV, V and VI of the periodic table. These elements possess higher directional binding forces and as a consequence show rather strong local order in their glassy compounds. Small deviations in the interatomic distances and in bond angles lead to a complete loss of translational order after a few co-ordination spheres.

1.7 b. Electrical Properties

The techniques employed for determining the electrical properties of amorphous solids are the same as those employed for crystalline materials. The most striking feature of amorphous semiconductors is that addition of atoms with valence band different from that of the host does not in general greatly affect the conductivity, i.e. they cannot be easily doped. Structural defects play a more effective role than do impurities in controlling the conductivity of amorphous semiconductors. Near room temperatures, for most of the materials with which we are concerned, the activation energy for electrical conduction is approximately equal to one half of the photon energy corresponding to the onset of strong optical absorption. The band of localised states which exists near the centre of the gap arise from specific defect characteristics of the material like dangling bonds, interstitials etc., the number of which will depend on the conditions of sample preparation and subsequent annealing treatments.

In amorphous semiconductors, three mechanisms of electrical conduction can be distinguished.

1) Conduction due to carriers excited beyond the mobility shoulders to the extended states. If energy values E_C and E_V separate the localized states from extended states and $(E_C - E_V)$ the energy difference defines the mobility gap as shown in Fig.(1.3), then

$$\sigma = \sigma_0 \exp\{-(E_F - E_V)/kT\} \quad (1.34)$$

where $\sigma_0 = 0.06 e^2 / h a_E$, and a_E is the atomic separation.

(2) Conduction due to carriers excited into the localized states at the band edges i.e. at E_A and E_B . If the main current is carried by holes and conduction is by hopping, then

$$\sigma = \sigma_1 \exp\{(-E_F - E_B + \Delta\omega_1)/kT\} \quad (1.35)$$

where $\Delta\omega_1$ is the activation energy for hopping and E_B is the energy at the band edge. σ_1 is expected to be less than σ_0 by a factor of 10^2 to 10^4 .

(3) Conduction due to carriers hopping between localized states near the Fermi energy, which is a process analogous to impurity conduction in heavily doped semiconductors. Conductivity is given by

$$\sigma = \sigma_2 \exp\{-\Delta\omega_2/kT\} \quad (1.36)$$

where $\sigma_2 < \sigma_1$ and $\Delta\omega_2$ is the hopping energy of the order of half the width of the defect band shown in Fig.1.3d. As temperature is lowered, the carriers tunnel to more distant sites and conductivity behaves like

$$\ln \sigma = A - BT^{-1/4} \quad (1.37)$$

This variable range hopping at low temperatures is one of the interesting properties of amorphous semiconductors. As one goes from extended to localized states, mobility decreases by a factor of 1000. This drop in mobility is called mobility shoulder [48]. The

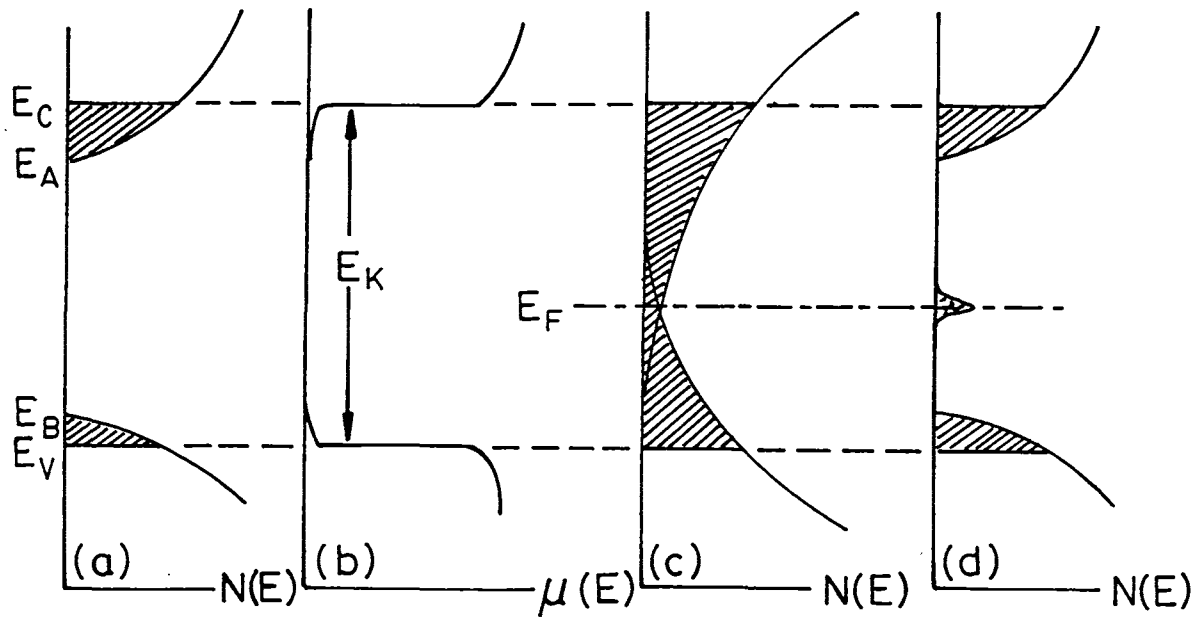


Fig.1.3 Density of states and mobility as a function of energy in amorphous semiconductors.

three mechanisms of charge transport that can contribute to d.c. current can also contribute to a.c. conductivity. The first is due to transport by carriers excited to the extended states near E_C or E_V . Conductivity could be given by a formula of the Drude type

$$\sigma(\omega) = \sigma(0)/(1+\omega^2\sigma_r^2) \quad (1.38)$$

where σ_r is the relaxation time. The second is due to transport by carriers excited to localised states at the edges of valance or conduction bands. Since transport here is by hopping, conductivity increases with frequency as $\omega^{0.8}$. The third is the transport by carriers with energies near the Fermi level. This again increases with frequency in the same manner as in the second case. Measurement of thermo power as a function of temperature provides the most direct way of determining the temperature coefficient γ of activation energy for conduction. Measurement of thermoelectric power in amorphous chalcogenide semiconductors have shown them to be p-type in the majority of cases reported. Hall coefficient yields a sign for carriers that is frequently in contradiction with thermoelectric power measurements which are explained by the theory of Friedman [64]. Magnetoresistance [48] which is the fractional change of resistivity in a magnetic field like Hall effect, can be used to determine the carrier mobilities. Magnetoresistance measurements on several amorphous semiconductors are found to be negative over a wide temperature range. For most materials, it is found to be proportional to B^n , where B is the magnetic induction with n being close to unity at high temperatures and falling to a value of the order of one half near room temperature. Only at very low magnetic fields and low temperatures it is found to be positive. Photoconductivity in amorphous semiconductors, in contrast to most crystalline semiconductors which exhibit a peak in conductivity at a photon energy corresponding to the onset of interband electronic transitions, have a spectral response that rise at approximately the same frequency as optical absorption edge and remains relatively constant at higher energies. Studies of transient photoconductivity in several amorphous semiconductors

indicate that the response is fast, with rise times measured in microseconds at low temperatures and fractions of microseconds at higher temperatures [65,66].

1.7 c. Optical Properties

The interaction with light provides a powerful means for probing the electronic and vibrational properties of a solid. Amorphous solids, lacking any special directions associated with crystallographic axis, are optically isotropic. The sharp features present in the crystal spectra are absent for glasses even at low temperatures. This spectral fine structure is a consequence of band structure of \mathbf{k} conservation in the crystalline state. Translational periodicity demands that only \mathbf{k} conserving transitions contribute to reflectivity spectra. Lacking long range order, amorphous solids do not show this fine structure in their comparatively blank spectra. In a crystalline solid, the lattice vibrational excitations are plane waves characterised by wave vector \mathbf{k} as well as frequency ν . Each mode of excitation is termed a phonon, and the $\nu(\mathbf{k})$ phonon dispersion relations provide an energy versus momentum representation of the vibrational modes which is analogous to the $E(\mathbf{k})$ band structure representation of the crystal's electron states. In amorphous solids the vibrational modes are no longer plane waves. While $\nu(\mathbf{k})$ is not a valid concept in glass, the concept of vibrational density of states $g(\nu)$ retains its validity. The overall shape of the band is similar for crystals and glasses because it reflects the same underlying chemical bonding structure. In an amorphous solid, contributions from the entire phonon density of states appear in the first order infrared and Raman spectra. Optical absorption in amorphous semiconductors can be separated into three regions, with absorption coefficients $\beta \geq 10^4 \text{ cm}^{-1}$, $1 \text{ cm}^{-1} < \beta < 10^4 \text{ cm}^{-1}$ and $\beta < 1 \text{ cm}^{-1}$ as shown in Fig.(1.4). Regions B and C are created by transitions within the fully co-ordinated system, perturbed to some extent by defects, while region A arises from transitions involving the defect states directly. The absorption edge has a defect induced tail at lower energies, an exponential region at intermediate energies and a power law region at higher energies. The defected amorphous states occur in numerous ways like voids arising

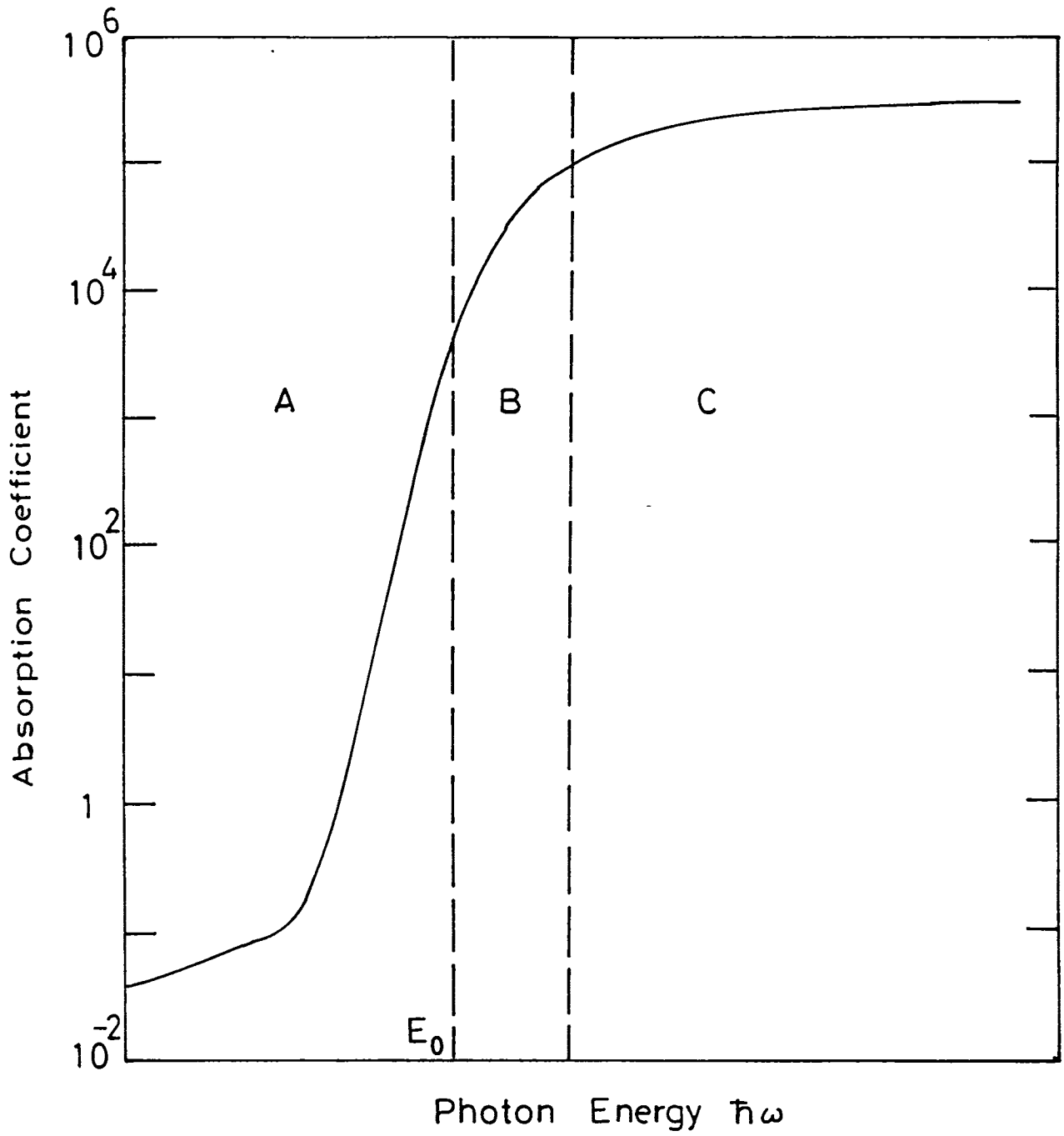


Fig. 1.4 Schematic representation of the absorption spectrum of amorphous semiconductors showing three different regions A, B and C.

from preparation techniques, occurrence of like bonds in a chemically ordered system or occasional occurrence of co-ordination variations. Perhaps the most important feature of the absorption process in amorphous semiconductors is that the \mathbf{k} -conservation rules, which apply to optically induced transitions in crystalline materials, are relaxed. In the high absorption region, absorption is governed by power law of the type

$$\beta = \text{const.}(h\nu - E_0)^\rho \quad (1.39)$$

where $\rho = 2$ for amorphous semiconductors under the assumption of parabolic bands. The constant E_0 can be used to define an optical gap. ρ assumes values 1 and 3 for elemental Se and multicomponent materials respectively. Beyond the fundamental absorption edge, amorphous semiconductors continue to absorb strongly. Since the selection rule is relaxed, all pairs of extended states with energy difference $h\nu$ can contribute to optical absorption. A plot of $\beta^{1/2}$ versus $h\nu$ yields a straight line and the extrapolated $h\nu$ at which $\beta^{1/2}$ tends to zero gives the value of E_0 .

The exponential tail in β is associated with the intrinsic disorder in amorphous semiconductors in the intermediate range of absorption coefficient. It has been suggested that it is due to disorder induced potential fluctuations [67]. In tetrahedrally co-ordinated materials, voids formed as a result of strain release mechanism provides a possible explanation for absorption tails.

In chalcogenide glasses, defects due to co-ordination variation explains several of the optical properties. In the weak absorption region, the shape of the absorption tail is found to depend on the preparation, purity and thermal history of the material [68]. It has been found that the mobility gap in many amorphous semiconductors corresponds to a photon energy at which the optical absorption coefficient has a value approximately 10^4cm^{-1} . The assumption here is that the mobility gap is equal to twice the activation energy for electrical conduction.

From measurements made using UV diffraction grating reflectometer, the optical constants can be derived from Kramers-Kronig analysis of reflectivity.

1.7 d. Thermal properties

A striking feature of amorphous solids at low temperature (below 50K) is that they exhibit markedly different behaviour from their crystalline counterparts in phonon related properties such as specific heat capacity, thermal conductivity and acoustic as well as dielectric absorption. The thermal properties of crystalline solids at low temperatures are well understood in terms of Debye's theory in which it is assumed that the distribution of phonons is cut off at some frequency to which a characteristic temperature θ_D may be associated. The specific heat of glass decreases much more slowly with temperature than the Debye T^3 prediction at low temperature ($0K < T < 1K$) [69,70]. The thermal conductivity is also markedly different being a monotonically decreasing function of temperature for glasses, in contrast to the peaked behaviour characteristic of crystals [71,72]. Near $\approx 10K$, thermal conductivity is only weakly temperature dependent and shows a plateau region. Upon further decrease in temperature, thermal conductivity is found to decrease roughly as T^2 . Hence the magnitude and temperature dependence appear to depend on the amorphous structure of the material rather than the chemical composition. Hence thermal transport below 10K is provided by phonons. The phonon mean free path has a magnitude and temperature dependence which is characteristic of the glassy state. Phonon scattering responsible for this mean free path is caused primarily by localized excitations. The elastic and dielectric behaviour of amorphous solids is strongly enhanced compared to crystals and a large absorption peak is found around liquid nitrogen temperature in many glasses. Below helium temperature, a number of anomalous effects are observed which can be attributed to low energy excitations closely related to the amorphous state. These excitations are responsible for the anomalously high C_P value and the observed elastic properties. To explain low temperature thermal properties, a number of theories have been proposed, the most successful of which has been that involving

“two-level systems” [TLS] proposed by Anderson et al [73] and Phillips [74]. At high temperatures, the atoms comprising the TLS change the configuration by means of thermally activated process by hopping over barriers while at low temperatures tunnelling through the barriers dominate.

1.8 Chalcogenide Glasses

Amorphous semiconductors while forming a single area of study often is divided into two subfields, the tetrahedrally co-ordinated silicon like materials and chalcogenide glasses. Arsenic from column V of the periodic table forms a bridge between the two classes of materials. Amorphous silicon, when nominally pure, is permeated with dangling bonds as evidenced by a detectable electron spin resonance. In contrast to amorphous silicon and other group IV tetrahedrally bonded semiconductors, the amorphous chalcogens and chalcogenide glasses do not exhibit a dangling bond spin resonance signal in their clean as-prepared state. Chalcogenide glasses are materials containing one or more of the chalcogen elements in the sixth column of the periodic table viz., sulphur, selenium or tellurium. Chalcogens with their two fold coordination and lone pair orbitals offer the network the dual channels of structural and electronic flexibility for the removal of dangling bonds. As a consequence, a typical chalcogenide has a relatively sharp optical absorption edge, a single electrical activation energy and efficient photoexcited conductivity and luminescence. All these properties are characteristic of a well defined and clear forbidden gap. Nevertheless, field-effect and doping experiments indicate that the Fermi level of a chalcogenide glass is nearly pinned. Within certain ranges of composition it is possible to form glasses by combination with one or more of the elements As, Ge, Si, Te, Pb, P, Sb, Bi among others. The problem of the classification of a large variety of ternary and quaternary systems becomes difficult due to the freedom to depart from stoichiometric proportions of the constituents. Multicomponent glasses of arbitrary compositions have been studied in connection with electrical switching. There have been several reports of the effect of impurities on the electrical conductivity of chalcogenide glasses. Sometimes they are quite marked, for example the addition of 1% of Ag to As_2S_3 has

been reported to raise the room temperature conductivity by several decades. Eventhough they cannot be doped, impurities with concentrations as high as 1% may play a role in modifying the structure (by crosslinking). The effect of this may be to increase or decrease the range of localized states at the band edges and hence change the conductivity. The d.c. conductivity of most of these glasses at room temperature obeys the relation

$$\sigma = C \exp(-E/kT) \quad (1.40)$$

Conduction in chalcogenide glasses is predominantly by carriers hopping between localized states at the band edge. The thermoelectric power of chalcogenide glasses are normally positive, with values consistent with the idea of a Fermi energy near the center of the gap, but nearer to the mobility edge in the valence band. In measurements made as a function of temperature, activation energies similar to those observed in electrical conductivity are found. Hall effect measurements on chalcogenide glasses are difficult, especially on those with low conductivity, because of the small magnitude of the effect. They are found to be negative. The optical absorption edge of chalcogenide glasses are characterised by absorption coefficients α that rises exponentially with increasing photon energy upto a value of α in the range 10^3 to 10^4 cm^{-1} . At higher values of absorption coefficients, the most frequently reported behaviour is

$$\alpha h\omega = \beta (h\omega - E_0)^2 \quad (1.41)$$

where β lies in the range 10^5 - $10^6 \text{ cm}^{-1} \text{ eV}^{-1}$ and E_0 is the optical band gap.

The network dimensionality is defined as the number of dimensions in which the covalently bonded molecular unit is macroscopically extended. Although chalcogenides primarily form 1D and 2D network glasses, 3 dimensional networks can also be obtained by the introduction of column IV elements like Ge which enter the covalent graph in four-fold

co-ordination. One of the interesting properties of chalcogenide glasses, which underlies an exciting potential application as computer memory materials is the possibility of producing a change of structure by means of incident light. The simplest such photoinduced structural change is crystallisation [75]. The compositional variability of this class of amorphous solids permits their properties to be tailored to specific application. In constructing a glass, the “8- n ” rule has been adopted as a central working assumption. The valence of each constituent atom is satisfied throughout the amorphous solid. Valence n in this context is taken to mean the number of single covalent bonds necessary for the neutral atom to complete via the shared electrons comprising the bonds, its outermost shell of s and p electrons. The “8- n ” rule has been proposed by Mott [76] in connection with the chalcogenide glasses, to account for the observation that the electrical properties of these solids do not exhibit great sensitivity to impurities and are insensitive to the composition changes of even a few percent. This rule ensures that all the valence electrons of the constituent atoms are taken up in bonds. This chemical condition is a reasonable one to invoke for melt quenched glasses. During the relatively slow formation of such bulk amorphous solids, there is enough time to attain this local energy-minimising chemical bonding configuration. The topological defects in glasses are the broken or dangling bonds and valence alternation pairs (VAPS) [77]. These types of defects were first proposed in chemically specific form in the pioneering work by Kastner, Adler and Fritzche [77]. The importance of VAP’s lies in the theoretical efforts to explain the unusual electrical and magnetic properties of chalcogenides.

As to chalcogenide glasses, one of the central problems concerns the question whether the structural order of layer types exists or not. Recently Phillips proposed a simple dynamical model for network glasses based entirely on topological considerations [78,79,80]. Phillips has demonstrated through a constraint counting analysis that the glassy structure has a maximum stability at $Z = 2.4$. He obtains this number under the argument that stable glasses satisfy the relation $N_d = N_{con}$, where N_d is the number of degrees of freedom for the atoms in the glassy network and N_{con} is the number of force field constraints per atom. The average co-ordination number (Z) at which the glass formation is optimised mechanically is

the critical average co-ordination number (Z_c). For $Z < Z_c$, the network is underconstrained and tends to disintegrate into non-polymerised fragments. When $Z > Z_c$, the network is overconstrained. Later, Thorpe extended this model to predict the elastic behaviour of covalent glasses in terms of the average number of constraints in the system [81-84]. Here, regions of lower co-ordination are called floppy and regions of higher co-ordination rigid regions. For low average co-ordination number the network is a polymeric glass ($N_d > N_{con}$) in which the rigid regions are isolated. As the mean co-ordination increases, the rigid regions increase in volume until at $Z = Z_c$ or $N_d = N_{con}$ the network transforms completely to a rigid glassy structure. This transition phenomenon is referred as to percolation transition phenomenon and the rigidity of the system is said to percolate in a threshold manner. This is schematically depicted in Fig.(1.5). By the application of shearing forces, these floppy regions can be elastically deformed admitting the displacement of groups of atoms with the provocation of restoring forces.

Considering a particular random network with N atoms constructed with n_r atoms having r bonds, we have,

$$N = \frac{\sum n_r}{r} \quad (1.42)$$

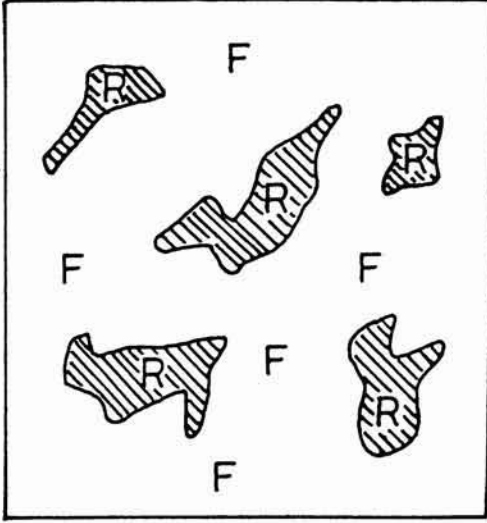
The largest forces in covalent networks are the nearest neighbour bond stretching and bond bending forces. There are three degrees of freedom. There is one constraint associated with each bond (giving $r/2$ per atom) and $(2r-3)$ angular constraints associated with each r co-ordinated atom. The fraction of zero frequency modes is then

$$\frac{3N - \sum n_r [r/2 + (2r - 3)]}{3N} \quad (1.43)$$

$$\text{i.e. } f = 2 - (5/6)\langle Z \rangle \quad (1.44)$$

where the mean co-ordination $\langle Z \rangle$ is defined as

I Polymeric Glass



II Amorphous Solid

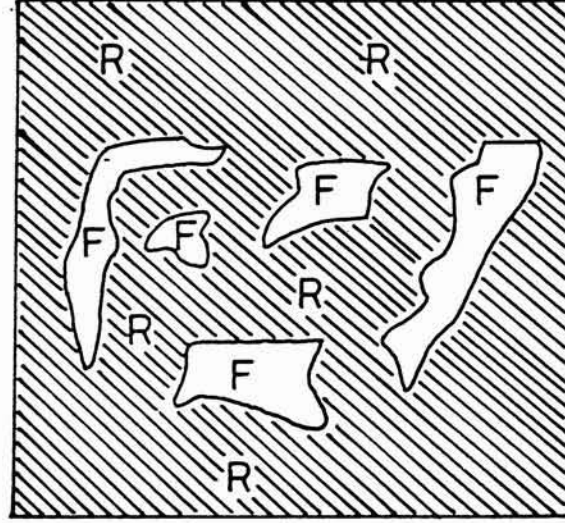


Fig. 1.5 Rigid and floppy regions in the network of polymeric glass and amorphous solid.

$$\langle Z \rangle = \sum r N_r / \sum N_r \quad . \quad (1.45)$$

As atoms with co-ordination higher than two are added to the network as crosslinks, f drops and goes to zero at $\langle Z \rangle = 2.4$ and the network becomes rigid as it goes through the above transition. This value of $\langle Z \rangle$ at which transition occurs is termed as the “mechanical threshold”.

Studies to verify the threshold behaviour on the ternary system Ge-As-Se are in accordance with the percolation model [85]. The ultrasonic pulse echo overlap technique used by the above authors to measure the room temperature elastic moduli shows a change of slope at $\langle Z \rangle = 2.4$. The experimental reports on a wide range of physical properties of various binary glasses indicate the threshold behaviour at $\langle Z \rangle = 2.4$ [86-98]. Some controversial results have been reported quite recently indicating a shift in $\langle Z \rangle$ value at which the threshold occurs. Reports on Ge-Se glasses show a slope change in the elastic constant versus $\langle Z \rangle$ at 2.60 [99] and 2.70 [100]. There have also been reports of anomalous behaviour at $\langle Z \rangle = 2.4$ and 2.67 in various properties of Ge-Se and Ge-S glasses [101-105]. Photodarkening, molar volume, X-ray diffraction, elastic constants, E_g values etc. of ternary glasses reported by Tanaka also show a departure in the threshold value [104-107]. The bulk modulus for these systems is nearly a constant when $\langle Z \rangle < 2.67$, but otherwise increase drastically with $\langle Z \rangle$. The magnitude of reversible photo-darkening is greatest at 2.67. All these properties reflect an intermediate structural order. Tanaka modified Phillips model by assuming a hypothetical material having a plane lattice laid in a 3-dimensional space [107]. Modifying the angular term, the number of angular constraints is reduced to $(r-1)$ instead of $(2r-3)$ as predicted by Phillips and Thorpe. The number of constraints then reduces to

$$N_{con} = r/2 + (r-1) \quad (1.46)$$

If such a cluster is laid in a three dimensional space, each atom must have 3 independent degrees of freedom of stable existence. This gives $\langle Z \rangle = 2.67$, i.e. the co-ordination number of glasses having stable layer structure becomes 2.67. This means a 2D

glass possessing a layered structure appears to be stably fixed in a 3D space if the co-ordination number of the glassy network is 2.67.

Other than the constraints model and the structural transition model, the chemically ordered covalent network (COCN) model have also been proposed to interpret data of various physical, elastic, thermal and electronic properties of chalcogenide glasses [108-111]. In this model, the glass structure is assumed to compose of crosslinked structural units of the stable chemical compounds and excess, if any, of the elements. Due to chemical ordering, features such as an extremum, a change in slope or a kink is observed in various properties as a function of composition at the tie-line or stoichiometric composition [112-117]. These tie line compositions are also referred to as the chemical thresholds [118-119] of the system. In COCN model for atomic arrangement in glasses, the formation of heteropolar bonds is always favoured over the formation of homopolar bonds. For a compound A_xB_y , this model envisages only A-B type of bonds for the tie-line composition, A-B and A-A types of bonds for A-rich and A-B and B-B types of bonds for B-rich compositions.

In glass systems containing group V-VI elements, the chemical threshold occurring at $\langle Z \rangle = 2.4$ coincides with one of the topological thresholds while in IV-VI elements, the chemical threshold occurring at $\langle Z \rangle = 2.67$ coincides with the other topological threshold. In IV-V-VI and IV-III-VI systems, the chemical thresholds occur at $\langle Z \rangle$ values other than the topological thresholds [120,121]. Variation of composition dependence with mean atomic volume for Ge-Ga-Se and Ge-In-Se glasses indicate a minimum at 2.4 and a peak at 2.67 due to the floppy to rigid transition and structural transition respectively [121]. Due to chemical ordering additional peaks are seen at the chemical threshold also [121-125]. Results are attributed to the coexistence of the effects which have a topological origin and effects due to chemical ordering. In this thesis, the validity of these conclusions are examined for selected systems by measuring the variation of optical band gap and thermal diffusivity with average co-ordination number $\langle Z \rangle$.

1.9 Applications of amorphous semiconductors

Amorphous solids have been used in a variety of applications for hundreds of years. Until very recently, silicate glasses were the only type of amorphous materials commonly used. The relatively recent discovery that very many other types of materials can be produced in the amorphous form, either as bulk glasses or as thin films, has led to very rapid expansion in the use of such materials in electronic, magnetic and optical applications.

Non-crystalline materials have many advantages over their crystalline counterparts when applications are concerned. In general, they are relatively easy to prepare. Large area homogeneous amorphous thin films can be prepared for solar cell or thin-film transistor applications. Bulk glasses can often be readily formed from the melt by relatively slow quenching procedures. More importantly, near the glass transition temperature the material remains workable over a range of temperatures so that it can be easily fashioned into fibres. Furthermore, amorphous materials, particularly bulk glasses, are often structurally homogeneous and isotropic over a macroscopic length scale as a result of which their physical properties are also isotropic. Thus large scale optical transparency is readily achievable in silicate glasses used for optical components and fibre optic cables. The absence of structural defects, such as grain boundaries or dislocations, also have a dramatic effect on the mechanical behaviour. They have a further distinct advantage over their crystalline counterparts in that homogeneous amorphous phases can often be formed in mixed component systems over rather wide ranges of compositions, not restricted to stoichiometric values. For this reason, physical properties of such amorphous materials can often be varied continuously by varying the composition. In many cases amorphous materials are used as passive and active elements in electronic devices [126,127]. One of the widespread current applications of amorphous semiconductors is in the field of xerography [128]. In order to fabricate large area flat displays, an array of thin film transistor devices need to be constructed and for this thin film deposition technology of amorphous semiconductors is very suitable [129]. Perhaps the most technologically developed and potentially the most important application is in the direct conversion of sunlight into electrical power [130]. The ability of

certain ions to diffuse readily in oxide or chalcogenide glasses in the presence of a concentration gradient or an electric field, opens up a range of possible electrochemical applications, for example, in the field of energy storage, displays or chemical sensors [131,132]. The most widespread use as an electrochemical sensor is in the so called “glass electrode” commonly used to monitor proton activity. Glasses have long been used extensively for optical communication applications, both for long distances and in local area networks as these materials have ultra low optical loss characteristics. There has also been some work recently on active optical devices as well [133,134] like LEDs.

Materials of the future should satisfy the stringent requirement of properties to provide the most efficient devices and at the same time should be cheap and suitable for mass production. For conventional applications the amorphous semiconductors have the advantage of being cheap, large area devices and compatibility with existing IC technology. Special devices use threshold switching behaviour based on structural changes. Threshold and memory switches show a rapid transition from a high impedance off state to a low impedance on state upon application of an voltage exceeding a threshold value. Photostructural changes have also been observed in amorphous semiconductors. The use of amorphous semiconductor thin films as storage target in an electron beam memory device has been reported [135]. Very good transmittance of chalcogenide glasses reaching up to the far infrared region and the possibility of a continuous shift of absorption edge make possible their utilisation in the form of IR filters and other IR optical elements [136].

REFERENCES

1. W.W.Wendlandt and H.G.Hecht, *Reflectance spectroscopy* [Wiley, New York, 1960].
2. Walks Jr. And T.Hirschfeld, *Appl. Spectrosc. Rev.* **1**, 99 (1968).
3. G.B.Wright (ed.), *Light scattering in solids*, (Springer-Verlag, Berlin, 1969).
4. M.J.Adams, B.C. Beadle and G.F.Kirkbright, *Analyst*, **102**, 569 (1977).
5. A.Rosencwaig and E.Pines, *Biochem. Et Biophys. Acta*, **493**, 10 (1977).
6. D.M.Munroe and H.S. Reichard, *Am. Lab*, **9**, 119 (1977).

7. A.Rosencwaig and A.Gersho, *J. Appl. Phys.* **47**, 64 (1976).
8. H.S.Bennett and R.A.Foreman, *J. Appl. Phys.* **48**, 1432 (1977).
9. M.J.Adams and G.F.Kirkbright, *Analyst* **102**, 281 (1977).
10. M.J.Adams, J.G.Highfield and G.F.Kirkbright, *Anal. Chem.* **49**, 1850 (1977).
11. W.Lahmann and H.J.Ludeweg, *Chem. Phys. Lett.* **45**, 177 (1977).
12. J.G.Parker, *Appl. Opt.* **12**, 2974 (1973).
13. F.A.Mc.Donald and G.C.Wetsel Jr., *J. Appl. Phys.* **49**, 2313 (1978).
14. L.C.Aamodt and J.C. Murphy, *J. Appl. Phys.* **49**, 3036 (1978).
15. A.Rosencwaig and A.Gersho, *J. Appl. Phys.* **47**, 64 (1976).
16. J.F.MacClelland and R.N.Kriseley, *Appl. Opt.* **15**, 2658 (1976).
17. G.C.Wetsel Jr. And F.A.MacDonald, *Appl. Phys. Lett.* **30**, 252 (1977).
18. A.Rosencwaig, *J. Appl. Phys.* **49**, 2905 (1978).
19. A.Rosencwaig, *Opt. Commun.* **7**, 305 (1973).
20. M.J.Adams, G.F.Kirkbright and K.R.Menon, *Anal. Chem.* **51**, 508 (1979).
21. J.I.Pankove, *Optical Processes in semiconductors* (1971), Prentice-Hall, New York.
22. A.Rosencwaig, *Anal. Chem.* **47**, 592A (1975).
23. A.Rosencwaig, *Phys. Today*, **28**, 23 (1975).
24. D.F.Nelson, L.F.Johnson and M.Gershonzon, *Phys. Rev.* **135A**, 1399 (1964).
25. R.B.Somoano, *Argen. Chem. Int. Ed. (Eng.)*, **17**, 234 (1978).
26. C.Tam, *Rev. of Modern Physics*, **58**, 2 (1986).
27. B.Ray, *International series of monographs in the science of solid state, II-VI compounds* (Oxford: Pergamon), Vol.2.
28. L.Baldassare, A.Cingolani, A.De Tommasi, G.Vailati, *Appl. Phys. Commun.* **2(3)**, 183 (1982).
29. A.Rosencwaig, M.J.Webber, R.A.Saroyan *FA5-I, Proceed. Of Ist Inter. Topical Meeting on PAS*, Aug. 1979, Ames, Iowa.
30. Patel and A.C. Tam, *Rev of Modern Physics* **53**, 13 (1981).

31. P.S.Bebton, S.F.Tanner, *Analyst* **108**, 591 (1983).
32. Lachaine, *J. Appl. Phys.* **57**, 11 (1985).
33. U.Zammet, M. Harinelli, R.Pezzoferrato, F.Scudiere and S.Martellucci, *J. Phys. E: Sci. Instrum.* **21**, 935 (1988).
34. T.Swimm, *Appl. Phys. Lett.* **42**, 955 (1983).
35. Lachaine and P. Poulet, *Appl. Phys. Lett.* **45(9)**, 953 (1984).
36. M.Rohde, *Thin Solid Films*, **238**, 199 (1994).
37. P.Charpentier, F.Lepoutre and L.Bertrand, *J. Appl. Phys.* **51**, 608 (1982).
38. O.Pessoa, C.L.Cesar, N.A.Patel, H.Vargas, C.C.Ghizone and L.C.H.Miranda, *J. Appl. Phys.* **59**, 1316 (1986).
39. P.Korpiun, R.Tilgner and D.Schmidt, *J. Phys. Colloq.* **44**, C6.43 (1983).
40. A.Torres-Filho, L.F.Perondi and L.C.M. Miranda, *J. Appl. Polym. Sci.* **35**, 103 (1988).
41. R.Florian, J. Pelzl, M.Rosenberg, H.Vargas and R.Wernhardt, *Phys. Status Solidi (a)*, **48**, 35 (1978).
42. P.Korpiun and R.Tilgner, *J. Appl. Phys.* **51**, 6115 (1980).
43. C.Pichon, M.Le Liboux, D.Fournier, A.C.Boccara, *Appl. Phys. Lett.* **35**, 435 (1979).
44. P.Korpiun, J. Baumann, E.Luoscher, E.Papamokes, R.Tilgner, *Phys. Status Solidi(a)*, **58**, K13 (1980).
45. P.S.Bechthold, M.Campagne, T.Schober, *Solid. Stat. Commun.* **36**, 225 (1980).
46. K.Junge, B.Bein, J. Pelzl, *J.Phys.* **44**, C6-55 (1983).
47. J.Extbarria, S.Uriate, J.Fernandez,M.J.Tello, *J.Phys. C.* **17**, 6601 (1984).
48. Mott and E.A. Davis in *Electronic processes in non-crystalline materials* (Clarendon Press) (1971).
49. A.C.Write and A.J.Leadbetter, *Phys. Chem. Glass* **17**, 122 (1976).
50. W.H.Zachariasen, *J. Amer. Chem. Soc.* **54**, 3841 (1932).
51. D.E.Polk, *J. Non-Cryst. Solid* **5**, 365 (1971).
52. G.N.Greques and E.A.Davis, *Phil. Mag.* **29**, 1201 (1974).

53. M.Long, P.Galiron, R.Alben and G.A.N. Connel, *Phy. Rev.B*, **13**, 1821 (1976).
54. J.C.Phillips, *Phy. Rev.B*, **21**, 5724 (1980).
55. J.E.Griffiths, G.P.Espinosa, J.R.Remeika and J.C.Phillips, *Solid State Commun.* **40**, 1077 (1981).
56. P.Bootchand, J. Grothaus, W.J.Bresser and P.Suranyi, *Phy. Rev.B.* **25**, 2975 (1982).
57. J.C.Phillips, *J. Non-Cryst. Solids* **35**, 1157 (1980).
58. J.C.Phillips, C.A.Beevers and S.E.B.Gould, *Phy. Rev.B.* **21**, 5724 (1980).
59. R.Grigorovici, *J. Non-Cryst. Solids* **1**, 303 (1969).
60. G.Lucovsky in *Physical Properties of Amorphous Materials*, ed. D.Adler (Plenum Press, New York,), 277 (1985).
61. L.Ley, M.Cardona and R.A.Pollak, in *Photoemission in Solids II* (Springer-Verlag, Berlin) 277 (1979) .
62. P.P.Seregin, A.R.Regel, A.A.Andreev and F.S.Wasredinov, *Phy. Stat. Solidi.a*, **74**, 373 (1982).
63. R.C.Mackenzie in *Differential Thermal Analysis* ed: R.C.Mackenzie (Academic Press, New York), (1970).
64. P.Nagels in *Amorphous Semiconductors*; ed. M.M.Brodsky (Springer-Verlag, Berlin) 113 (1979).
65. H.Scher and E.W.Montrell, *Phy. Rev.B.* **12**, 2455 (1975).
66. R.Zallen in *Physics of Amorphous Solids* (Wiley, New York, 1983).
67. J.Tauc in *Amorphous and Liquid Semiconductors*, ed: J.Tauc (Plenum Press, New York, 1974) 159.
68. A.Vasko, D.Lezal and I.Srb., *J. Non-Cryst. Solids* **4**, 311 (1970).
69. R.C.Zeller, R.O.Pohl *Phy. Rev. B* **4**, 2029 (1971).
70. Stephens, *Phys. Rev. B* **13**, 852 (1976).
71. R.Berman, *Proc. R. Soc. London A* **208**, 96 (1951).
72. W.A.Phillips in *Amorphous Solids:Low Temperature Propertis* (Springer-Verlag) 65 (1981).

73. P.W.Anderson, B.I.Halperin and C.M.Varma, *Phil. Mag.* **25**, 1 (1972).
74. W.A.Phillips, *J. Low Temp. Phys.* **7**, 351 (1972).
75. E.Finkman E, A.P.Denfonzo and J.Tauc in *Proc. of the 12th Int. Conf. On the Physics of Semiconductors* ed: H.H.Piekuhn (1974), 1022.
76. N.F.Mott, *Phil. Mag.* **19**, 835 (1969).
77. M.Kastner, O.Adler and H.Fritzsche, *Phys. Rev. Lett.* **37**, 1504 (1976).
78. Phillips, *J. Non-Cryst. Solids* **34**, 153 (1974).
79. Phillips, *J. Non-Cryst. Solids* **43**, 37 (1981).
80. J.C.Phillips, *Phys. Status Solidi.(b)* **101**, 473 (1980).
81. M.F.Thorpe, *J. Non-Cryst. Solids* **57**, 355 (1983).
82. J.C.Phillips and M.F.Thorpe, *Solid State Commun.* **53**, 699 (1985).
83. S.Feng, M.F.Thorpe and E.Garborzi, *Phys. Rev.B* **31**, 276 (1985).
84. H.He and M.F.Thorpe, *Phys. Rev. Lett.* **54**, 2107 (1985).
85. B.L.Halfpap and S.M.Lindsay, *Phys. Rev. Lett.* **57**, 847 (1986).
86. R.Ota, T.Yamate,N.Soga, M.Kunugi, *J. Non-Cryst. Solids* **29**, 67 (1978).
87. K.Murase, K.Yakushiji and T.Fukunaga, *J. Non-Cryst. Solids* **59-60**, 855 (1983).
88. M.Bensoussan, *Rev. Phys. Appl.* **12**, 753 (1977).
89. K.S.Gilroy and W.A.Phillips, *Phil. Mag. B* **47**, 655 (1983).
90. K.N.Madhusoodanan and J.Philip, *Phy. Stat. Solidi.(a)* **108**, 775 (1988).
91. A.Denewville, J.P.Keradec, P.Gerrad and A.Mini, *Solid State Commun.* **14**, 341 (1974).
92. K.N.Madhusoodanan, J. Philip, G.Parthasarathy, S.Asokan and E.S.R.Gopal, *Phil. Mag. B* **50**, 123 (1983).
93. K.E.Peterson; U.Birkholz and A.Adler, *Phys. Rev. B.* **8**, 1453 (1973).
94. S.Asokan, G.Parthasarathy and E.S.R.Gopal, *Phys. Rev. B.* **35**, 8269 (1987).
95. K.N.Madhusoodanan, J. Philip, S.Asokan, G.Parthasarathy and E.S.R.Gopal, *J. Non-Cryst. Solids* **109**, 255 (1989).

96. K.N.Madhusoodanan, K.Nandakumar, J. Philip, S.S.K.Titus and E.S.R.Gopal, *Phys. Stat. Solidi(a)*, **114**, 525 (1989).
97. R.Ota, N.Soga and M.Kunugi, *Yogyokyokaishi* **81**, 131 (1973).
98. K.Madhusoodanan and J.Philip, *Pramana-J.Phys.* **33**, 705 (1989).
99. S.S.Yun, H.Li, R.L.Cappeletti, R.N.Enzweiler and P.Bookhand, *Phys. Rev. B* **39**, 8902 (1989).
- 100.J.Y.Duquesne and G.Bellessa, *Europhys. Lett.* **9**, 453 (1989).
- 101.A.Feltz, H.Aust. and A.Blayer, *J.Non-Cryst.Solids* **55** 179 (1983).
- 102.S.Asokan, M.V.N.Prasad, G.Parthasarathy and E.S.R.Gopal, *Phys. Rev. Lett.* **62**, 808 (1989).
- 103.R.A.Street, R.J.Nemanich and G.A.N.Conenell, *Phys. Rev. B* **18**, 6915 (1978).
- 104.K.Tanaka, T.Nakagawa and A.Odajima, *Phil. Mag. B* **54**, L3 (1986).
- 105.K.Tanaka, Y.Kasanuki and A.Odajima, *Thin Solid Films* **117**, 251 (1984).
- 106.K.Tanaka, *Solid Stat. Commun.* **60**, 295 (1986).
- 107.K.Tanaka, *Phys. Rev. B* **39**, 1270 (1989).
- 108.G.Lucovsky, F.L.Galeena, R.H.Geils, and R.C.Keezer in “*The Structure of Non-Crystalline Materials*”, ed: P.H.Gaskell (Taylor & Francis, London) 127 (1977).
- 109.G.Lucovsky, R.J.Nemanich and F.L.Galeener in: *Proc. 7th Int. Conf. On Amorphous and Liquid Semiconductors*, Edinburg, 1977 ed: W.Spear (Univ. of Edinburg), 130.
- 110.F.Betts, A.Beinenstock and S.R.Ovishinsky, *J. Non-Cryst.Solids* **4**, 554 (1970).
- 111.G.Lucovsky, F.L.Galeener, R.C.Keezer, R.H.Geils and H.A.Six, *Phys. Rev. B* **10**, 5134 (1974).
- 112.C.H.Hurst and E.A.Davis in *Proc. 5th Int. Conf. Of Amorphous and Liquid Semiconductors*, ed: J.Stuke and W.Brenig, Vol.7 (Taylor and Francis, London) 34 (1974).
- 113.M.K.Rockstad and J.P.de Neufville in *Proc. 11th Int. Conf. On Physics of Semiconductors* (P.W.N.Polish Scientific Publishers, Warsaw) 542 (1972).

- 114.P.S.L.Narasimham, A.Giridhar and S.Mahadevan, *J. Non-Cryst. Solids* **43**, 365 (1981).
- 115.A.Giridhar and P.S.L.Narasimham and S.Mahadevan, *J. Non-Cryst. Solids* **43**, 29 (1981).
- 116.A.Giridhar and S.Mahadevan, *J. Non-Cryst. Solids*, **51** 305 (1982).
- 117.S.Mahadevan, A.Giridhar and A.K.Singh, *J. Non-Cryst. Solids* **103**, 179 (1988).
- 118.P.Bodehard, *Key. Eng. Mater.* **13**, 31 (1987).
- 119.S.Mahadevan and A.Giridhar, *J.Non-Cryst. Solids* **110**, 118 (1989).
- 120.A.Feltz, M.Aust and A.Blayer, *J. Non-Cryst. Solids* **55**, 179 (1983).
- 121.S.Mahadevan and A.Giridhar, *J.Non-Cryst.Solids* **134**, 94 (1991).
- 122.A.Giridhar and S.Mahadevan, *J.Non-Cryst.Solids* **126**, 161 (1990).
- 123.S.Mahadevan and A.Giridhar, *J.Non-Cryst.Solid* **42**, 152 (1993).
- 124.S.Saffarine, *Solid State Commun.* **91**, 577 (1994).
- 125.S.Mahadevan and A.Giridhar, *J.Non-Cryst.Solids* **143**, 52 (1992).
- 126.Hamakawa: in *Non-Crystalline Semiconductors*, ed: M.Pollak, Vol.1 (CRC Press) 229 (1987).
- 127.A.Madan and M.P.Shaw in *The Physics and Applications of Amorphous Semiconductors* (Academic Press) (1988).
- 128.I.Shimizu, *J.Non-Cryst.Solids* **77**, 1363 (1985).
- 129.P.G.Le Comber, A.J.Snell, K.D.Mackenzier and W.E.Spear, *J. Phys.* **42**, C4-423 (1981).
- 130.C.H.Henry, *J. Appl. Phys.* **51**, 4494 (1980).
- 131.J.P.Gabona, in *Glass: Current Issues* (1985).
- 132.G.Eisenman, ed: *Glass Electrodes for Hydrogen and Other Cations, Principle and Practice* (Marcel Dekker) (1967).
- 133.T.Miya, Y.Terunuma, T.Hosaka and T.Miyashita, *Electronics Lett.* **15**, 106 (1979).
- 134.H.Weber, *Wiss Zutschr Friedrich-Schiller Univ.* **32**, 239 (1987).
- 135.A.C.M.Chen, A.M.Dunham and J.M.Wang, *J. Appl. Phys.* **44**, 1436 (1973).
- 136.Z.Cimpe and F.Kosek, *J.Non-Cryst.Solids* **90**, 577 (1987).

CHAPTER II

INSTRUMENTATION

2.1 Introduction

In this chapter the experimental setup of the PA measurement technique is described. The application of this technique in measuring both optical band gap and thermal diffusivity of solid samples are outlined. This chapter also outlines an accurate temperature controller which we have designed and fabricated to control the furnace temperature while preparing bulk chalcogenide glasses.

A basic PA spectrometer consists of a radiation source of sufficient intensity with wavelength range of interest, a light intensity modulator, PA cell in which the sample is placed, which also incorporates the acoustic transducer, and a signal processing unit. The block diagram of the various modulus of a typical PA spectrometer is shown in Fig.(2.1). The basic instrumentation has been modified by different workers depending upon their application areas.

Details of the various modulus in a PA spectrometer are briefly outlined below.

2.1 a. Radiation source

The important parameters for the selection of a light source are the available power per usable bandwidth, the wavelength range, tunability and the ease of intensity modulation. Both coherent and incoherent sources are widely used. Arc lamps and lasers are the two popular types of light sources currently in use for PA experiments. Continuous tunability from infrared to ultraviolet can be provided by the lamp-monochromator combination. High pressure Xe arc lamps, high pressure Hg lamps, tungsten lamps, etc. are the commonly used incandescent sources. The relatively low bandwidth - throughput product is the major drawback of these sources. For a high pressure Xe arc lamp - monochromator combination,

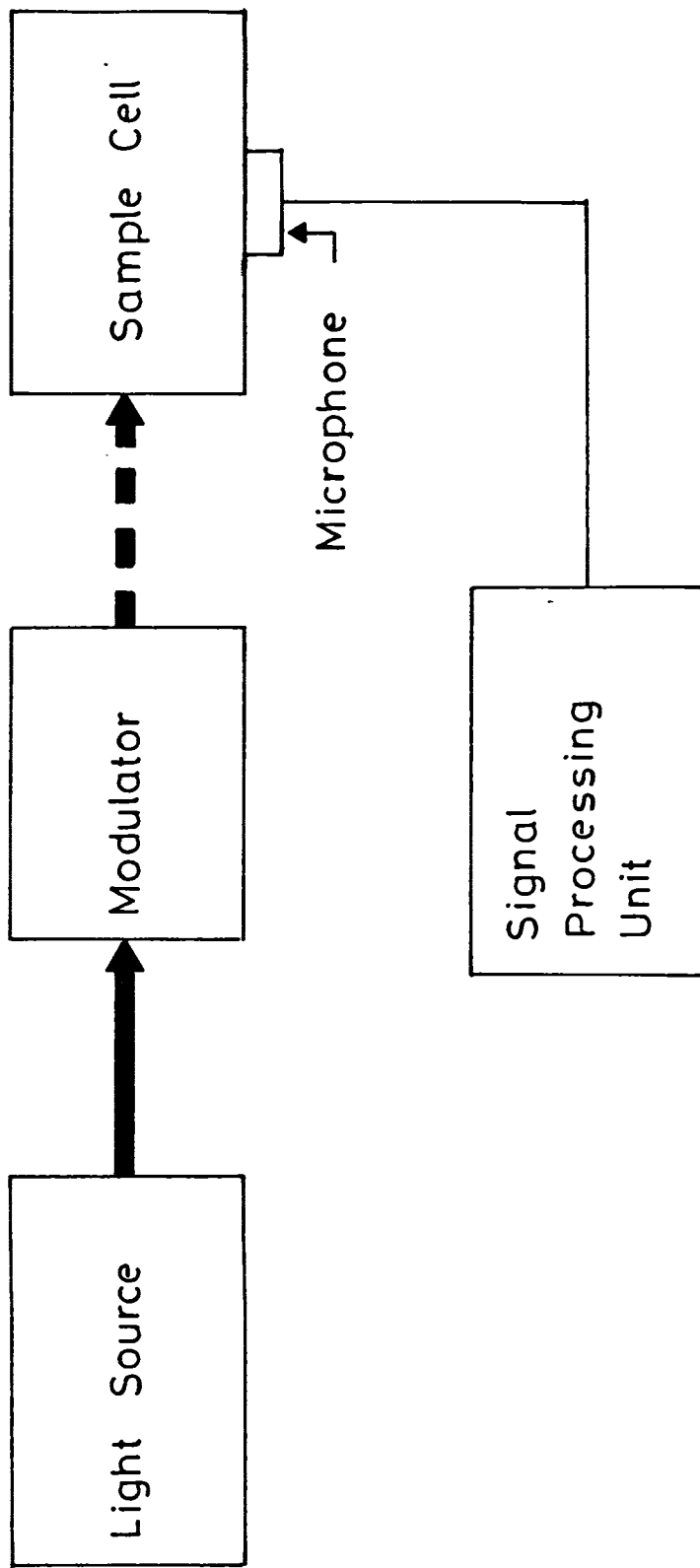


Fig. 2.1 Basic set up of a gas - microphone PA spectrometer.

an output power of 0.1 mW is typical for 1 nm resolution. Consequently it can be used with strongly absorbing samples or where low resolution suffices. The strength of the PA signal is found to be proportional to the intensity of radiation. Hence optical sources should have high spectral radiance. The wide acceptance of lasers in PA spectroscopy as radiation source is due to their highly collimated beam of high spectral brilliance. The high peak power available from pulsed lasers is especially attractive for measuring very weak absorption. The limited tunability is the main drawback of lasers.

2.1 b. Modulation

For the generation of PA signal, modulation of the incident light beam is essential. Either amplitude or frequency of the incident beam can be modulated. Amplitude modulation is the most commonly used one, which can be achieved by one of the several methods such as mechanical, electrical, electro-optic etc. The depth of modulation using a mechanical chopper is nearly 100% and is an efficient, inexpensive and hence the most commonly used method. In this type of modulation, care should be taken to minimize the vibration noise which may interfere with the PA signal and cannot be filtered away even by lock-in-detection. Electrical modulation can be achieved by varying the discharge current from the output of electric discharge lasers such as CO₂, CO etc. The application of a modulated electric field across a crystal changes the plane of polarization of the incoming polarized light beam in a nonlinear crystal giving rise to electro-optic modulation. Frequency modulation can be employed to eliminate the PA signals generated due to wavelength independent absorption at the cell windows. This type of modulation is well achieved in dye lasers using an electro-optic tuner and it is well suited for narrow line width absorbers such as atomic and diatomic species.

2.1 c. PA Cell

The heart of the PA spectrometer is the PA cell in which the sample is mounted and the region where the PA signal is generated. In order to generate PA signal of detectable

amplitude the cell should be properly designed. The major criteria that one should consider while designing a PA cell are the following:

- (i) The acoustic isolation of the cell from the ambient should be good. The cell should be designed with good acoustic seals and with walls of sufficient thickness to form good acoustic barriers. For this the thermal mass of the cell walls should be large. Precautions should be taken to isolate the whole PA cell from building vibrations.
- (ii) The interior of the cell should be made highly reflective and windows should be made transparent in the wavelength range of interest if the PA signal that arises from the walls and windows of the cell is to be minimised. If the thermal mass of the walls are very large, the resulting PA signal that arises due to absorption of the incident and scattered light will be quite weak. The interior surfaces of the cell should also be free from any kind of contamination.
- (iii) The PA signal from the solid sample is found to vary inversely with the volume of the gas inside the cell [1]. Attempts are to be made to minimise this volume, though not to a point that the signal suffers appreciable dissipation before reaching the microphone. The length ' l ' of the gas column between the sample and the window should be greater than the thermal diffusion length μ' of the gas at the lowest chopping frequency of interest. PA signal is generated as a result of this layer of gas of thickness μ' at the sample boundary acting as an acoustic piston on the rest of the air column [1]. Tam [2] has suggested the optimum gas column length to be $l' \approx 1.8 \mu'$. One should also take into account thermoviscous damping while determining the dimensions of the signal path since this could be a source of signal dissipation at the cell boundaries. Thermoviscous damping results in an $e^{-\varepsilon x}$ damping where ε is the damping coefficient given by [3].

$$\varepsilon = [1 / d\nu][\eta_e \omega / 2\rho_0]^{1/2} \quad (2.1)$$

where d is the closest distance between the cell boundaries in the path, v is the sound velocity, ω is the frequency, ρ_o is the density of the gas and η_e is the effective viscosity which depends both on the ordinary viscosity and the thermal conductivity of the gas. At low frequencies the thermal diffusion length which varies as $\omega^{-1/2}$ is predominant. Thus a cell designed to be used over a wide range of frequencies should have a minimum distance between the sample and window and minimum dimensions for signal path, which is of the order of 1-2 mm [4]. The operational principles underlying the different types of PA cell including resonant and non-resonant ones are given by Rosengreen [5] and Dewey [6]. Cylindrical cell design, which is the most common one, is one in which the light beam is centered along the axis. Resonance enhancement of the PA signal is a useful technique to increase the sensitivity of PA detection. Longitudinal, azimuthal and radial resonant modes are the different types of acoustic resonances. PA cells with very high quality factor have been constructed [7,8] of which the Helmholtz resonator type configuration is of particular interest [9,10,11]. Here the sample and microphone chambers, having volumes V_1 and V_2 , are connected by a narrow coupling tube of length L and cross sectional area σ , and the resonance frequency is given by [12]

$$2\pi f = v \left[\frac{(1/V_1 + 1/V_2)\sigma}{L + 1/2(\pi\sigma)^{1/2}} \right]^{1/2} \quad (2.2)$$

where v is the speed of sound. Spurious acoustic signals due to absorption at microphone surface as a result of light scattered from the sample, holder and window onto the microphone can be reduced by means of this configuration. Another advantage of this configuration is that it can be used to perform temperature dependent PA studies with the microphone kept at room temperatures and the sample chamber kept at high or low temperature if sufficiently long coupling tubes are used [13,14]. Geometries other than cylindrical symmetry have also been used in PA cell design [15]. Brewster windows for minimum light scattering, acoustic

baffler for reduced effects due to window absorption etc. can be incorporated for improved performance. The effects due to window heating can be eliminated using a differential cell design [16].

2.1 c. Acoustic detectors

PA cell also incorporates the acoustic transducer which usually is a microphone. Both conventional condenser microphone with external biasing and electret microphones with internal self biasing provided by charged electret foil are good ones in use to detect photoacoustic signals. A condenser microphone produces an electrical signal when a pressure wave impinges on a diaphragm. Such microphones generally have flat frequency response upto ≈ 15 KHz, low distortion and are not sensitive to mechanical vibrations [17]. Electret microphones [17] constructed from solid materials of high dielectric constant which are electrically polarised can also be used. Due to large capacitance per area possible they can be made into miniaturised microphones. Piezoelectric devices can also be used to sense the elastic waves generated in radiation absorbing solids [18,19,20,21]. These devices offer better acoustic impedance matching to solid samples and can detect high frequency signals.

2.1 d. Signal processing

The PA signal is often several orders of magnitude lower than the ambient noise and so special care is to be taken while processing the microphone output signal. The fact that the PA signal has the same frequency as that of modulation enables one to take advantage of the lock-in detection technique [21]. High signal to noise ratio can be easily obtained using a lock-in-amplifier. Also by lock-in detection, the amplitude and phase of the PA signal can be measured and by using a dual phase lock-in amplifier the measurements can be made more easily when both amplitude and phase vary simultaneously.

2.2 Basic PA spectrometer for spectral studies

When the surface of a solid material is not highly reflective, PAS can provide optical absorption data about the bulk material itself. The PAS technique can thus be used to study insulator, semiconductor and even metallic systems that cannot be studied readily by conventional absorption or reflection techniques like substances that are in the form of powders or are amorphous. Several points concerning PA spectra of semiconductors can be made. First, the PAS technique gives the correct spectrum for both direct and indirect band gap semiconductors [22]. Second, the samples can consist of powders taken off the shelf without further purification or of single crystals that are ground to reduce the reflectivity and increase the surface area. Third, the sample mass need only be a few milligrams. Fourth, each spectrum is obtained in a few minutes. Thus PAS provides a convenient tool for physicists to quickly screen, characterize and correlate the optical properties of numerous semiconductors for use in many different systems. In addition, PAS can also be used at cryogenic temperatures and at higher resolutions (eg. using lasers) to study excitonic and other fine structure in crystalline, powder or amorphous semiconductors and thus enables one to investigate the effect of impurities, dopants etc. In spectroscopy applications one should normalize the PA spectrum with the power spectrum of the radiation source, as the PA signal is proportional to the intensity of the incident beam. The power spectrum of the source can be obtained either by using a conventional power meter or using another reference PA cell with a saturable absorber like carbon black as the sample. While using a reference PA cell, part of the incident modulated beam is allowed to fall onto the reference cell using a beam splitter and the signal from the sample cell is divided by that of the reference cell using a ratiometer and the spectrum is directly recorded by plotting the normalized PA signal as a function of the wavelength of incident radiation.

The block diagram of the PA setup which we have used to carry out spectral measurements is shown in Fig.(2.2). Different parts of the set up are

1. 1000W Xe arc lamp

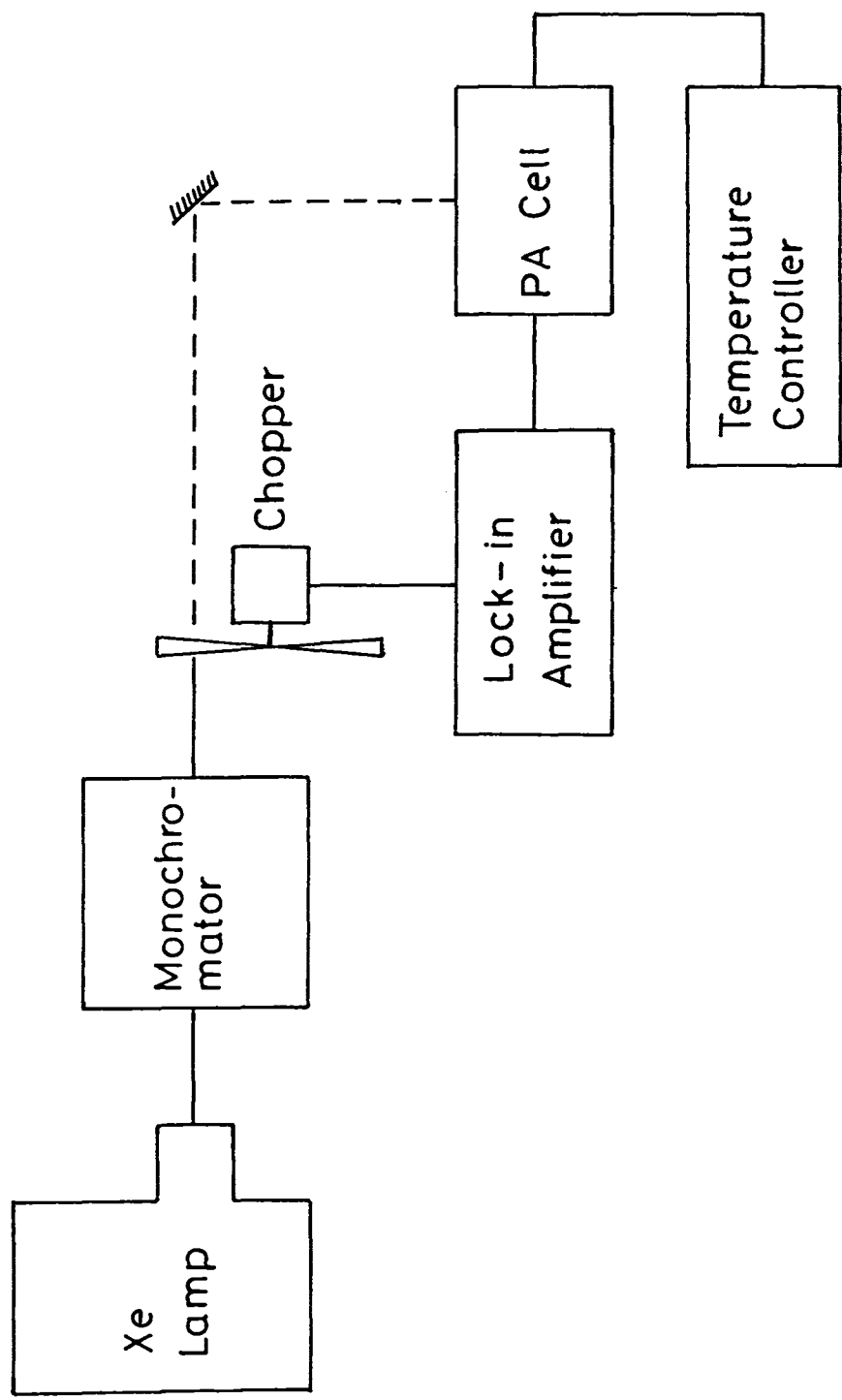


Fig. 2.2 Block diagram of the experimental set up.

2. 0.2m grating monochromator
3. electromechanical chopper
4. PA cell
5. lock-in amplifier

The light source we have used is a 1000W high pressure Xe arc lamp (M/s.Spectroscopy Instruments, Model SVX 1000). It has got continuous emission from 280 to 2500 nm. A 0.2 m grating monochromator (Mc Pherson, Model No.275) has been used to select the wavelength of the incident radiation. The output wavelength can be varied from 190 nm to 24 μm with appropriate gratings. Intensity modulation of the incident beam is accomplished by an electromechanical chopper (Photon Technology International, Model OC 4000). The chopping frequency can be varied continuously from 4 to 4000Hz with two chopper discs. The chopper also provides appropriate reference signal to the lock-in amplifier with excellent phase stability.

A single phase lock-in amplifier (Stanford Research Systems, Model SR 510) is used to process the detected PA signal. The built in preamplifier of the lock-in amplifier provides a full scale sensitivity of 10 nV maximum and has an operating frequency range from 0.5 Hz to 100 KHz. Phase can be adjusted in large steps of 90° and fine steps of 0.025° . Phase shift as well as frequency can be read on a four digit LCD display. The signal amplitude can be read either on the analogue meter or on the autoranging digital display.

The PA cell is the most important part of the PA spectrometer. We have designed and fabricated a PA cell which makes use of the front and rear surface illumination technique in determining the thermal diffusivity of solid samples at a single chopping frequency. A detailed description of this cell is given in the next chapter. The same cell under front surface illumination has been used to carry out spectral studies presented in this thesis.

A small size flat type electret microphone (Knowles, Model BT 1759) is used in the PA cell to pickup the generated acoustic signal. It has got a flat frequency response in the range 10 to 5000 Hz and a high sensitivity of 10 mV/Pascal. The microphone has a built-in FET buffer amplifier in order to provide proper impedance matching. A 3V cell to supply

bias voltage to the FET, a miniature switch and a BNC connector to take the output are all fit to the microphone housing.

2.3 Basic PA setup to study thermal diffusivity of solids

Thermal diffusivity, α , of solids is usually determined through a frequency analysis of the amplitude or phase of the PA signal generated at the front [23] or rear surface [24] of illumination and by determining the characteristic frequency. Thus measuring the amplitude of the PA signal as a function of the chopping frequency is the most widely used method of determining α .

One of the parameters which determine the amplitude of the PA signal is the thermal diffusion length μ given by

$$\mu = [\alpha / \pi f]^{1/2} \quad (2.3)$$

where f is the chopping frequency. In the thermally thick regime ($\mu < l$, where l is the thickness of the sample) the PA signal is independent of the thermal properties of the backing material on which the sample is mounted, whereas in the thermally thin regime ($\mu > l$) the PA signal gets modified by the thermal properties of the backing material as well. For an appropriate sample thickness, one can obtain a cross-over from a thermally thin regime to a thermally thick regime by increasing the chopping frequency. The amplitude versus chopping frequency plot hence shows a change in slope at the characteristic frequency f_c at which the cross-over takes place. This f_c is related to the thermal diffusivity of the sample as shown below.

According to Rosencwaig-Gersho theory, the complex expression for the pressure variation Q inside the PA cell can be expressed as

$$Q = qe^{-i\psi} \quad (2.4)$$

where q is the amplitude of the PA signal and ψ is the phase shift between Q and the excitation. Eqn. (2.4) can be written as the product of two terms A and B such that A depends on the modulation frequency f and B is independent of f as given by

$$B = \frac{P_0 \gamma W_a l^2 \sqrt{\alpha}}{2 l' T_0 K \sqrt{\alpha}} \quad (2.5)$$

and

$$A = \left[1 + g \frac{d^+ + d^-}{d^+ - d^-} \right]^{-1} \left[\frac{d^+ + d^-}{d^+ - d^-} + g \right] \frac{1}{(\sigma l)^2} \quad (2.6)$$

where

$$d^+ = e^{(\sigma l)}$$

$$d^- = e^{-(\sigma l)}$$

$$\sigma = (1 + J) \sqrt{(\pi f / \alpha)} \quad (2.7)$$

and g is the ratio of the thermal effusivities of the backing material (e'') and the sample (e), which is given by

$$g = e''/e = (K''/K)(\sqrt{\alpha} / \sqrt{\alpha''}) \quad (2.8)$$

In the above equation l , k and α are the thickness, thermal conductivity and thermal diffusivity respectively. Unprimed, singly primed and doubly primed quantities refer to sample, gas and backing material respectively. T_0 and P_0 are the static temperature and pressure, γ is the ratio of specific heats of the gas and W_a is the amount of absorbed light. The effusivity of the gas in the cell is neglected compared to the effusivity of the sample. The term A depends on the modulation frequency through the product σl which can be written as

$$\sigma l = (1 + i) \sqrt{(\pi f / f_c)} \quad (2.9)$$

where the characteristic frequency f_c is defined by

$$f_c = \alpha / l^2 \quad (2.10)$$

The dependence of A on the modulation frequency for different values of g have been demonstrated by Carpentier et. al [24]. When $f > f_c$, the variation of A is independent of α and A decreases as f^{-1} . When $f < f_c$, the variation of A depends on both α and g . Thus it is possible to determine f_c by measuring the amplitude of the PA signal as a function of f . However, if $g = 1$, the variation of the amplitude is the same for all frequencies and the determination of f_c becomes impossible. Once f_c is determined, thermal diffusivity can be obtained from eqn. 2.10 as

$$\alpha = f_c l^2 \quad (2.11)$$

Thermal diffusivity α , although a derived characteristic of a substance, is of direct importance in heat flow studies as it determines the rate of periodic or transient heat propagation through the medium. Knowledge of α can be used to calculate the thermal conductivity since it is the ratio of the thermal conductivity to the specific heat and density of the material and has dimensions $(\text{length})^2 (\text{time})^{-1}$. Although K and α are directly related, the measurement of these two parameters are made by completely different experimental techniques. K , when measured directly by a steady state method, requires the measurement of a thermal flux and temperature gradient. Thermal diffusivity on the other hand requires the measurement of the time for the thermal disturbance to propagate to a known distance. This points out the importance of thermal diffusivity measurements because lengths and time intervals can be measured more easily and accurately than heat fluxes and temperature

gradients. Moreover, thermal diffusivity measurements are insensitive to radiative heat losses from the sample. In the transient heat flow method an addition or removal of thermal energy from the sample will induce a transitory temperature change and α is determined from a measurement of the temperature as a function of time at one or more point along the sample. In periodic temperature methods the thermal energy supplied to the sample is modulated at a fixed period. Consequently the temperatures at all points in the sample vary with the same period and α is then determined from the measurement of the amplitude and phase of the thermal wave in the sample. Time resolved measurement techniques for determining α are based on the work carried out by Angstrom [25], King [26] and Abels et al [27]. In these methods the variation of sample temperature is usually sensed by thermocouples. The PA technique which belongs to the periodic heat flow method can effectively be used for studying the thermal properties of the sample which enables one to measure indirectly and with high sensitivity the surface temperature of the sample by non-contact means.

2.4 Preparation of amorphous materials

There are at least a dozen different techniques that can be used to prepare materials in the amorphous state. The different techniques use all three phases of matter - vapour, liquid or solid - as the starting material for preparing amorphous solids. Since the amorphous phase is thermodynamically less stable than the corresponding crystalline form, its preparation can be regarded as the addition of excess free energy in some manner to the crystalline polymorph, which can be done by faster rate of cooling.

One of the several ways of producing amorphous solids by deposition from a vapour is thermal evaporation. The starting compound is vapourized and the material is collected on a substrate. The principal disadvantage of thermal evaporation as a preparative technique lies in the variations in purity and composition of the resulting films (in the case of alloys). It is a thin film preparative technique. Sputtering process is rather more complicated than thermal evaporation but enjoys the advantage of being far more flexible. It consists of the

bombardment of a target by energetic ions from a low pressure plasma, causing erosion of the material, either atom by atom, or as clusters of atoms, and subsequent deposition of a film on a substrate. Most factors which cause variation in the film produced by thermal evaporation are also applicable in this case. Another technique which can produce thin films of amorphous materials is glow discharge (GD) deposition in the vapour phase. Prepared in this manner certain amorphous semiconductors can be subsequently doped to control their electronic properties as discovered by Spear and LeComber [28]. This technique like sputtering relies on the production of a plasma in a low pressure gas, but instead of ions from the sputtering material, chemical decomposition of the gas takes place, leading to deposition of a solid film on a substrate placed in the plasma. Another technique which is the chemical vapour deposition (CVD) is analogous to GD method in that both depend on the decomposition of a vapour species. The difference is that the CVD process relies on thermal energy for the decomposition.

The oldest established method of producing an amorphous solid is to cool the molten form of the material sufficiently quickly. Amorphous materials produced in this manner are often been termed as glasses. The distinguishing feature of the melt quenching process of producing amorphous materials is that the amorphous solid is formed by continuous hardening (i.e. increase in viscosity) of the melt. In contrast, crystallization of the melt occurs as a discontinuous solidification process. An essential prerequisite for glass formation from the melt is that the cooling be sufficiently fast to preclude crystal nucleation and growth. The crystalline phase is thermodynamically more stable and crystal growth will always dominate over the formation of amorphous phase if allowed to take place. Cooling rate is often a critical factor in determining glass formation. Certain "easy glass-formers", such as B_2O_3 will form an amorphous solid even under conditions of very slow cooling (say 1 Ksec^{-1}) whereas other materials, notably mettalic glasses, require very high rates of cooling indeed before they form an amorphous phase; otherwise polycrystalline materials are produced. The most usual way of producing samples of easy glass formers is to seal a charge (1 to 10 gms) in a fused silica ampoule under a good vacuum ($\sim 10^{-6}$ Torr) and keep the ampoule in a

rocking or rotating furnace at sufficiently elevated temperature that the constituents become molten and can react. The rocking motion ensures that a through mixing of the mixture takes place. The melt can be quenched either slowly or simply switching off the oven, or more rapidly by bringing the ampoules into the air, or yet more rapidly by plunging the ampoule immediately from the oven into a liquid, preferably one with a high thermal conductivity and high latent heat of vapourization so that heat is conducted away from the sample as fast as possible without the formation of a thermally insulating vapour layer around the ampoule. In this manner cooling rates of the order of 10^2 to 10^3 Ksec⁻¹ are achievable. Some parameters which are important in the ampoule method of melt quenching are the following

1. Temperature of the oven
2. Rate of cooling
3. Volume of charge in the ampoule
4. Thickness of the wall of the ampoule

Materials produced in this manner is often in the form of a plug or rod. For certain materials, however, notably metals, even the fastest cooling rates achieved by the above methods are insufficient to prevent crystallization and still faster cooling rates, in excess of $\sim 10^6$ K sec⁻¹, are required. The melt spinning and melt extraction techniques which make use of a rapidly spinning copper disc as a chill-block produce thin ribbons or wires. In contrast to other melt quenching methods, this cannot produce material in the bulk form, but only in the form of ribbons. If attempts are made to produce ribbons of thickness greater than a few tens of microns, only polycrystalline material is produced, since beyond a critical thickness conduction of heat through the ribbon becomes a critical factor.

Faster rates of cooling are achievable by "laser glazing" and it begins with the material in the crystalline form. Cooling rates of 10^{10} to 10^{12} K sec⁻¹ are achieved by this method. A very short and very intense single laser pulse is focused onto a very small spot on the crystal surface with the laser wavelength selected so that high energy is absorbed in an extremely thin (~ 100 Å) layer of the solid, which melts it but is swiftly quenched and

resolidified by the surrounding crystal. The small, very thin layer is found to be amorphous (eg. Si).

In this work we have prepared chalcogenide glass samples by the melt quenching technique. Samples in quartz ampoules are kept at high temperatures at high temperatures in a rotating furnace and are quenched in ice water. The method employed for preparing each sample is described in the corresponding chapters.

2.5 A temperature controller for high temperature applications

In order to control the furnace temperature while preparing the samples and to maintain a high temperature constant over long periods and wide variations in ambient temperature we have designed a general purpose temperature controller capable of maintaining the temperature constant to within $\pm 0.5^\circ\text{C}$ over the range 50-1200°C. It has a stable and sensitive thermocouple amplifier with an active cold junction compensation and low noise pick-up. The input configuration permits easy reading of the set temperature and the actual temperature by a digital panel meter. A proportional plus integral mode of control is adopted to prevent any oscillations in temperature when the set value is attained. The controller gives a pulse width modulated control signal which is used to drive a solid state relay. A block diagram of the temperature controller is given in Fig.(2.3).

The schematic diagram of the controller is given in Fig.(2.4). The thermocouple amplifier is built around op-amp. A_1 whose gain is set at 260 which gives a $10.5 \text{ mV}^\circ\text{C}^{-1}$ output signal with a chromel-alumel thermocouple. The transistor T_1 which is in thermal contact with the thermocouple cold junction provides the required cold junction compensation. The potential divider formed by R_2 and R_3 makes the temperature coefficient of V_{BE} of T_1 match the thermocouple sensitivity and is applied to the inverting input of A_1 . This compensation scheme will not work for temperatures below the ambient temperature. The potentiometer R_1 is adjusted to take the output to the required voltage for a known temperature. The input offset voltage of A_1 should be initially adjusted to zero using R_4 since this is necessary for the amplifier to operate with minimum drift. External frequency

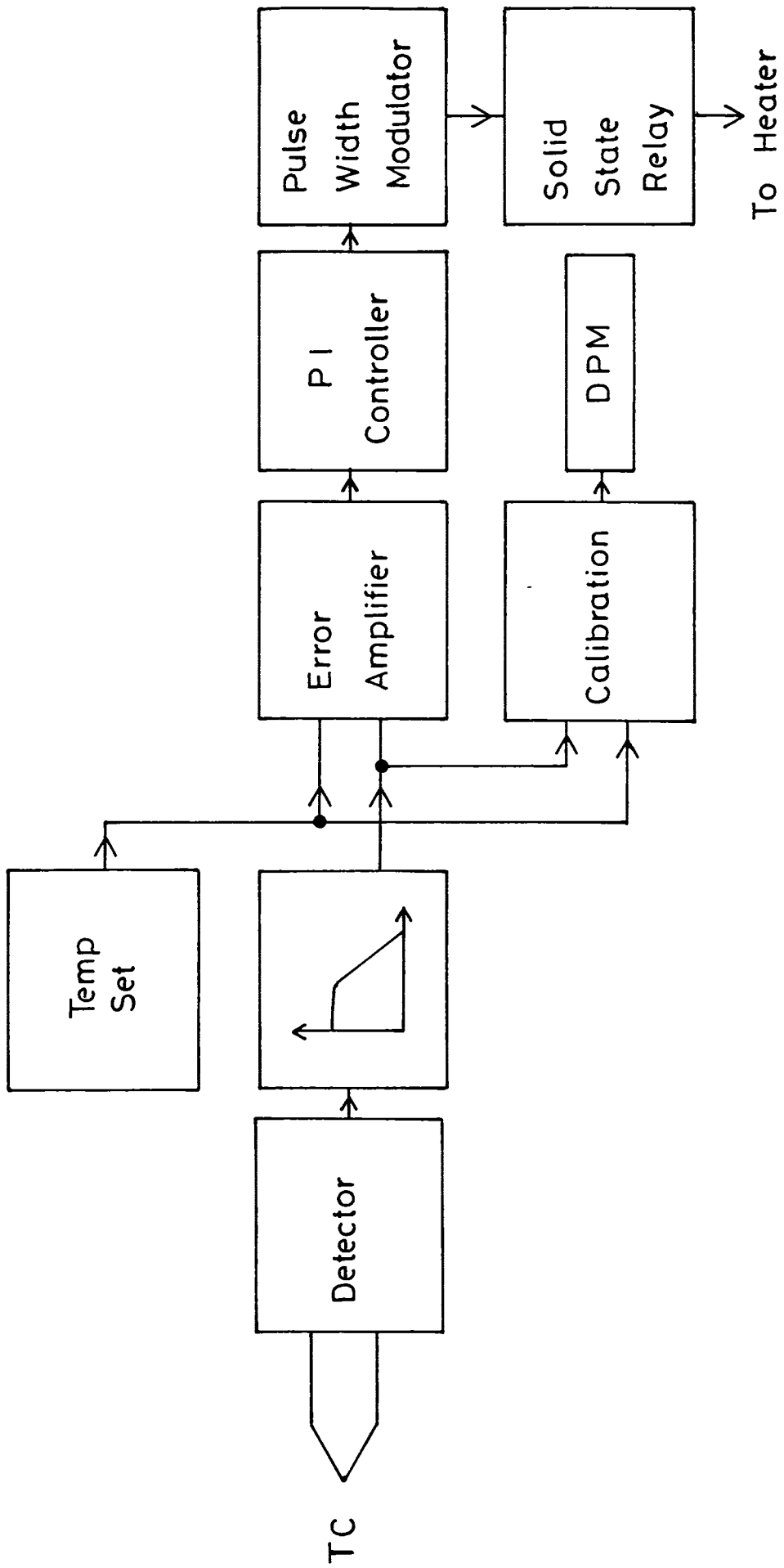


Fig. 2.3 Block diagram of the temperature controller.

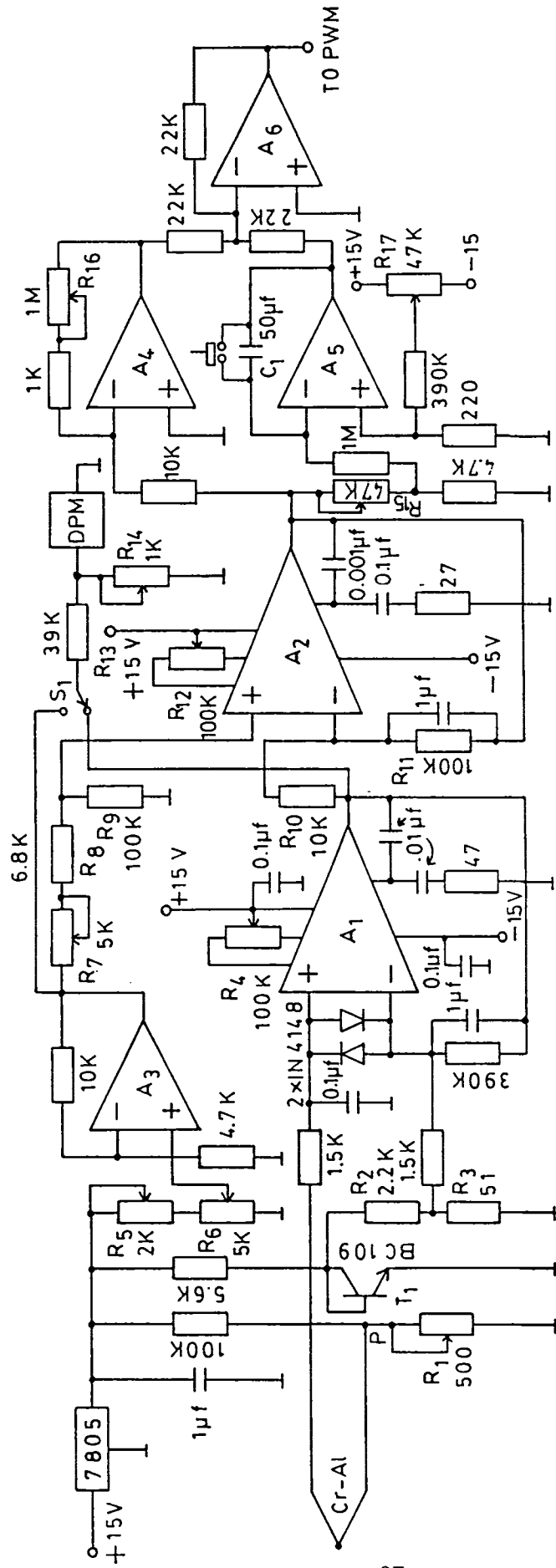


Fig. 2.4 Schematic diagram of the controller. A₁-A₂ LM 725, A₃, A₆ μ A 741, A₄-A₅ LF 353 JFET input dual op. - amp. All resistors are metal film resistors with 1% tolerance.

compensation is provided at pin 5 of A_1 and the component values are found to give an optimum performance for this circuit configuration and gain. The $1\ \mu\text{F}$ capacitor connected across the feedback resistor limits the bandwidth of the amplifier to 0.4 Hz, thereby avoiding the need for additional low pass filtering to minimize the noise.

The output of the thermocouple amplifier is fed to a differential amplifier formed by op.amp. A_2 and its associated components. The other input to the differential amplifier is derived from A_3 which is the set temperature amplifier. By using a 10-turn potentiometer R_6 the output of A_3 can be varied from 0 to 12.6V which is the output voltage of A_1 at 1200°C . This upper limit can be fixed by adjusting R_5 . The common mode rejection ratio of the differential amplifier can be adjusted to a maximum by trimming R_4 so that $(R_{11}/R_{10}) = R_9/(R_7 + R_8)$. The offset voltage of A_2 can be adjusted using R_{12} . The outputs of A_3 and A_1 , selected through the switch S_1 , are used to read the set temperature and actual temperature respectively, using a $3^{1/2}$ -digit panel meter (DPM). The present values of the voltage divider resistors, R_{13} and R_{14} are chosen for a full-scale sensitivity of 200 mV in the DPM. R_{14} may be adjusted to read the temperature in $^\circ\text{C}$.

The error signal derived from the differential amplifier is fed to the input of a proportional plus integral control amplifier composed of op.amps A_4 , A_5 and A_6 . Amplifier A_4 constitute the proportional path whose gain determines the amount of corrective action to be applied for a given temperature change. Its gain is varied by R_{16} from -20dB to +40 dB. A_5 and the associated components form the integrater which is included in the control network to overcome the offset problem inherent in proportional control. It allows the controller to stabilize the desired temperature with no error signal from the error amplifier. A detailed description of the working of the proportional plus integral controller has been given by Forgan [29] and Grubic et al [30]. Unlike the scheme described by Handchy [31], here the proportional and integral paths are fed independently from the error amplifier. This gives greater flexibility of the control parameter setting which is desirable for a controller designed for a wide temperature range. The integration time can be varied by the potentiometer R_{15} from 50s to 500s. The integrating capacitor C_1 should be of non-polar type and the parallel

insulation resistance should be very high. The offset null potentiometer R_{17} should be adjusted so that the output of the integrator is steady with time when its input is zero. The control signal is obtained from the output of the summing amplifier A_6 .

The output power to the heater is varied using a Solid State Relay (SSR) by varying the on-off time in accordance with the control signal obtained from A_6 . This is achieved by pulse-width modulating the control signal. Fig.(2.5) shows the schematic diagram of the pulse width modulator used in the present controller. The standard practice of comparing the signal to be modulated with a triangular wave of suitable amplitude and frequency is followed here. A_7 and A_8 constitute a symmetrical triangular wave generator, A_9 is a level shifter and A_{10} acts as a comparator. The peak to peak amplitude of the triangular wave is made equal to the maximum value of the control signal by adjusting R_{19} and is level shifted in the positive direction to make its minimum coincide with zero by adjusting R_{20} . The frequency of the triangular wave is given by $f = V_{sat} / 2AR_{18}C_2$ where V_{sat} is the output saturation voltage of A_7 and A is the peak-to-peak amplitude of the triangular wave. The present values give a frequency of 0.5Hz. The pulse width modulated control signal obtained from A_{10} is fed to a solid state relay through an opto-isolator driven by transistor T_2 . A SSR with zero crossover switching is used, the schematic diagram of which is given in Fig.(2.6). The transistors TR_4 and TR_5 act as zero crossover detectors, giving short positive going pulses at the zero crossing points of the a.c. voltage. This method prevents the large inrush of current which occurs when a rather high voltage is suddenly applied to a very low resistance load thus preventing thermal shock to the load. It also eliminates electromagnetic interference which results when there is a sudden inrush of current.

To obtain a highly regulated +15V and -15V power supply, a circuit is designed and fabricated as shown in Fig.(2.7). The circuit is a conventional one with bridge rectifiers and two separate filter capacitors. The performance of the controller has been tested on a vertical tubular furnace for the entire range of temperatures and for long times by monitoring the error signal at the output of A_2 . The temperature is found to be stable at the set value with random fluctuations of about 0.5°C. These fluctuations are due to convectional air currents in the

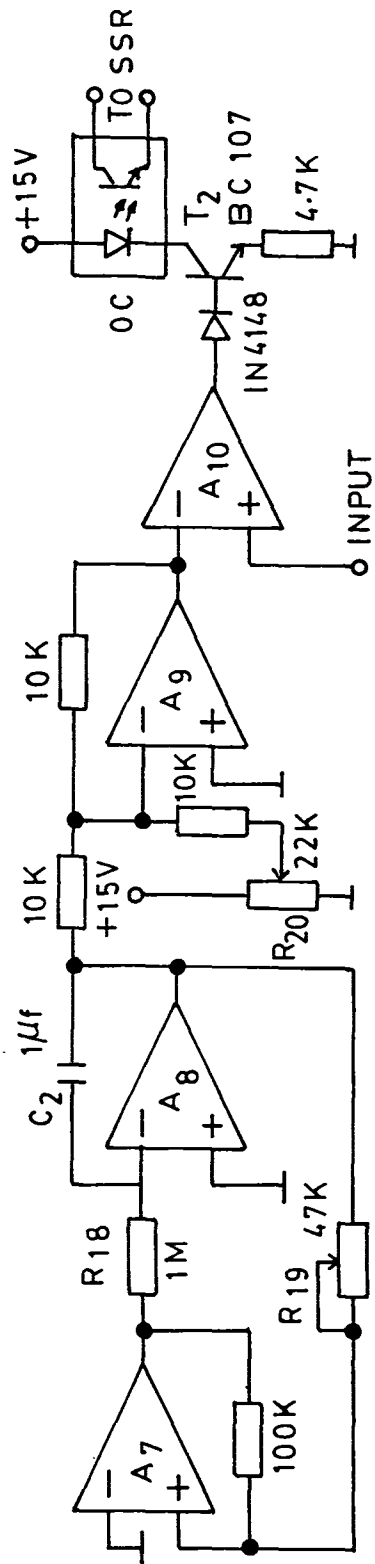


Fig. 2.5 Schematic diagram of pulse width modulator. A₇ - A₁₀ LM 324 quad. op. amp., OC -optocoupler.

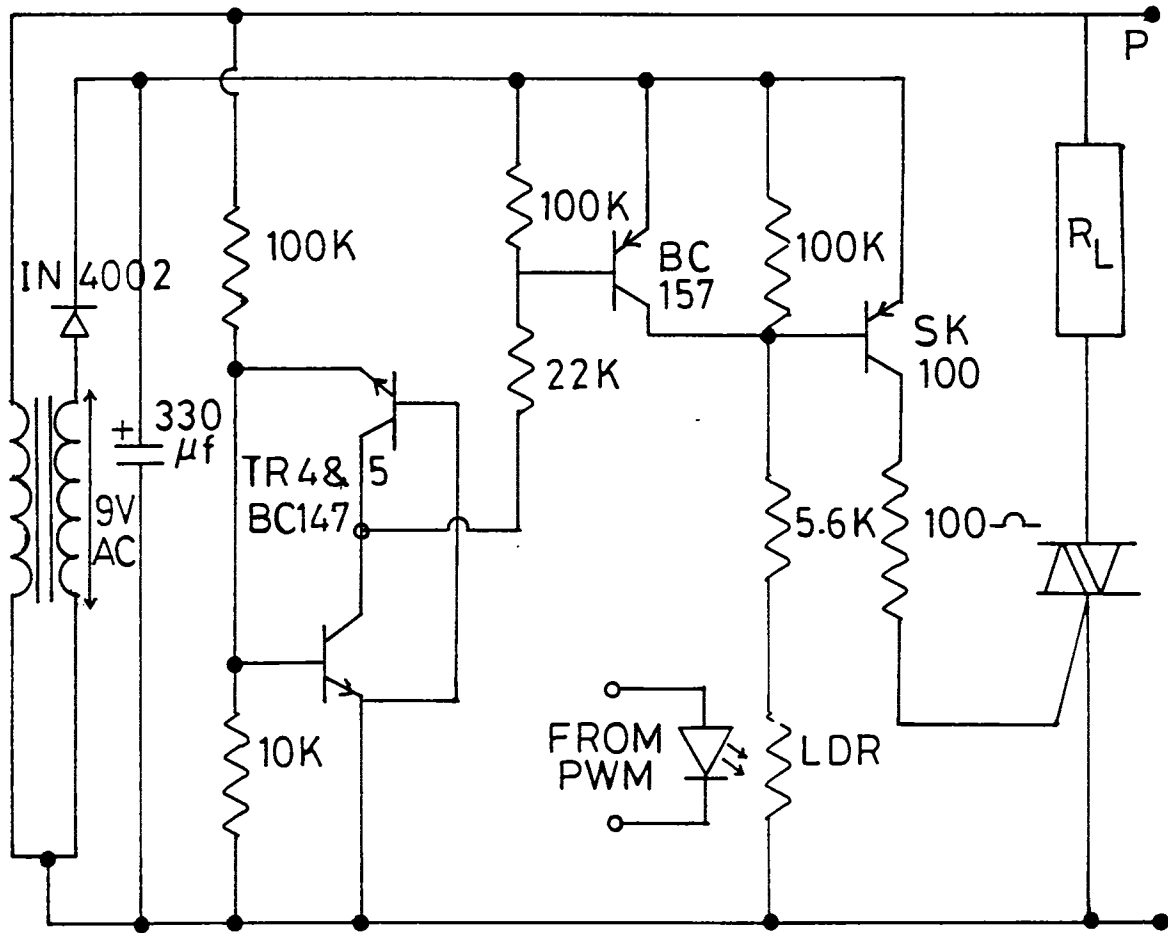


Fig. 2.6 Schematic diagram of solid state relay.

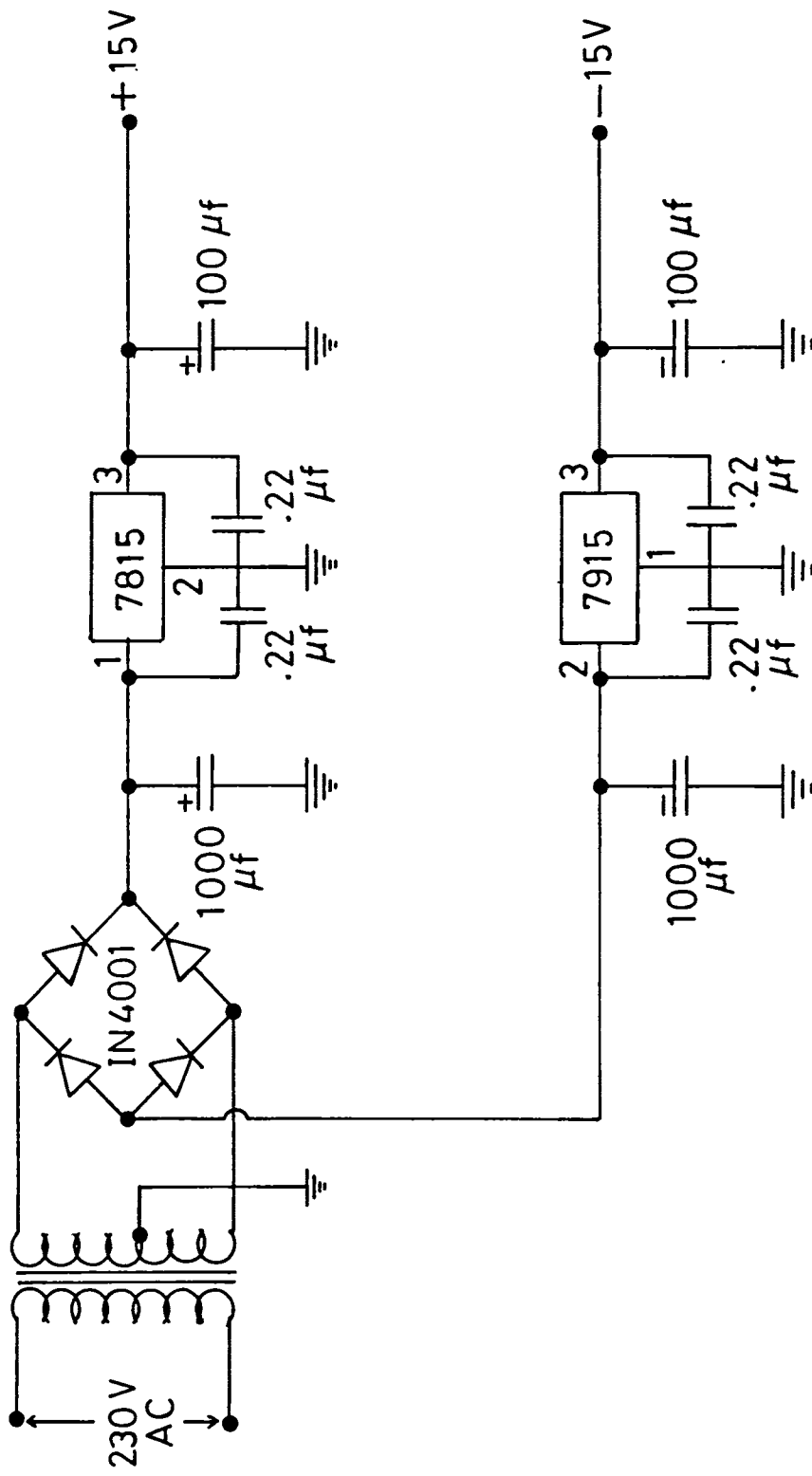


Fig. 2.7 Schematic diagram of the power supply.

long tube and are expected to be much lower for a well isolated thermostat. The major factors that affect the temperature stability of the present controller are drift in the input offset voltage of A_1 and the cold junction compensation mismatch. The former can cause a total temperature error of 0.3°C for an ambient temperature variation of 20°C . The thermocouple amplifier has been tested independently for different ambient temperatures and the error is found to be well within the specified range. The cold junction compensation mismatch can be reduced to a sufficiently low level by trimming R_3 so that $\tau_{V_{BE}} R_3/(R_2+R_3)$, where $\tau_{V_{BE}}$ is the temperature coefficient of V_{BE} of T_1 , exactly matches the thermocouple sensitivity. The whole circuit has been assembled on a single printed circuit board. It is necessary to shield T_1 and the thermocouple cold junctions to protect them from air currents. The electrical noise pick up by the thermocouple is found to be practically absent when the whole circuit is grounded at point P in Fig.(2.4).

The above temperature controller has been used to control furnace temperatures during the sample preparations done in this work.

REFERENCES

1. A.Rosencwaig and A.Gersho, *J. Appl. Phy.* **47**, 64 (1976).
2. A.C.Tam, *Ultrasensitive Laser Spectroscopy* (D.Klinger Ed.), Academic Press, New York (1983).
3. L.E.Kinsler and A.R.Frey, *Fundamentals of Acoustics*, Chap.9, Wiley, New York (1962).
4. A.Rosencwaig, *Rev. Sci. Instrum.* **48**, 1133 (1977).
5. L.G.Rosengreen, *Appl. Opt.* **14**, 1960 (1975).
6. C.F.Dewey, *Optoacoustic Spectroscopy and Detection* (Y.H.Pao, Ed.) Academic Press, New York (1977).
7. L.D.Thomas, M.J.Kelley and N.M.Amer, *Appl. Phys. Lett.* **32**, 736 (1978).
8. E.Nodov, *Appl. Opt.* **17**, 1110 (1978).
9. N.C.Femelius and T.W.Hass, *Appl. Opt.* **17**, 3348 (1978).

10. N.C.Fernelius and T.W.Hass, *Appl. Opt.* **18**, 1784 (1979).
11. R.S.Quimby, P.M.Selzer and W.M.Yen, *Appl. Opt.* **16**, 2630 (1977).
12. Lord Rayleigh, *Theory of Sound*, Vol. **2**, Dover, New York (1948), p.189.
13. J.C.Murphy and L.C.Aamodt, *J. Appl. Phys.* **48**, 3502 (1977).
14. P.A.Bechthold, M.Campagna and J.Chatzipetros, *Opt. Commun.* **36**, 369 (1981).
15. N.Ioli, P.Vidino and M.Meucci, *J. Phys. E.* **12**, 168 (1979).
16. T.F.Deaton, D.A.Dapatee and T.W.Walker, *Appl. Phys. Lett.* **26**, 300 (1975).
17. G.M.Sessler and J.E.West, *J. Acoust. Soc. Amer.* **53**, 1589 (1973).
18. A.Hordvik and H.Scholossberg, *Appl. Opt.* **16**, 101 (1977).
19. C.K.N.Patel and A.C.Tam, *Appl. Phys. Lett.* **34**, 467 (1979).
20. C.L.Sam and M.L.Shand, *Opt. Commun.* **31**, 174 (1979).
21. M.L.Meade, in *Lock-in amplifiers; Principles and Applications* (Peter Peregrinuss Ltd. London) (1983).
22. R.B.Somoano, C.Angew. *Chem. Int. Ed. (Engl.)* **17**, 234 (1978).
23. A.Lachaine and P.Poulet, *Appl. Phys. Lett.* **45**, 953 (1984).
24. P.Charpentier, F.Lepoutre and L.Bertrand, *J. Appl. Phys.* **53**, 608 (1982).
25. A.J.Angstrom, *Phil. Mag.* **26**, 161 (1963).
26. R.W.King, *Phys. Rev.* **6**, 437 (1975).
27. B.Abeles, G.D.Cody and D.S.J. Beers, *J. Appl. Phys.* **31**, 1585 (1960).
28. W.E.Spear and Le Comber, P.G., *Solid State Commun.* **17**, 1193 (1975).
29. E.M.Forgan, *Cryogenics* **14**, 207 (1974).
30. M.Grubic and U.Wurz, *J. Phys. E* **11**, 692 (1978).
31. M.A.Handchy, *J. Phys. E.* **13**, 998 (1980).

CHAPTER III

PHOTOACOUSTIC PHASE LAG TECHNIQUE TO DETERMINE THERMAL DIFFUSIVITY OF SOLIDS

3.1 Introduction

In order to determine the thermal diffusivity of solids by means of photoacoustic effect various methods have been put forward by several workers [1-3]. Usually, thermal diffusivity α is measured by a frequency analysis of the amplitude or the phase of the PA signal generated at the front or rear surface of illumination. Adams and Kirkbright [1] calculated α for various samples by plotting the phase $-\psi$ of the PA signal obtained by rear surface illumination versus $\sqrt{\omega}$, where ω is the chopping angular frequency. Their assumption that $\psi = l_s a_s$, where $a_s = (\omega / 2\alpha)^{1/2}$ and l_s is the sample thickness is an approximation for thermally thick case ($l_s a_s \gg 1$). Charpentier et al [2] have described an equivalent procedure which measures the attenuation of the magnitude of thermal oscillation as a function of $\sqrt{\omega}$ again for rear surface illumination. The frequency ω for which the slope of the attenuation curve diverges from the value of -3 is typical of thermally thick samples, and indicates an $l_s a_s = 1$ point, at which extraction of α can be made. Another alternative is to vary the distance x_0 between the point where the heat is generated and one point at which the thermal oscillation is detected. Cesar et al [3] adapted this method to photoacoustics by varying the position of a laterally incident laser beam on a transparent sample. The plot of both the PA phase and magnitude versus x_0 provided α by a data fit to expressions with a linear and exponential dependence on $-a_s x_0$ respectively. For samples not necessarily thermally thick, but having a large optical absorption coefficient β , an attractive and simple method has been introduced by Yasa and Amer [4]. They have measured the attenuation of the rear surface illumination signal (S_R) relative to the front surface illumination signal (S_F). Using appropriate formulas they were able to obtain α from the ratio

$$S_F/S_R = [I_F/I_R] [\cosh^2 (l_s a_s) - \sin^2 (l_s a_s)]^{1/2} \quad (3.1)$$

The advantage of this two beam technique is that, it is valid for both thermally thin and thick samples and measurements can be carried out at a single chopping frequency. However, the magnitude ratio of the signals do depend upon the front and rear surface conditions of the sample. This difficulty has been overcome by measuring the relative phase lag $\Delta\psi = (\psi_F - \psi_R)$ instead of (S_F/S_R) as proposed by Pessoa Jr. et al [5]. In this two beam setup, the beams to be incident at the front and rear surfaces of the sample are derived from a single chopped laser beam using a beam splitter. It is difficult to arrange the setup with an incoherent source due to involved complexities in optics. We have overcome this difficulty with a single beam PA technique in which the front and rear surface signals are measured one after the other by rotating the PA cell through 180° about a vertical axis [6]. The principle of this method, experimental realisation of the technique, required cell design, its calibration and all other details of this technique are given in the following sections.

3.2 Principle of the method

The principle underlying PA phase lag method can be derived from the one dimensional theory of Rosencwaig and Gersho which shows that the pressure variation δP_1 at the front surface of an optically thick sample depends on the thermal diffusivity α of the sample. The theoretical expression of δP_1 may be written as the product of two terms; A_1 depending on the modulating frequency f of the excitation while the other term B is independent of f , as explained in the previous chapter. Thus,

$$\delta P_1 = B A_1 \quad (3.2)$$

where

$$A_1 = \left[1 + g \frac{d^+ + d^-}{d^+ - d^-} \right]^{-1} \left[\frac{d^+ + d^-}{d^+ - d^-} + g \right] \frac{1}{(\sigma_s l_s)^2} \quad (3.3)$$

and

$$d^+ = \exp(\sigma_s l_s)$$

$$d^- = \exp - (\sigma_s l_s)$$

$$\sigma_s = (1 + i) a_s$$

$$a_s = \sqrt{\pi f / \alpha} \quad (3.4)$$

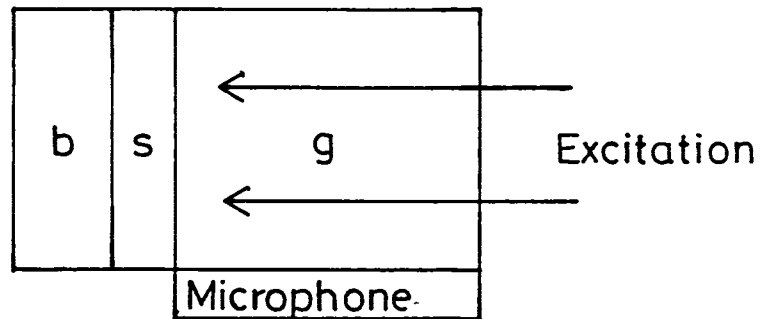
and $g = e_b / e_s$ is the ratio of thermal effusivities of the backing (e_b) and sample (e_s), ($e = (K\rho C)^{1/2}$ where K , ρ and C are thermal conductivity, density and specific heat at constant pressure respectively). The expression for the dynamic pressure at the rear surface can be written in a similar manner as

$$\delta P_2 = BA_2 \quad (3.5)$$

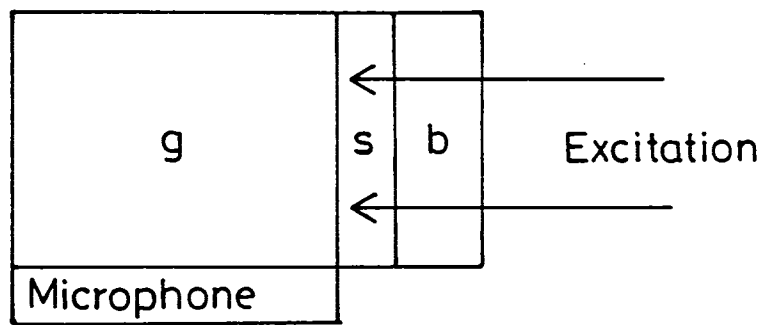
where

$$A_2 = \frac{2}{d^+ + d^-} \left[1 + g \frac{d^+ + d^-}{d^+ - d^-} \right]^{-1} \frac{1}{(\sigma_s l_s)^2} \quad (3.6)$$

The principle and scheme of the front and rear surface excitation is illustrated in Fig.(3.1). For solid samples with air as the backing medium, g can be neglected. Hence the corresponding phase of the signals relative to that of the excitation can be obtained from the above expression as follows.



Front surface illumination



Rear surface illumination

Fig. 3.1 Principle and scheme of the front and rear surface excitation. **b** - backing, **s** -sample, **g** - gas meduim.

For front surface illumination

$$A_1 = \left[\frac{d^+ + d^-}{d^+ - d^-} \right] \frac{1}{(\sigma_s l_s)^2} \quad (3.7)$$

$$= \left[\frac{\exp[(1+i)a_s l_s] + \exp -[(1+i)a_s l_s]}{\exp[(1+i)a_s l_s] - \exp -[(1+i)a_s l_s]} \right] \frac{1}{(1+i)^2 a_s^2 l_s^2} \quad (3.8)$$

$$= \frac{1}{2ia_s^2 l_s^2} \left[\frac{\exp[a_s l_s][\cos(a_s l_s) + i\sin(a_s l_s)] + \exp -[a_s l_s][\cos(a_s l_s) - i\sin(a_s l_s)]}{\exp[a_s l_s][\cos(a_s l_s) + i\sin(a_s l_s)] - \exp -[a_s l_s][\cos(a_s l_s) - i\sin(a_s l_s)]} \right] \quad (3.9)$$

$$= \frac{1}{2ia_s^2 l_s^2} \left[\frac{\cos(a_s l_s)2\cosh(a_s l_s) + i\sin(a_s l_s)2\sinh(a_s l_s)}{\cos(a_s l_s)2\sinh(a_s l_s) - i\sin(a_s l_s)2\cosh(a_s l_s)} \right] \quad (3.10)$$

$$= \frac{-1}{2a_s^2 l_s^2} \left[\frac{\cos(a_s l_s)\sin(a_s l_s) + i\cosh(a_s l_s)\sinh(a_s l_s)}{\cos^2(a_s l_s)\sinh^2(a_s l_s) - \sin^2(a_s l_s)\cosh^2(a_s l_s)} \right] \quad (3.11)$$

Hence the phase of the front surface signal can be obtained as

$$\tan \psi_F = \frac{\cosh(a_s l_s) \sinh(a_s l_s)}{\cos(a_s l_s) \sin(a_s l_s)} \quad (3.12)$$

Similarly for rear surface illumination

$$A_2 = \left[\frac{2}{d^+ - d^-} \right] \frac{1}{(\sigma_s l_s)^2} \quad (3.13)$$

$$= \left[\frac{2}{\exp[(1+i)a_s l_s] - \exp -[(1+i)a_s l_s]} \right] \frac{1}{(1+i)^2 a_s^2 l_s^2} \quad (3.14)$$

$$= \frac{1}{i a_s^2 l_s^2} \left[\frac{1}{\exp[a_s l_s][\cos(a_s l_s) + i \sin(a_s l_s)] - \exp -[a_s l_s][\cos(a_s l_s) - i \sin(a_s l_s)]} \right] \quad (3.15)$$

$$= \frac{1}{i a_s^2 l_s^2} \left[\frac{1}{\cos(a_s l_s) 2 \sinh(a_s l_s) + i \sin(a_s l_s) 2 \cosh(a_s l_s)} \right] \quad (3.16)$$

$$= \frac{1}{2 a_s^2 l_s^2} \left[\frac{\cosh(a_s l_s) \sin(a_s l_s) + i \sinh(a_s l_s) \cos(a_s l_s)}{-\sin^2(a_s l_s) \cosh^2(a_s l_s) - \sinh^2(a_s l_s) \cos^2(a_s l_s)} \right] \quad (3.17)$$

The rear surface phase can be obtained from the above expression as

$$\tan(\psi_R) = \frac{\cos(a_s l_s) \sinh(a_s l_s)}{\cosh(a_s l_s) \sin(a_s l_s)} \quad (3.18)$$

From equations (3.12) and (3.18) we get

$$\tan(\psi_F - \psi_R) = \frac{\tan(\psi_F) - \tan(\psi_R)}{1 + \tan(\psi_F) \tan(\psi_R)} \quad (3.19)$$

$$= \frac{\left[\frac{\cosh(a_s l_s) \sinh(a_s l_s)}{\cos(a_s l_s) \sin(a_s l_s)} \right] - \left[\frac{\cos(a_s l_s) \sinh(a_s l_s)}{\cosh(a_s l_s) \sin(a_s l_s)} \right]}{1 + \left[\frac{\cosh(a_s l_s) \sinh(a_s l_s)}{\cos(a_s l_s) \sin(a_s l_s)} \right] \left[\frac{\cos(a_s l_s) \sinh(a_s l_s)}{\cosh(a_s l_s) \sin(a_s l_s)} \right]} \quad (3.20)$$

$$= \frac{\sinh(a_s l_s) \sin(a_s l_s)}{\cosh(a_s l_s) \cos(a_s l_s)} \left[\frac{\cosh^2(a_s l_s) - \cos^2(a_s l_s)}{\sinh^2(a_s l_s) + \sin^2(a_s l_s)} \right] \quad (3.21)$$

This equation simplifies to

$$\tan(\Delta\psi) = \tan(\psi_F - \psi_R) = \tanh(a_s l_s) \tan(a_s l_s) \quad (3.22)$$

Thermal diffusivity α can be calculated from the above expression using the relation between α and a_s given earlier.

In order to demonstrate the usefulness, generality and accuracy of the phase lag technique, we have designed and fabricated a single beam PA cell, the design, fabrication and calibration of this temperature variable cell is given in the following sections.

3.3 PA phase lag cell design

A single beam PA cell which can be rotated through 180° about a vertical axis and can be used over a wide range of temperatures has been designed and fabricated with which measurements can be made from 90K to 520K. Fig.(3.2) shows the schematic diagram of the experimental setup. The sample compartment is made of a copper rod in the form of a cold finger, one end of which is in contact with liquid nitrogen chamber and to the other end a heater is wound. The sample cell having a volume of approximately 1 cc is sealed with two windows at the front and rear surfaces against vacuum outside using 'O' rings made of Indium (for low temperature measurements) or silicone rubber (for room temperature and high temperature measurements). The microphone compartment is acoustically coupled to the sample cell through a thin walled stainless steel tube of inner diameter 1.8 mm and length 8 cms. The PA cell configuration is thus that of an acoustic Helmholtz resonator [7-9] which for several reasons is an appropriate design for a variable temperature PA cell, whether heated [10] or cooled [11]. This configuration permits large variation in sample temperature

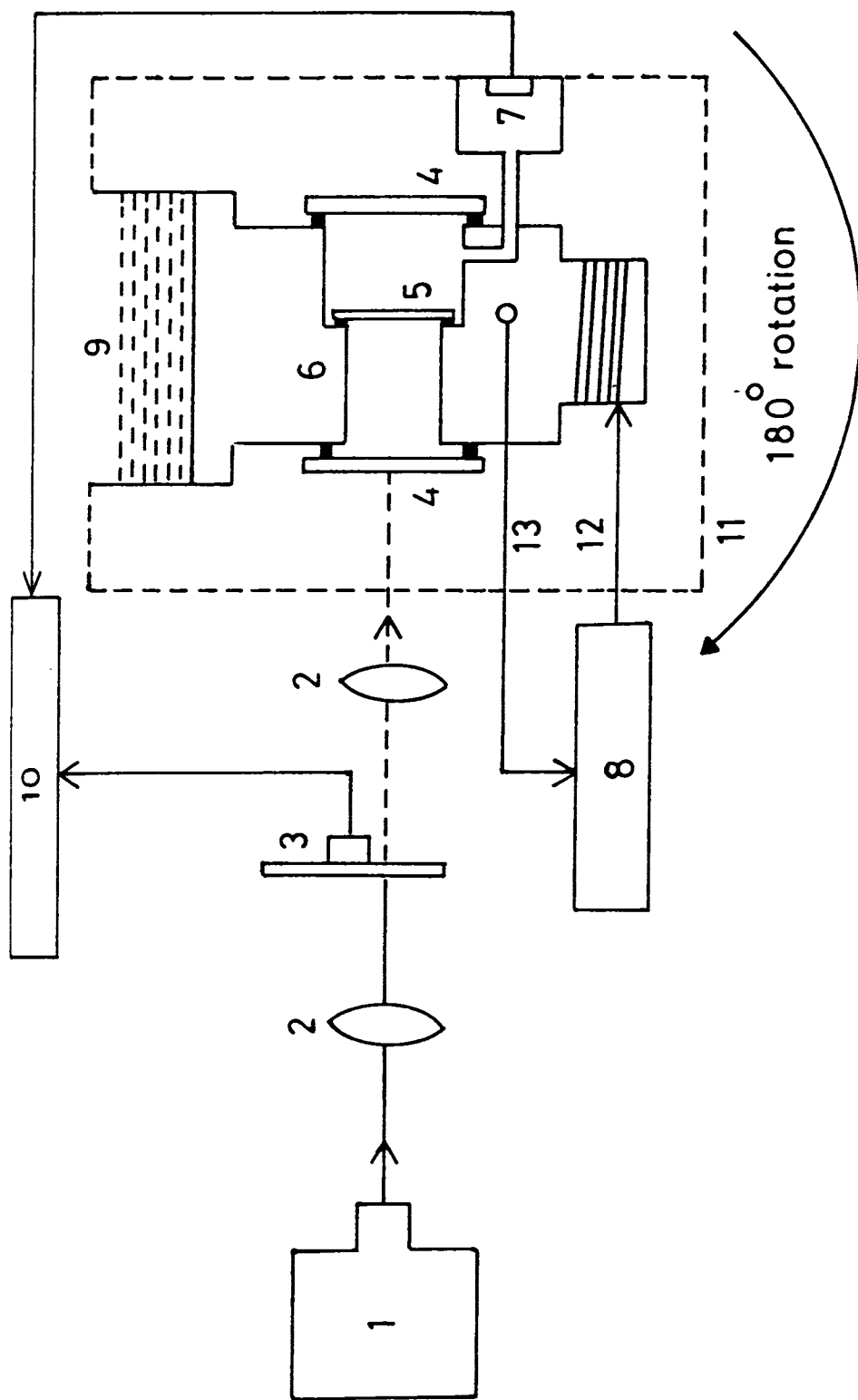


Fig. 3.2 Schematic diagram of the experimental set up. **1**-source, **2**- lenses, **3**- chopper, **4**-cell windows, **5**- sample, **6**- sample holder, **7**- microphone, **8**-temperature controller, **9**- liquid nitrogen chamber, **10**- lock-in amplifier, **11**- outer chamber, **12**- heater, **13**- temperature sensor.

without altering the microphone temperature appreciably. In order to avoid convection of the gas inside the cell at low temperatures, the microphone chamber is slightly lifted with respect to the sample cell and this bend of the coupling tube helps to compensate for thermal contraction. The microphone housing is sealed with rubber 'O' rings to have good acoustic isolation. A cross-section of the sample chamber along with the microphone compartment is shown in Fig.(3.3). The whole arrangement is kept in a metallic outer chamber of inner diameter 22 cm and wall thickness 5 mm (Fig.3.4). The sample chamber is connected to the outer chamber by means of thread provided at one end of the cold finger. With the help of a circular groove and ball bearing arrangement at the bottom of the outer chamber, the cell can be rotated freely about a vertical axis. Provision is also made to clamp the cell after rotation onto a sturdy base plate. The sample temperature is detected with a platinum resistance sensor. Both the temperature sensor and heater are connected to a temperature controller. A miniature flat type electret microphone (Knowles BT 1759) is used to detect the acoustic signal. A 3V cell to supply bias voltage to the FET, a switch and a BNC connector to take the microphone output are all fitted to the outer chamber.

3.4 Calibration of the cell

The performance of the cell has been evaluated by determining the thermal diffusivities of a number of standard samples such as copper, silicon, aluminium and Ge-Ga-Se glass. For this, measurements have been taken at different chopping frequencies between 20 and 40 Hz, the average of which is taken. Table 3.1 shows the measured values of α of these samples along with the literature values. The standard deviation of the measurements are also given in the table. The signal magnitude is relatively low in the case of copper, silicon and aluminium samples due to their high reflectivities which has resulted in a larger standard deviation in the data. When the signal level from the sample is low signals originating from the cell window and side walls of the cell can introduce phase errors. The use of thin absorbing coatings on the sample surfaces as proposed by Pessoa Jr. et al [5] is not a solution to this because in such cases there should be proper thermal matching ($g = 1$)

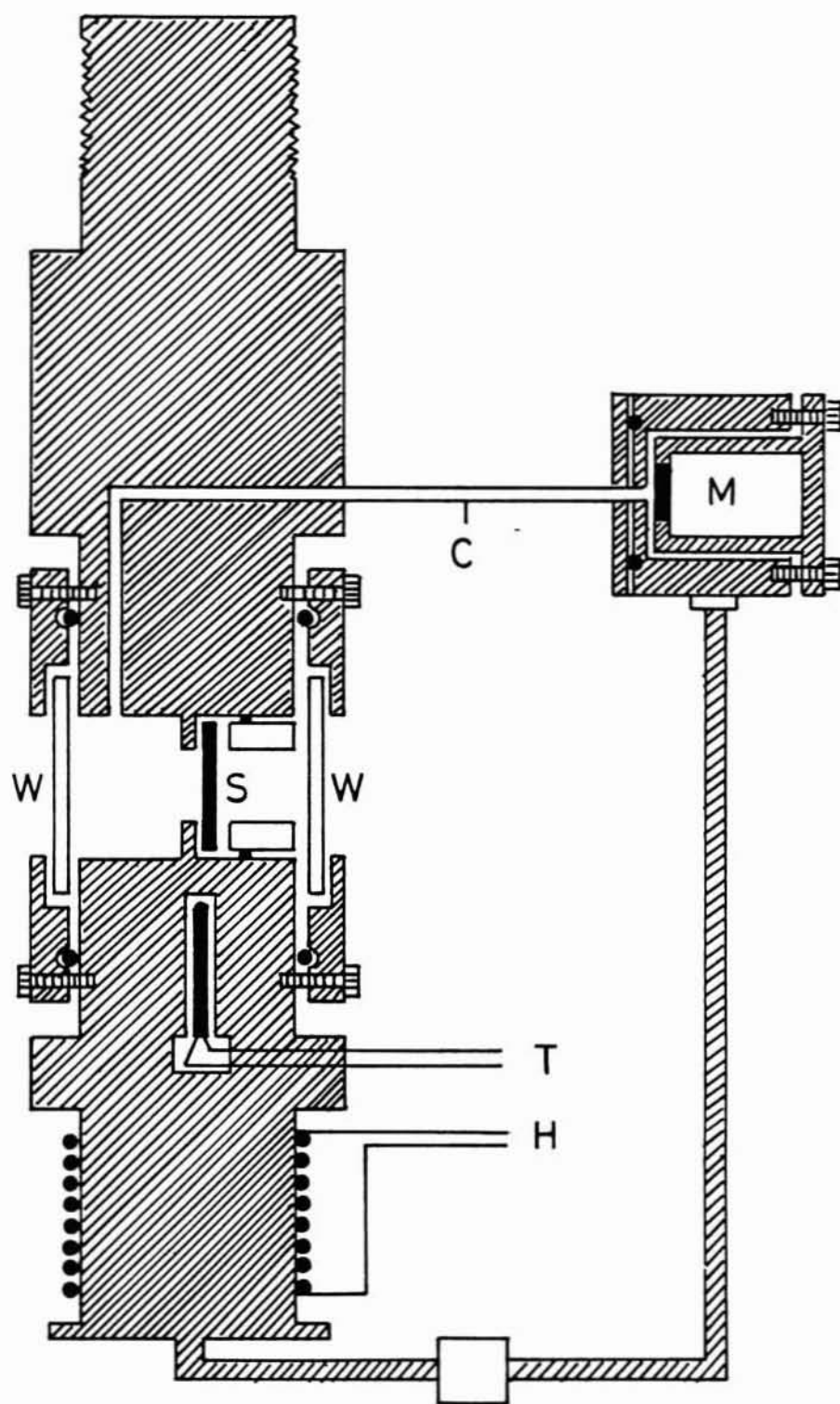


Fig. 3.3 Schematic diagram of the sample chamber and microphone compartment. W- cell windows, S- sample, C- coupling tube, M- microphone, T- temperature sensor, H - heater winding.

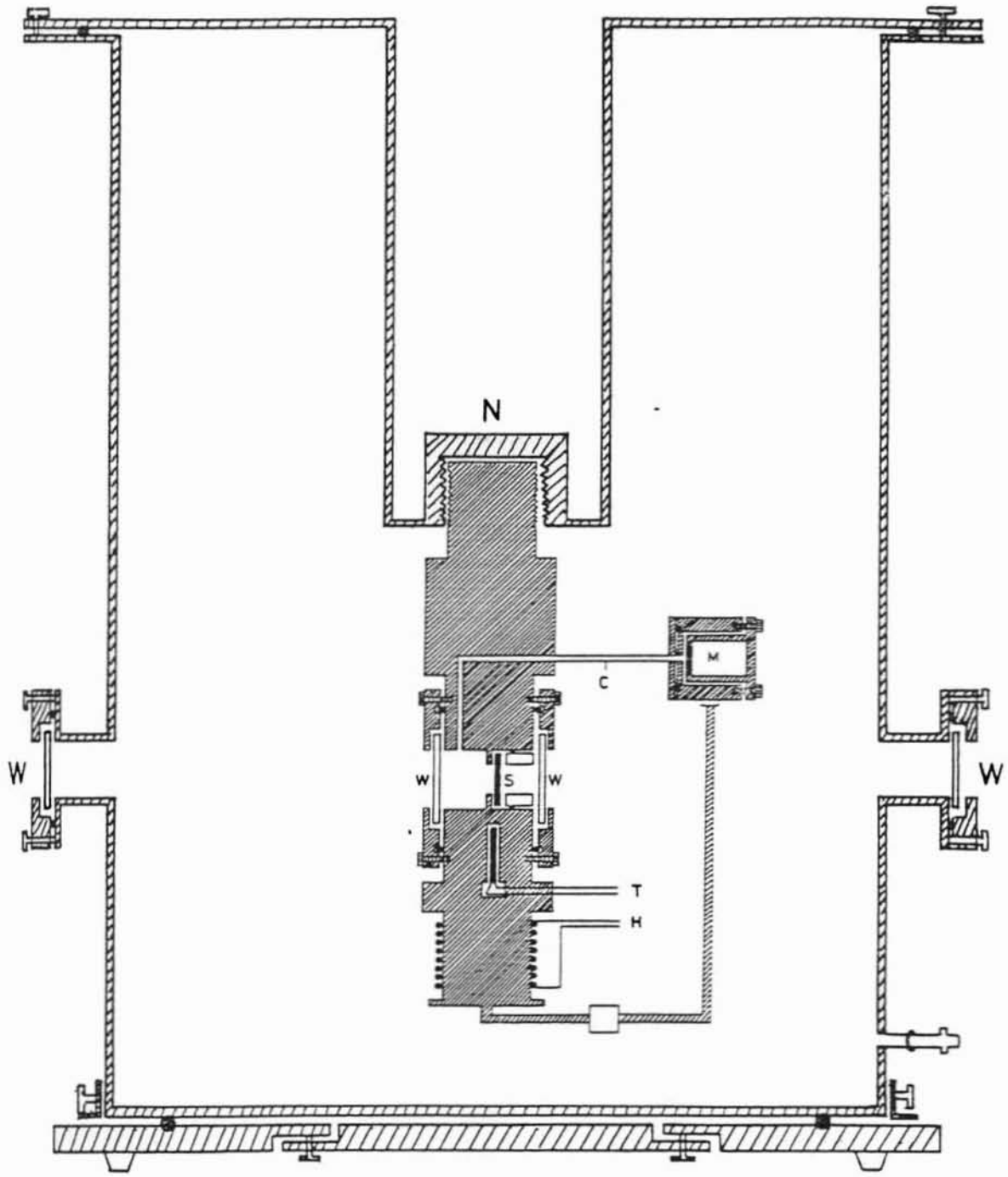


Fig. 3.4 Schematic diagram of the variable temperature PA cell.

Table 3.1The measured and literature values of thermal diffusivity α of selected samples

| Material | Sample thickness (μm) | Measured α (cm^2s^{-1}) | Standard deviation | Literature value (cm^2s^{-1}) |
|----------------|------------------------------------|--|--------------------|---|
| Copper | 415 | 1.10 | 0.10 | 1.12 |
| Silicon | 380 | 0.95 | 0.05 | 0.92 |
| Aluminium | 510 | 0.78 | 0.10 | 0.81 |
| Ge-Ga-Se glass | 630 | 0.019 | 0.0001 | -- |

between the absorber and the sample; otherwise thermal wave reflection will take place at the sample absorber interface causing significant error in signal phase. The Ge-Ga-Se glass sample gives a very good signal to noise ratio and consequently there is excellent agreement between the values measured at different chopping frequencies and for different sample thicknesses. The variation of α with temperature for silicon sample has been measured from 135 to 370K with the sample kept under a temperature controlled environment. The results obtained are shown in Fig.(3.5) along with the results taken from literature [12]. The experimental points shown in the figure are averages of four measurements at different chopping frequencies. Since temperature variation of α could not as such be found in literature, they have been determined from thermal conductivity and specific heat values at each temperature, assuming density to be constant.

3.5 Conclusions

In conclusion, the present single beam phase lag method is found to be simple and convenient for accurate determination of α of solid samples. The measured values are found to be in good agreement with literature values for known samples. The advantage of this technique is that measurements can be carried out at a single chopping frequency and also it is seen that sample thickness is not so critical. The complexities involved in optics while using an incoherent source is overcome by rotating the cell through 180° about a vertical axis. Provision is also made to carry out temperature variation measurements of α accurately. Moreover, it is very convenient to mount the sample and measurements can be completed in a comparatively short time.

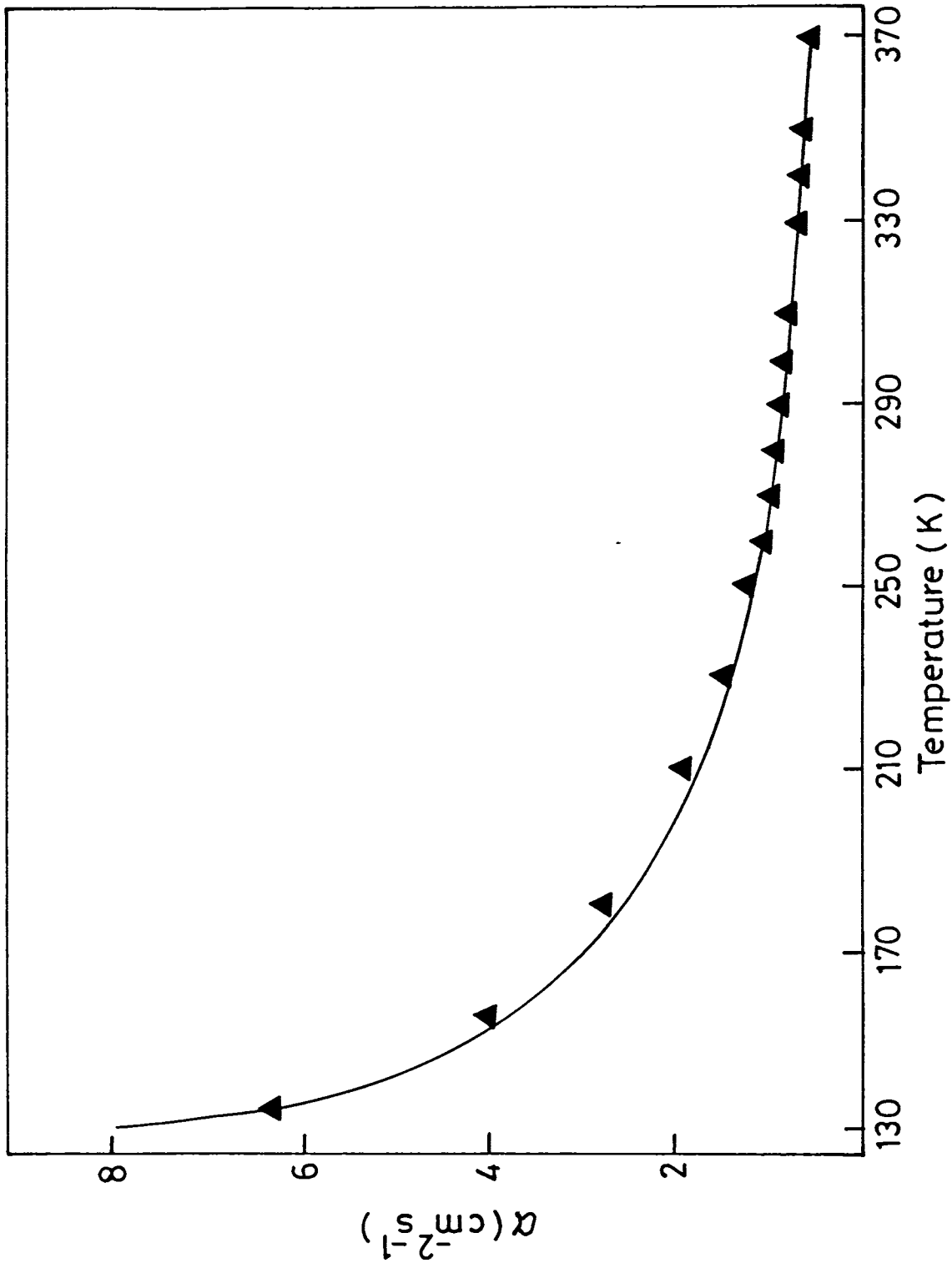


Fig. 3.5 Temperature variation of the thermal diffusivity of silicon.
 (-) literature values; (\blacktriangle) experimental values.

REFERENCES

1. Adams and G.F. Kirkbright, *Analyst*, **102** 678 (1977).
2. P.Charpentier, F. Lepoutre and L. Bertrand, *J. Appl. Phys.* **53**, 608 (1982).
3. C.L.Cesar, H.Vargas, J.M.Filho and L.C.M.Miranda, *Appl. Phys. Lett.* **43**, 555 (1983).
4. Z.Yasa and N.Amer, in *Tropical Meeting on Acoustic Microscopy*, Ames, Iowa, WAS-1 (1979).
5. O.Pessoa, Jr., C.L.Cesar, N.A.Patel, H.Vargas, C.C.Ghizone and L.C.N.Miranda, *J. Appl. Phys.* **59**, 1316 (1986).
6. Sheenu Thomas, J. Isaac and J.Philip, *Rev. Sci. Instrum.* **66**, 3908 (1995).
7. N.C.Fernelius, *Appl. Opt.* **18**, 1784 (1979).
8. R.S.Quimby, P.M.Selzer and W.M.Yen, *Appl. Opt.* **16**, 2630 (1977).
9. Lord Rayleigh, *Theory of Sound*, Vol.2, Dover, New York, 189 (1945).
10. P.S.Beehthold, M.Campagna and T.Schober, *Solid State Commun.* **36**, 225 (1980).
11. J.C.Murphy and L.C.Aamodt, *J. Appl. Phys.* **48**, 3502 (1977).
12. Hodgman, ed. *Handbook of Chemistry and Physics*, 44th ed., (Chemical Rubber Publishing, Cleveland) (1963).

CHAPTER IV

OPTICAL AND THERMAL PROPERTIES OF Ge-Ga-Se SEMICONDUCTING GLASSES

4.1 Introduction

Systematic studies on the variation of various mechanical, optical, chemical, thermal and electrical properties [1-7] of chalcogenide glasses with average coordination number have recently gained considerable interest among solid state physicists and electronic engineers in view of their many potential technological applications in solid state devices. The applications of chalcogenide glasses as materials for threshold switching, memory switching, inorganic photoresist, xerography, IR detection and transmission etc. are well documented in literature. Since these glasses do not absorb infrared radiation, they are suitable for fabricating infrared optical elements such as cells, windows, prisms and as FIR beam splitters, condensers and other accessories. One advantage of these glasses is that they can easily be formed by melt quenching over a wide range of compositions, making them suitable model systems for systematic studies of composition dependence of physical, thermal and optical properties. A good understanding of the gap states in disordered systems is of particular interest because they govern the electron transport in these materials. Thermal diffusivity α is of direct importance in thermal transport properties as it determines the rate of periodic or transient heat propagation through a medium. The chemically ordered covalent network (COCN) model [8,9] and topological models based on constraints theory [10-14] and structural dimensionality considerations [15-18] are used to explain the features observed in the composition dependence of various properties of chalcogenide glasses. According to COCN model, heteropolar bonds are at maximum, thereby favouring chemical order which results in features such as extremum or change of slope in physical parameters at stoichiometric compositions of these glasses. The topological models emphasize the concept

of the average coordinators number Z in determining many of the physical properties of tetrahedrally coordinated glasses.

According to Phillips and Thorpe [10-14] who interpreted the dynamical properties of chalcogenide glasses in terms of Z , the average number of atoms in the network is a measure of the balance between the force field constraints acting on the glassy system and the number of degrees of freedom which predicts a mechanical threshold at $Z = 2.4$, at which a threshold percolation of rigidity occurs. This idea was later modified by Tanaka [15-18], who proved that medium range order exists in chalcogenide glasses as indicated by the presence of layered structures. The inclusion of this structural feature predicts another threshold value at $Z = 2.67$. There have been a number of studies [19-21] aimed at verifying the validity of these models in various glasses. Anomalous features in many physical properties have been reported around $Z = 2.4$ in several systems, which have been explained on the basis of the constraints model. The existence of extrema in the properties at $Z = 2.67$ indicating a structural transition are observed in the composition dependent studies of many other physical properties [17,22].

We have carried out investigations on the optical and thermal properties of $\text{Ge}_x\text{Ga}_5\text{Se}_{(95-x)}$ glasses. These samples which are easy glass formers form good glasses in the entire range covering $Z = 2.4$ and 2.67 . It is seen that in this glass system containing IV-III-VI elements, the chemical threshold occurs at $Z = 2.73$ which is again different from $Z = 2.4$ or $Z = 2.67$, whereas in glasses containing V-VI or IV-VI elements, the chemical threshold coincides with the topological threshold. So the $\text{Ge}_x\text{Ga}_5\text{Se}_{(95-x)}$ system is an ideal one to get an insight into the variations in properties around different predicted thresholds which in turn helps to test the validity of different models. Measurements of optical band gap E_g and thermal diffusivity α of bulk $\text{Ge}_x\text{Ga}_5\text{Se}_{(95-x)}$ glasses have been carried out using the photoacoustic (PA) technique. This work is presented in this chapter. The PA technique has proved to be a very convenient and efficient method for the study of thermal and optical properties of amorphous semiconductors as described in chapter I. The advantages of the PA technique over conventional spectroscopic absorption techniques makes it convenient for the

study of glassy semiconductors. The energy band gap and thermal diffusivity measurements greatly help in selecting materials of desired optical absorption properties and thermal transport properties for special technological applications.

4.2 Sample preparation

Bulk $\text{Ge}_x\text{Ga}_y\text{Se}_{(95-x-y)}$ ($10 \leq x \leq 31$) glasses have been prepared by the melt quenching technique generally adopted for preparing chalcogenide glasses. Appropriate atomic proportions of 5N purity constituents are weighed and sealed in cylindrical quartz ampoules under a vacuum of 10^{-5} Torr. The ampoules are then placed in a furnace in which the mixture is heated and a temperature of 850°C is maintained constant for nearly 24 hrs. The molten sample is periodically rotated to ensure thorough mixing of the constituents. The ampoules are then quenched in ice water at a cooling rate of 10^2 K/sec. to make the glass. The amorphous nature of the samples have been confirmed from their powder X-ray diffractograms as shown in Fig.(4.1). The Ge-Ga-Se system forms glasses upto about 35 at% germanium and 20 at% gallium, the remainder being selenium [23]. The glass forming region for the Ge-Ga-Se system is shown in the phase diagram given in Fig.(4.2). The Z values of the compositions $\text{Ge}_x\text{Ga}_y\text{Se}_z$ ($x+y+z=1$) are given by $Z = 8-4x-3y-6z$.

4.3 Composition dependence of E_g using PA and UV-VIS-NIR methods

Optical band gap E_g is determined graphically using PA technique by measuring the variation of the normalized PA signal amplitude as a function of incident wavelength at a particular chopping frequency. The PA spectrum obtained for a highly absorbing carbon black sample is used to normalize the spectrum obtained for each sample. The normalized PA spectra recorded for the samples of Ge-Ga-Se family are shown in Figs.(4.3, 4.4 and 4.5). Since the PA signal is directly proportional to the optical absorption coefficient [24], these spectra provide information about the features of optical absorption in the samples. The normalized PA signal increases as the photon energy is increased and reaches a saturation

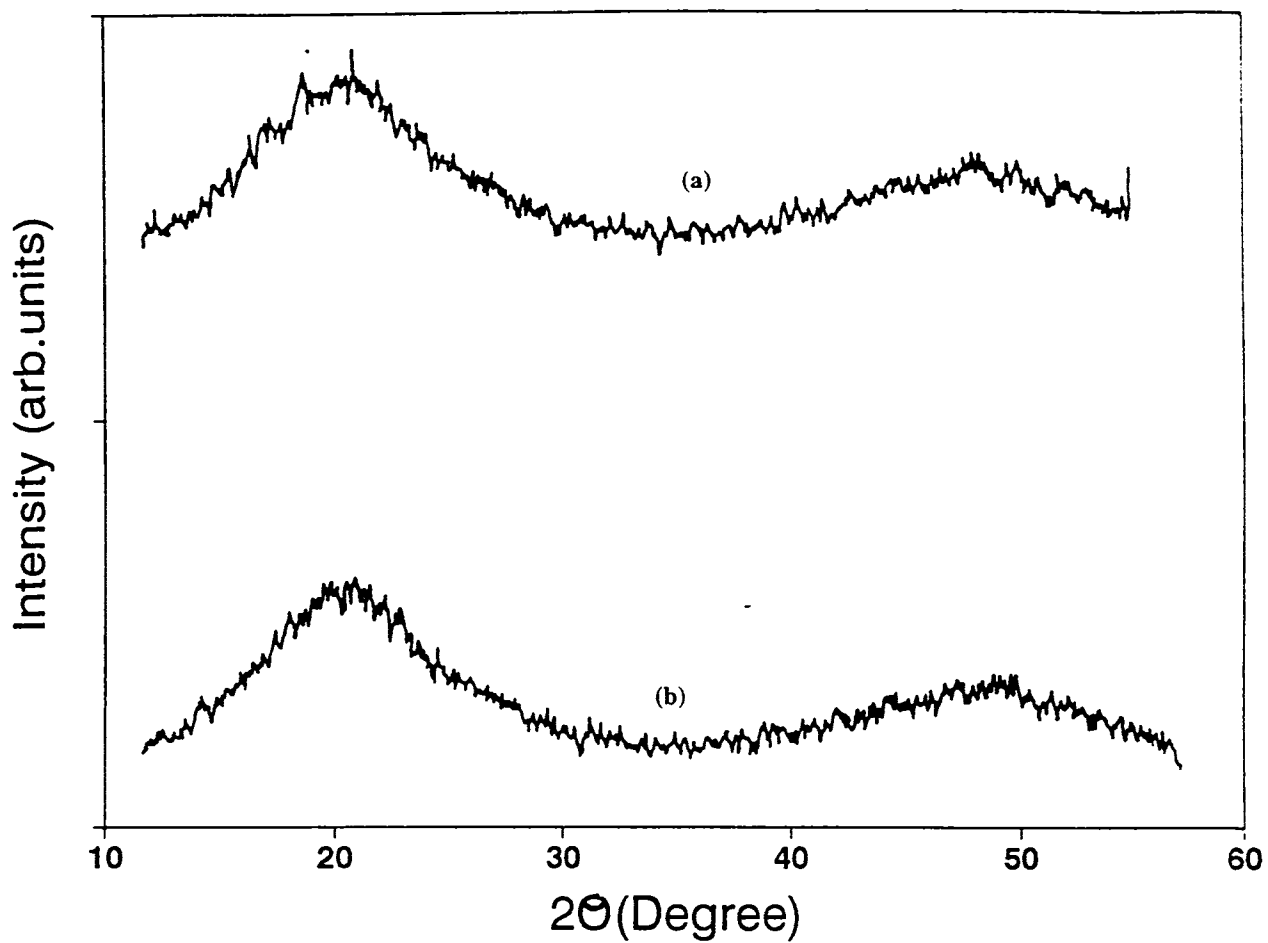


Fig. 4.1 X-ray diffraction pattern of (a) $\text{Ge}_{12.5}\text{Ga}_5\text{Se}_{82.5}$ and (b) $\text{Ge}_{26}\text{Ga}_5\text{Se}_{69}$ glasses.

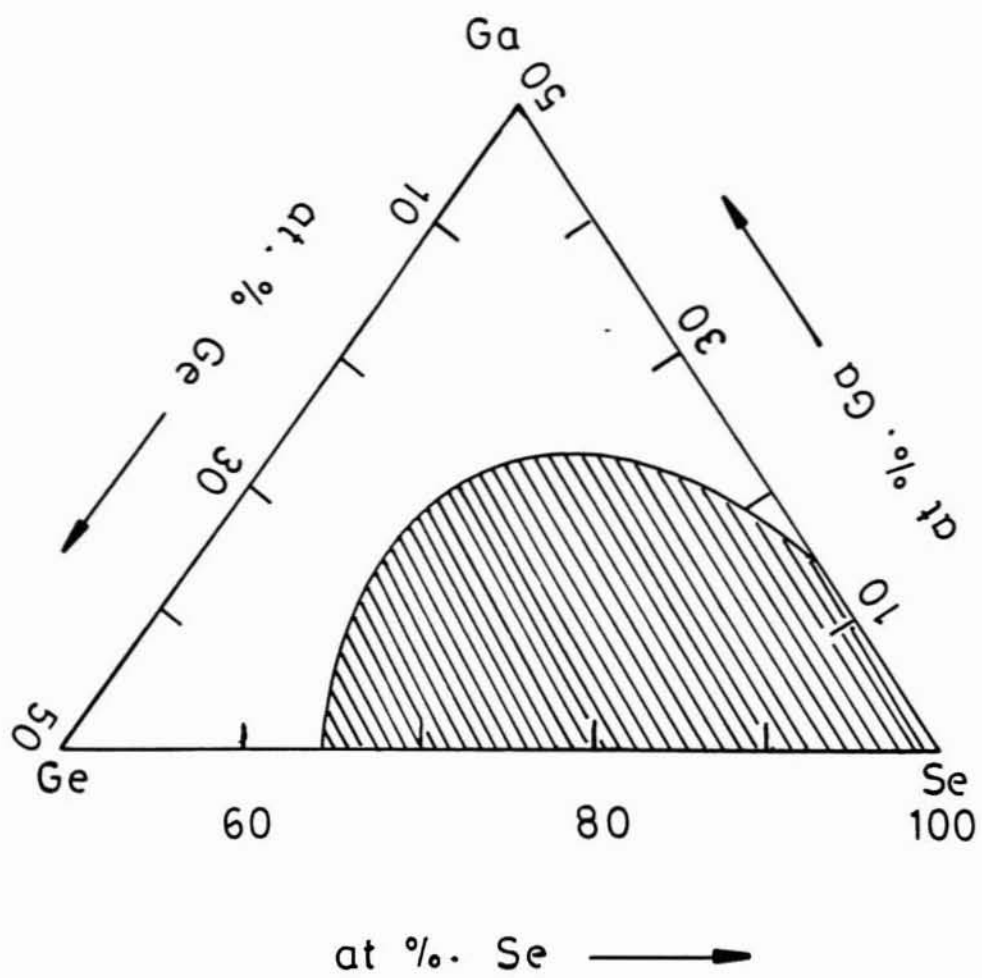


Fig. 4.2 Glass forming regions of Ge-Ga-Se system.

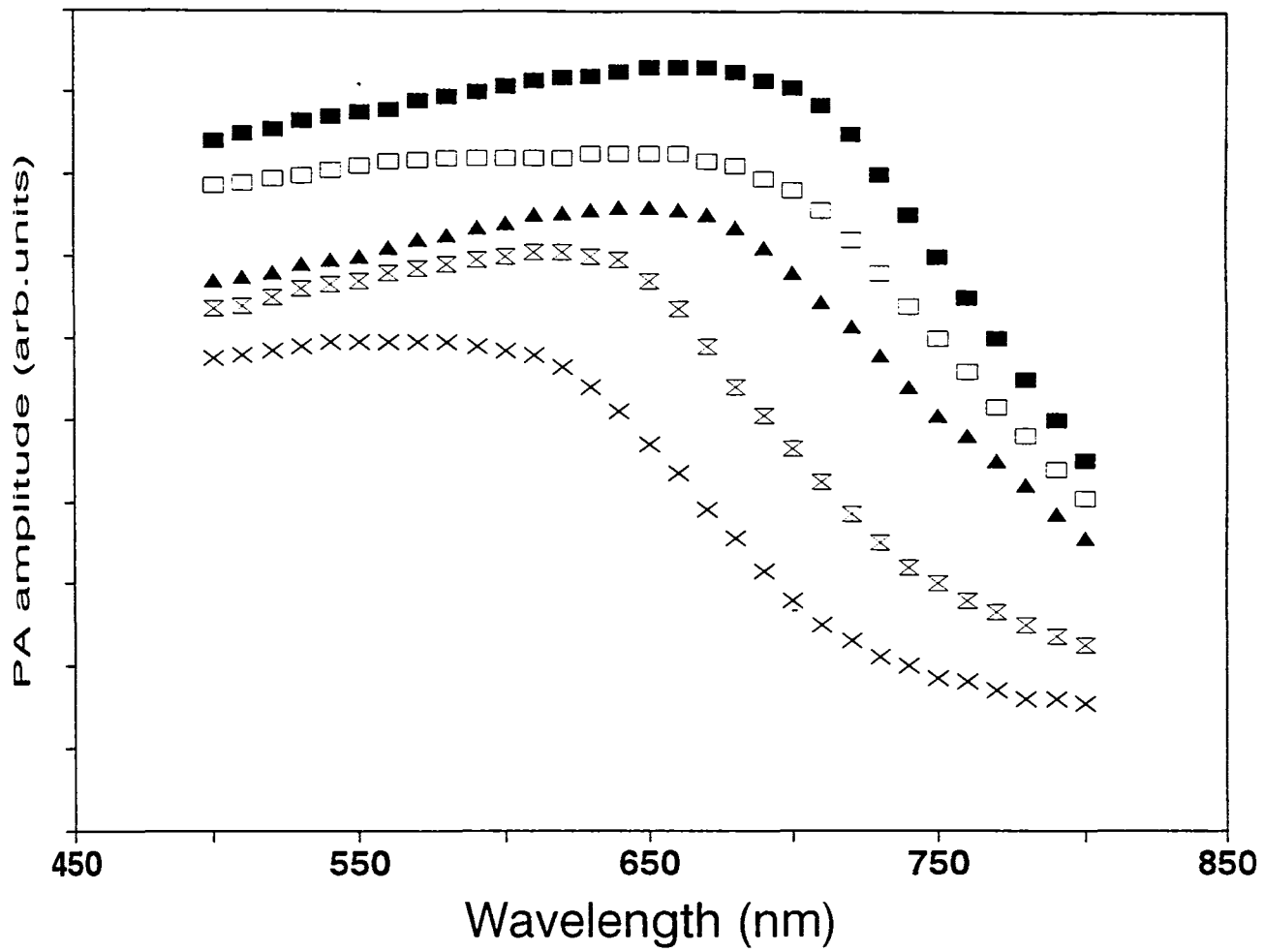


Fig. 4.3 PA spectra of $\text{Ge}_x\text{Ga}_5\text{Se}_{95-x}$ glasses.
 (■) $\text{Ge}_{10}\text{Ga}_5\text{Se}_{85}$ (□) $\text{Ge}_{12.5}\text{Ga}_5\text{Se}_{82.5}$ (▲) $\text{Ge}_{15}\text{Ga}_5\text{Se}_{80}$
 (⊗) $\text{Ge}_{17.5}\text{Ga}_5\text{Se}_{77.5}$ (X) $\text{Ge}_{20}\text{Ga}_5\text{Se}_{75}$.

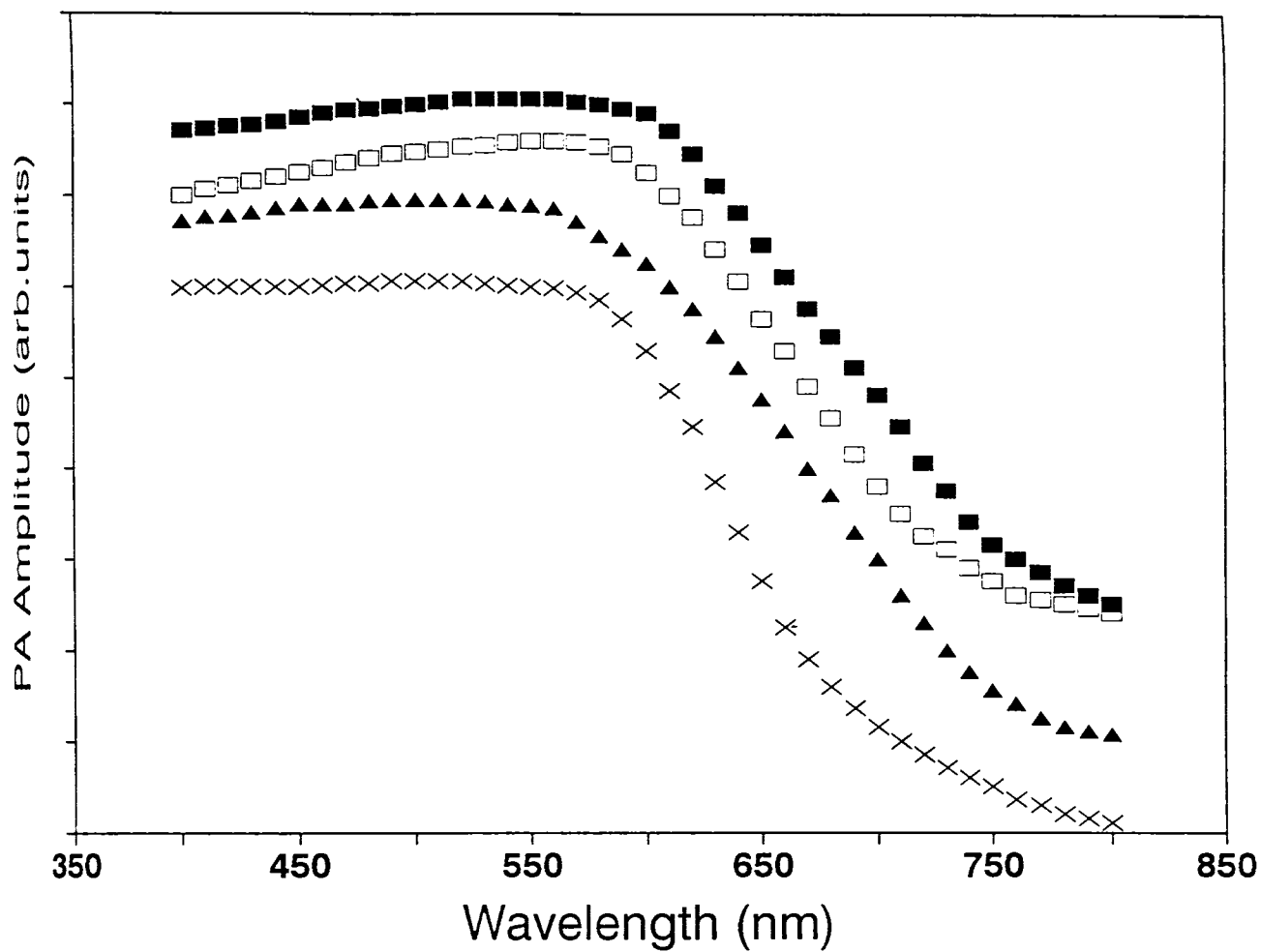


Fig. 4.4 PA spectra of $\text{Ge}_x\text{Ga}_5\text{Se}_{95-x}$ glasses.
 (■) $\text{Ge}_{22.5}\text{Ga}_5\text{Se}_{72.5}$ (□) $\text{Ge}_{25}\text{Ga}_5\text{Se}_{70}$ (▲) $\text{Ge}_{26}\text{Ga}_5\text{Se}_{69}$ (⊗) $\text{Ge}_{27}\text{Ga}_5\text{Se}_{68}$.

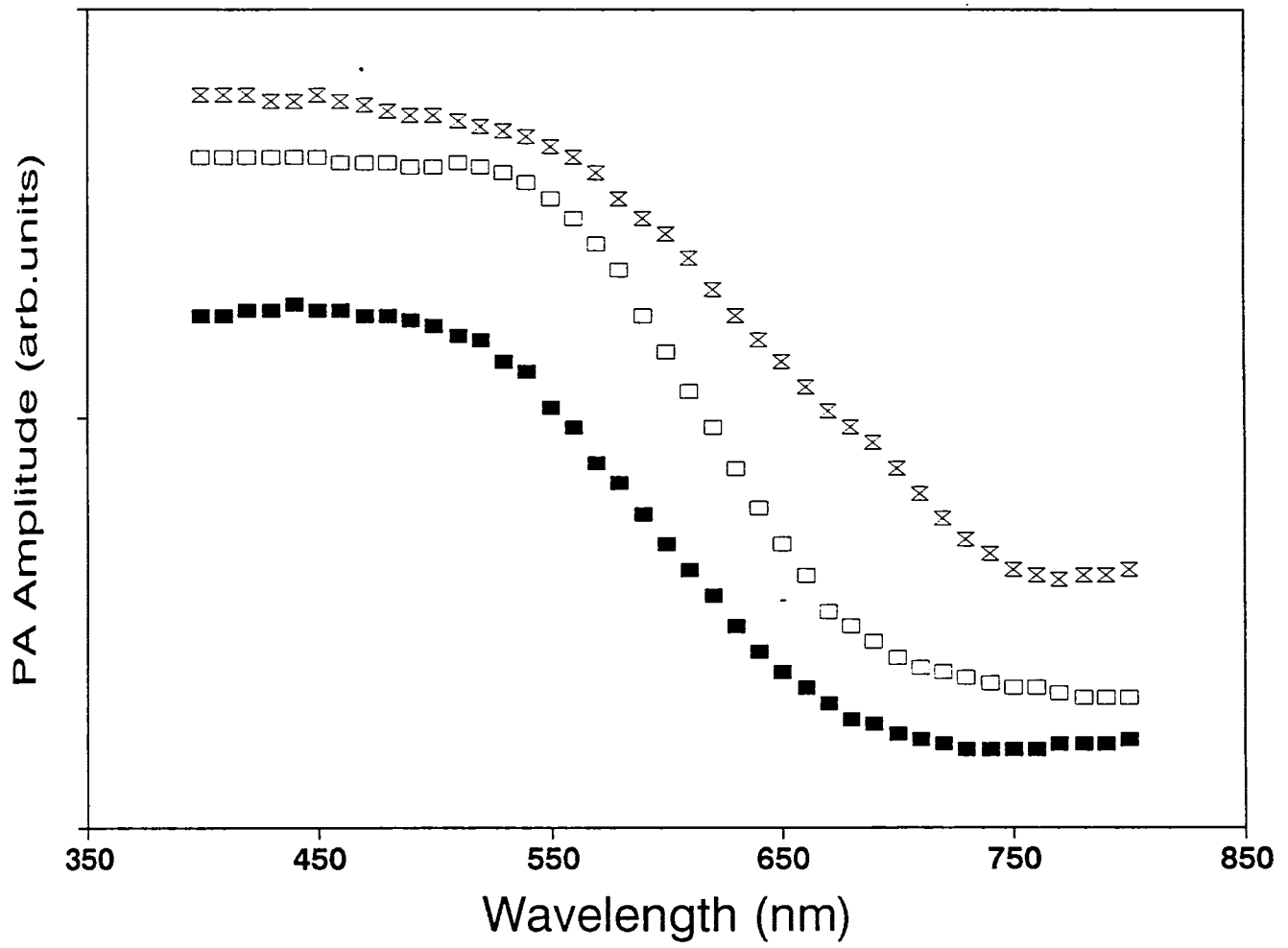


Fig. 4.5 PA spectra of $\text{Ge}_x\text{Ga}_5\text{Se}_{95-x}$ glasses.
 (■) $\text{Ge}_{29.17}\text{Ga}_5\text{Se}_{65.73}$ (□) $\text{Ge}_{30}\text{Ga}_5\text{Se}_{65}$ (X) $\text{Ge}_{31}\text{Ga}_5\text{Se}_{64}$.

level for photon energy $h\nu > E_g$ where E_g is the optical energy gap. As described by Tauc [25], for an amorphous semiconductor there are three different regions in the optical absorption curve corresponding to the three different ranges of the optical absorption coefficient β . The saturated region of the normalized PA signal is characterized by a very high absorption value ($\beta \gg 10^4 \text{ cm}^{-1}$). R-G theory [26] predicts this type of behaviour for highly absorbing samples with $l_\beta < l_s$ and $\mu_s > l_\beta$. In this region the absorption coefficient β has an energy dependence given by

$$h\nu \beta(h\nu) = B (h\nu - E_g)^2 \quad (4.1)$$

where B is a constant.

The absorption edge in an amorphous semiconductor has an exponential part associated with disorder induced potential fluctuations which extends in the absorption coefficient range $1 \text{ cm}^{-1} \leq \beta \leq 10^4 \text{ cm}^{-1}$. The absorption in this region depends on the photon energy according to the relation

$$\beta(h\nu) = \beta_0 \exp[h\nu/E] \quad (4.2)$$

where E characterizes the slope of the exponential absorption region. In the PA spectra this corresponds to the region where the normalized PA signal increases with photon energy. In the weak absorption tail region with $\beta < 1 \text{ cm}^{-1}$, the absorption depends on the preparation, purity and thermal history of the material. The optical energy gap E_g of all the samples have been determined graphically from the PA spectra. For this the logarithmic plot of the PA amplitude where it obeys the exponential rule as a function of the incident photon energy is plotted for each sample and the energy corresponding to the point at which it deviates from the straight line is taken as the band edge above which the transition is purely due to extended states.

The optical band gap has also been determined by recording the optical absorption spectra using a UV-Vis-NIR spectrophotometer. A Hitachi Model U-3410 recording spectrophotometer has been employed for this purpose. The model U-3410 comprises of a monochromator section (including control section), display section, floppy disk section, graphics plotter and operating section. The system is equipped with various functions which can be used in combination with the variety of optional accessories in all types of analytical fields and is especially suited for material characterization. This unit has a wavelength range 187 to 2600 nm with 0.07 nm resolution. The wavelength accuracy is 0.2 nm in the UV-Vis range.

The absorption spectra recorded using UV-Vis-NIR spectrophotometer for $\text{Ge}_x\text{Ga}_5\text{Se}_{(95-x)}$ glasses are shown in Figs.(4.6, 4.7 and 4.8). The E_g values are determined in a similar manner as in the case of the PA method and the E_g values obtained using the above two methods are compared. The agreement is found to be very good. In these glasses, the variation of E_g with composition parameter x , with $10 < x < 31$, are shown in Fig.(4.9). The E_g values determined using PA technique and UV-Vis-NIR method at different average coordination numbers, Z , are tabulated in Table 4.1. The average coordination numbers have been evaluated as outlined in Chapter I. The uncertainty in the values of E_g is of the order of 2%. It is found that E_g increases with increasing Ge content upto the tie-line composition corresponding to $Z = 2.73$ and decreases thereafter for Ge-rich glasses.

4.4 Thermal diffusivity by PA phase lag method

The thermal diffusivity α of bulk $\text{Ge}_x\text{Ga}_5\text{Se}_{(95-x)}$ glasses have been determined using the PA phase lag technique already described in Chapter III. To carry out α measurements, bulk samples of thickness approximately 0.5 mm and diameter 5 mm have been prepared. The advantage of this modified technique is that it can be used with thermally thick as well as their samples and, moreover, measurements can be carried out at a single chopping frequency.

The sample is fixed on to a metallic ring using vacuum grease and placed in the sample

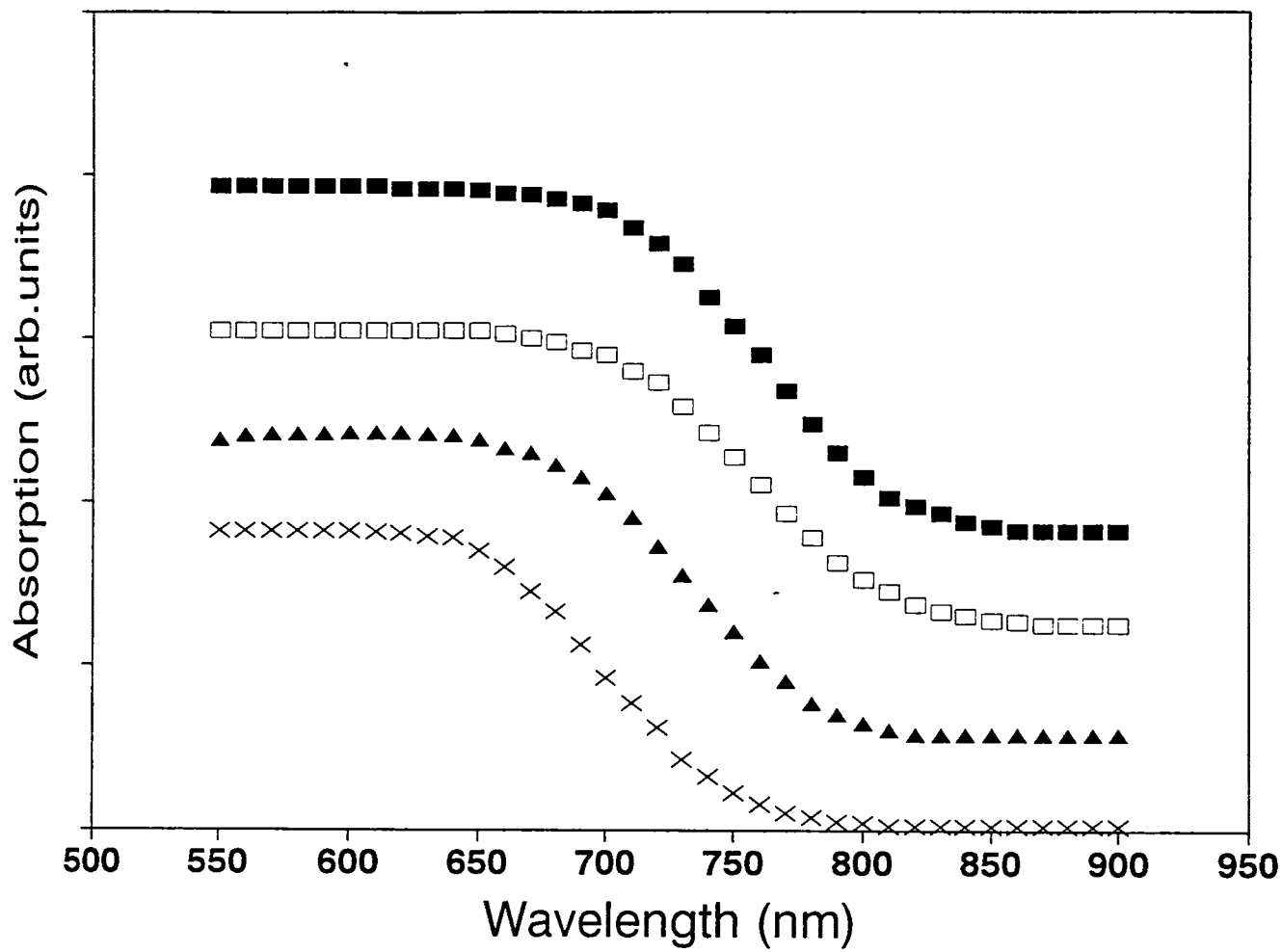


Fig. 4.6 UV-Vis - NIR spectra of $\text{Ge}_x\text{Ga}_5\text{Se}_{95-x}$ glasses.
 (■) $\text{Ge}_{10}\text{Ga}_5\text{Se}_{85}$ (□) $\text{Ge}_{12.5}\text{Ga}_5\text{Se}_{82.5}$ (▲) $\text{Ge}_{15}\text{Ga}_5\text{Se}_{80}$ (X) $\text{Ge}_{17.5}\text{Ga}_5\text{Se}_{77.5}$.

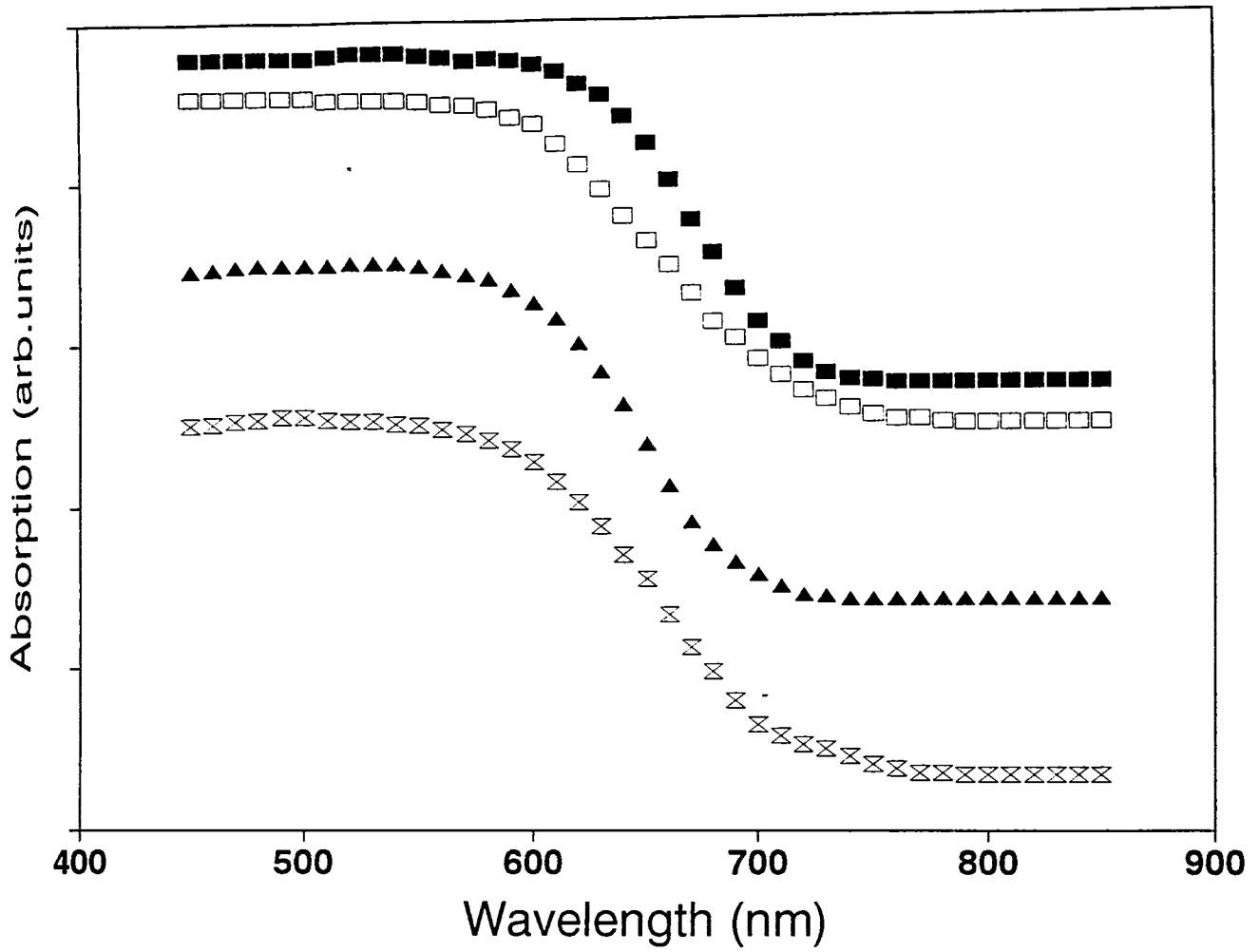


Fig. 4.7 UV-Vis - NIR spectra of $\text{Ge}_x\text{Ga}_5\text{Se}_{95-x}$ glasses.
 (■) $\text{Ge}_{20}\text{Ga}_5\text{Se}_{75}$ (□) $\text{Ge}_{22.5}\text{Ga}_5\text{Se}_{72.5}$ (▲) $\text{Ge}_{25}\text{Ga}_5\text{Se}_{70}$ (⊗) $\text{Ge}_{26}\text{Ga}_5\text{Se}_{69}$.

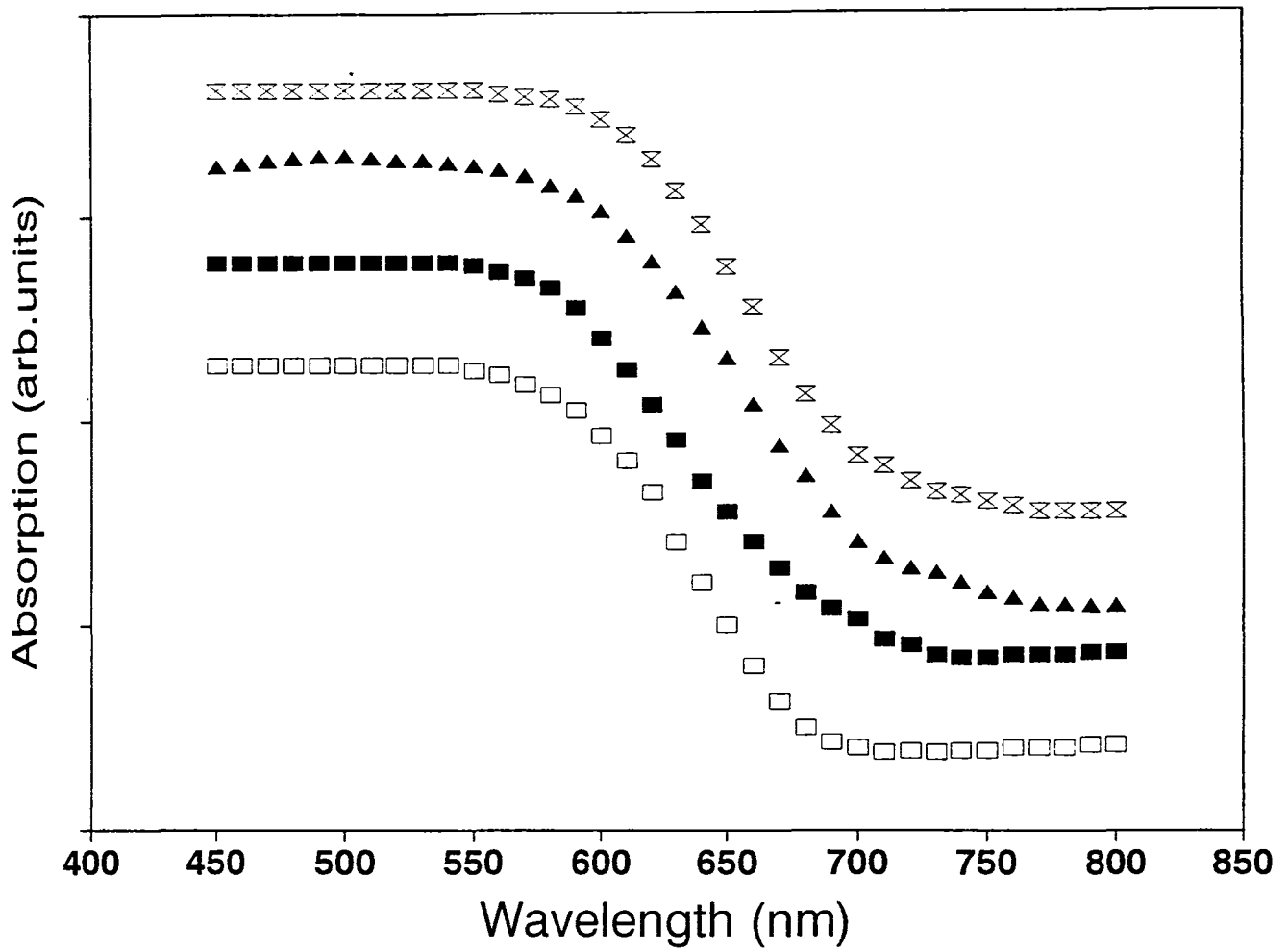


Fig. 4.8 UV - Vis - NIR spectra of $\text{Ge}_x\text{Ga}_5\text{Se}_{95-x}$ glasses.
 (■) $\text{Ge}_{27}\text{Ga}_5\text{Se}_{68}$ (□) $\text{Ge}_{29.17}\text{Ga}_5\text{Se}_{65.73}$ (▲) $\text{Ge}_{30}\text{Ga}_5\text{Se}_{65}$ (X) $\text{Ge}_{31}\text{Ga}_5\text{Se}_{64}$.

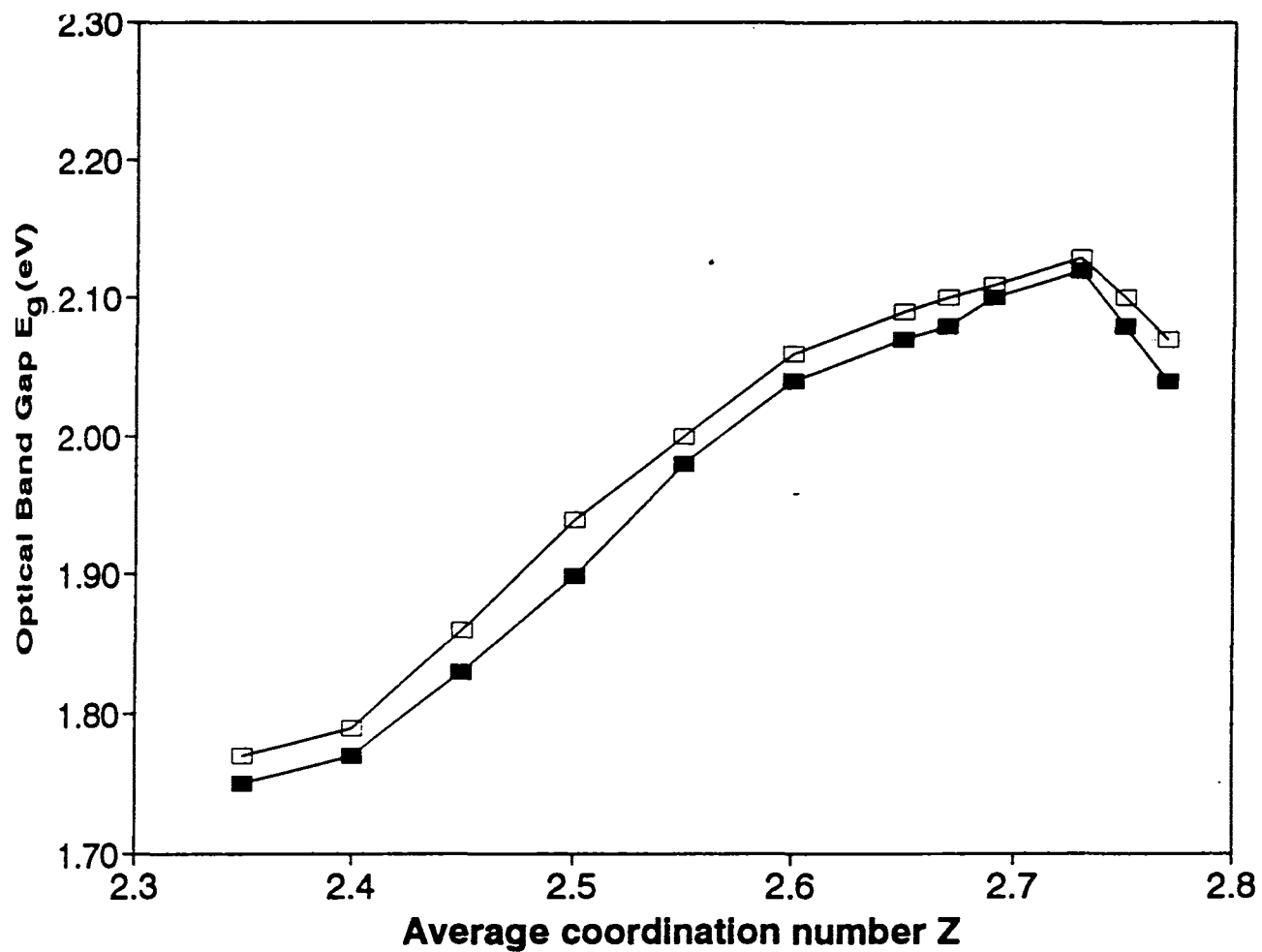


Fig. 4.9 Variation of the optical band gap E_g with average coordination number Z for the $\text{Ge}_x\text{Ga}_3\text{Se}_{95-x}$ glasses using PA technique (\square) and UV-Vis-NIR absorption technique (\blacksquare).

Table 4.1

Average co-ordination number Z , optical band gap E_g and thermal diffusivity α of Ge-Ga-Se glasses.

| Composition | | | Z | E_g (eV) | | α ($10^{-2} \text{ cm}^2 \text{ s}^{-1}$) |
|-------------|------|-------|------|--------------|----------------------|---|
| Ge : | Ga : | Se | | PA technique | UV-Vis-NIR method | |
| 10 | 5 | 85 | 2.35 | 1.77 | 1.75 | 0.34 ± 0.004 |
| 12.5 | 5 | 82.5 | 2.40 | 1.79 | 1.77 | 0.94 ± 0.009 |
| 13.5 | 5 | 81.5 | 2.42 | - | - | 1.83 ± 0.008 |
| 15 | 5 | 80 | 2.45 | 1.86 | 1.83 | 1.66 ± 0.02 |
| 16 | 5 | 79 | 2.47 | - | - | 1.35 ± 0.01 |
| 17.5 | 5 | 77.5 | 2.50 | 1.94 | 1.90 | 1.17 ± 0.01 |
| 20 | 5 | 75 | 2.55 | 2.00 | 1.98 | 1.38 ± 0.02 |
| 22.5 | 5 | 72.5 | 2.60 | 2.06 | 2.04 | 1.42 ± 0.02 |
| 25 | 5 | 70 | 2.65 | 2.09 | 2.07 | 1.36 ± 0.01 |
| 26 | 5 | 69 | 2.67 | 2.10 | 2.08 | 1.89 ± 0.02 |
| 27 | 5 | 68 | 2.69 | 2.11 | 2.10 | - |
| 29.17 | 5 | 65.83 | 2.73 | 2.13 | 2.12 | 1.32 ± 0.01 |
| 30 | 5 | 65 | 2.75 | 2.10 | 2.08 | 1.01 ± 0.01 |
| 31 | 5 | 64 | 2.77 | 2.07 | 2.04 | 0.88 ± 0.009 |

chamber. Care is taken to provide good acoustic isolation between the front and rear surfaces so that the front surface signal do not interfere with the rear surface signal. Relative phase lag $\Delta\psi = \psi_F - \psi_R$ of the generated PA signals between the front and rear surfaces of illumination when the sample is irradiated by a single light beam is determined by rotating the PA cell freely by 180° about a vertical axis. Thus α is determined using equation (3.22) as given in Chapter III. The variation of α with Z is shown in Fig.(4.10). These values are also tabulated in Table 4.1. It is seen that α has extrema at the two topological thresholds $Z = 2.42$ and 2.67 while no special feature is observed at $Z = 2.73$ which corresponds to the chemical threshold in these glasses.

4.5 Discussions based on COCN model and constraints theory

According to COCN model, Ge-Ga-Se glasses are made of GeSe_2 and Ga_2Se_3 structural units and excess of Ge or Se, if any. We can attribute the peak in E_g occurring at the chemical threshold to the chemical ordering since as per the above model of atomic arrangement formation of heteropolar bonds is always favoured over homopolar bonds. At this composition, only cross-linked structural units of GeSe_2 and Ga_2Se_3 exist, with neither Ge or Se in excess. The bond energies of Ge-Ge, Se-Se, Ge-Se and Ga-Se bonds estimated using listed electronegativities of elements are 49.1, 44, 55.4 and 65 kcal/mole respectively [27]. With the tie line composition as the reference as we consider the Ge-rich glasses, there is a progressive replacement of GeSe_2 structural units by Ge units. Since the bond energies of Ge-Ge bonds are less than those of Ge-Se bonds, the average bond energy of the system decreases. Using Kastner's model [28] for the band structure of chalcogenide glasses, the decrease in average bond energy of the system tends to decrease the energy of the conduction band edge. This effectively decreases the optical band gap E_g . Similarly, for Se-rich compositions also the replacement of strong heteropolar Ge-Se bonds by Se-Se bonds results in a decrease in E_g . The E_g values evaluated from the activation energy (δE) for electrical conductivity using the relation $2(\delta E) = E_g$, which has been reported earlier [29], also shows

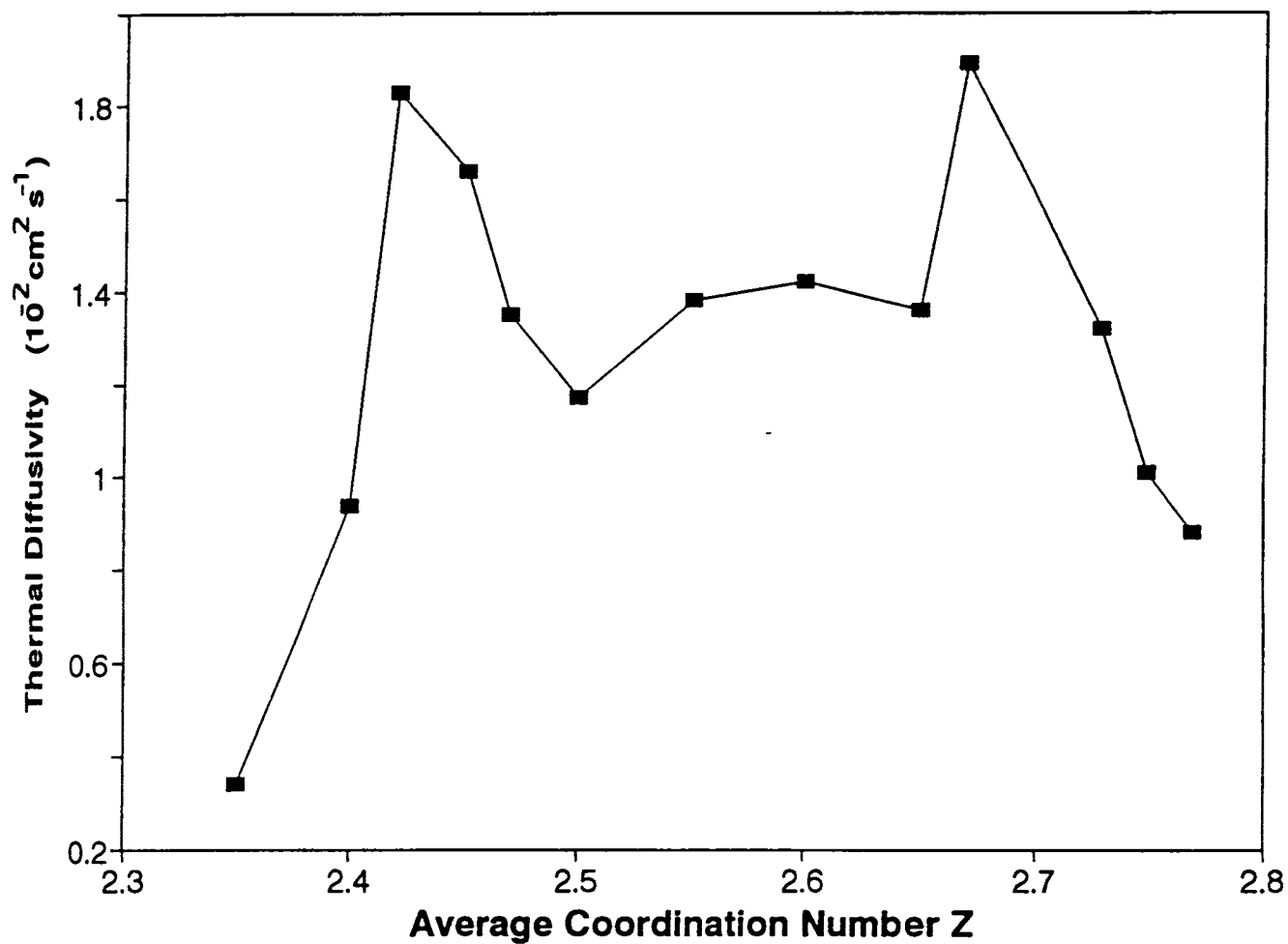


Fig. 4.10 Variation of thermal diffusivity α with average coordination number Z for $\text{Ge}_x\text{Ga}_5\text{Se}_{95-x}$ glasses.

an increase in E_g with Ge content upto the tie-line composition. Thereafter, a decrease in E_g occur for Ge-rich glasses. The results of the measurement on the variation of the glass transition temperature T_g with Z also report a maximum in T_g at $Z = 2.73$ [30].

The nature of the dependence of α on composition for these glasses show threshold maxima at $Z = 2.42$ and 2.67 . The peak at $Z = 2.42$ can be attributed to a mechanical threshold or a critical point at $Z = 2.4$ due to constraint balancing condition getting satisfied as predicted by Phillips and Thorpe [14,31]. Salient features of the constraints model, developed by Phillips, Thorpe and others, are already described in chapter I. The underconstrained glass with $N_c < N_d$ or $Z < 2.4$ contain large floppy or spongy regions with a few rigid inclusions, whereas overconstrained glasses with $N_c > N_d$ or $Z > 2.4$ contain rigid regions having percolated to form a rigid network extending into the whole solid with a few floppy or spongy inclusions. The network with $N_c = N_d$ at $Z = 2.4$ is the percolation threshold where the network changes from a floppy to rigid type driven by the average coordination number. As has been stated earlier experimental results on elastic constants [32] and slow neutron scattering [33] support this model. In order to explain the observed peak in thermal diffusion at $Z = 2.42$, one has to invoke the role played by low frequency modes in the underconstrained glass. At $Z = 2.4$, the network becomes more and more rigid and the number of low frequency modes correspondingly decrease. Scattering of the propagating thermal waves by the low frequency modes limit the thermal diffusivity of the underconstrained glass with $Z < 2.4$. As Z approaches 2.4, the number of low frequency modes approaches zero resulting in a corresponding enhancement in thermal diffusion. As Z increases beyond 2.4, the elastic forces build up fast giving rise to an increase in the values of elastic constants. Correspondingly, the allowed phonon modes characteristic of a rigid elastic network build up fast. Scattering of thermal waves by these modes lead to a reduction in thermal diffusivity for the overconstrained network with $Z > 2.4$.

The presence of a threshold maximum in the value of α again at $Z = 2.67$ may be considered as due to the topological transition from two dimensional to three dimensional

structure of the system as predicted by Tanaka [15-18]. We believe that this system essentially consists of Ge-Se network with Ga-Se bonds dispersed in it. The Ge-Se bonds fixed in a three dimensional network undergo mechanical stiffening at $Z = 2.4$. The Ga-Se bonds prevalent in them form a layer like structure for $Z < 2.67$. So essentially we have a material having a plane Ga-Se lattice laid in a three-dimensional Ge-Se space. The layer structure of the Ga-Se lattice is fully evolved at $Z = 2.67$ and the constraint balancing equation is getting satisfied and the network undergoes a topological transition from two to three dimensional structure at this composition. For $Z < 2.67$, the Ga-Se layers form a lattice misfit and act as scattering regions for propagating thermal waves resulting in a reduced thermal diffusivity. As Z tends to 2.67, the lattice misfit decreases and a uniform 3D structure is evolved at $Z = 2.67$. But at this transition composition, the elastic forces are not fully developed (as at 2.40 for the Ge-Se network) and hence the phonon modes are not fully evolved. This results in the observed maximum in α at this composition. As Z exceeds 2.67, the network becomes a uniform three dimensional one with elastic forces characteristic of a three dimensional glassy solid. The phonon modes also develop correspondingly and they scatter the propagating thermal waves causing further reduction in α for $Z > 2.67$. Reports on variation of mean atomic volume V with Z also show anomalies at $Z = 2.45$ and $Z = 2.63$ which are also explained based on topological models [29,30]. Finally, at $Z = 2.73$, corresponding to the chemical threshold, the system forms a stoichiometric glass.

4.6 Conclusions

Effects due to chemical ordering in this glass system are marked by a maximum in E_g in the Z dependence of E_g at $Z = 2.73$ in $\text{Ge}_x\text{Ga}_5\text{Se}_{(95-x)}$ glasses. Topological thresholds at $Z = 2.42$ and 2.67 due to floppy to rigid transition and a two to three dimensional structural transition respectively in these glasses are registered by maxima in the Z dependence of thermal diffusivity investigated using PA technique. Results on Ge-Ga-Se glasses indicate that the thresholds occur at three different average coordination numbers in the glass forming

range making this a model system for experimentation. Arguments such as occurrence of a two dimensional layered structure dispersed in a three dimensional network which is mechanically rigid are still controversial and need to be resolved with more investigations.

REFERENCES

1. S.Mahadevan and A.Giridhar, *J. Non-Cryst. Solids* **110**, 118 (1989).
2. D.R.Swiler, A.K.Varshneya and R.M.Callahan, *J. Non-Cryst. Solids* **125**, 250 (1990).
3. K.N.Madhusoodanan and J. Philip, *Phys. Status Solidi(b)* **108**, 77 (1988).
4. S.Mahadevan and A Giridhar, *J. Non-Cryst. Solids* **143**, 52 (1992).
5. A.N.Sreeram, D.R.Swiler and A.K.Varshneya, *J. Non-Cryst. Solids* **127**, 287 (1991).
6. S.Mahadevan, A. Giridhar and A.K.Singh, *J. Non-Cryst. Solids* **169**, 133 (1994).
7. A.Srinivasan, K.Ramesh, K.N.Madhusoodanan and E.S.R.Gopal, *Phil. Mag. Lett.* **65**, 249 (1992).
8. P.Tronc, M.BenSoussan, A.Brenac and C.Sebenne, *Phys. Rev. B* **8**, 5947 (1973).
9. G.Lucovsky, F.L.Galeener, R.C.Keezer, R.H.Geils and H.A.Six, *Phys. Rev. B* **10**, 5134 (1974).
10. J.C.Phillips, *J. Non-Cryst. Solids* **34**, 153 (1979).
11. J.C.Phillips, *J. Non-Cryst. Solids* **43**, 37 (1981).
12. J.C.Phillips, *J. Non-Cryst. Solids* **57**, 355 (1983).
13. H.He and M.F.Thorpe, *Phys. Rev. Lett.* **54**, 2107 (1985).
14. J.C.Phillips and M.F.Thorpe, *Solid State Commun.* **53**, 699 (1985).
15. K.Tanaka, *Solid State Commun.* **53**, 699 (1985).
16. K.Tanaka, *J. Non-Cryst. Solids* **103**, 149 (1988).
17. K.Tanaka, *Phys. Rev. B* **39**, 1270 (1989).
18. K.Tanaka, *J. Non-Cryst. Solids* **97-98**, 391 (1987).
19. C.F.Niederriter, R.L.Cappelletti and P. Boolchand, *Solid State Commun.* **61**, 527 (1987).
20. W.Bresser, P. Boolchand and P.Suranyi, *Phys. Rev. Lett.* **56**, 2493 (1986).

21. P. Boolchand, *Phys. Rev. Lett.* **57**, 3233 (1986).
22. S. Mahadevan and A. Giridhar, *J. Non-Cryst. Solids* **162**, 294 (1993).
23. S. Mahadevan and A. Giridhar, *J. Non-Cryst. Solids* **126**, 161 (1990).
24. A. Rosencwaig, in *Photoacoustics and Photoacoustic Spectroscopy* (Wiley, New York, 1980).
25. J. Tauc, in *Amorphous and Liquid Semiconductors*, ed: J. Tauc (Plenum Press, New York) 159 (1974).
26. A. Rosencwaig and A. Gersho, *J. Appl. Phys.* **47**, 64 (1976).
27. R. T. Sanderson, in *Chemical Bonds and Bond Energy*, ed. Ernest M. Loeble, (Academic Press, New York) 21 (1976)
28. M. Kastner, *Phys. Rev. Lett.* **28**, 355 (1972).
29. S. Mahadevan and A. Giridhar, *J. Non-Cryst. Solids* **152**, 42 (1993).
30. A. Giridhar and S. Mahadevan, *J. Non-Cryst. Solids* **151**, 245 (1992).
31. M. F. Thorpe, *J. Non-Cryst. Solids* **182**, 135 (1995).
32. S. S. Yun, H. Li, R. L. Cappelliti, P. Boolchand and R. N. Engweiler, *Phys. Rev. B* **39**, 8702 (1989).
33. P. Boolchand, R. N. Engweiler, R. L. Cappelliti, W. A. Kamitakahara, Y. Cai and M. F. Thorpe, *Solid State Ionics* **39**, 81 (1990).

CHAPTER V

COMPOSITION DEPENDENCE OF OPTICAL AND THERMAL PROPERTIES OF Ge-In-Se GLASSES

5.1 Introduction

Interpretation of the composition dependence of some of the physical and structural properties of network glasses in terms of the average coordination number Z is an outcome of the constraints theory developed by Phillips [1], Thorpe [2,3] and others. This theory is based on balancing the force field constraints acting on the glassy network with available degrees of freedom. Halpap et al [4] considered a network of N atoms, N_z of which have Z bonds per atom. If the number of degrees of freedom $3N$ exceeds the sum of the bond length [$Z/2$ per atom] and bond angle [$2Z-3$ per atom] constraints corresponding to linear and bending motions of atoms respectively, then the excess degrees of freedom are low energy [2] or floppy modes. The density of floppy modes [4], ρ_f is the number of floppy modes divided by N given by

$$\rho_f = 6 - (5/2) Z \quad (5.1)$$

The mean field result should apply to poorly cross-linked materials consisting mainly of chains of divalent atoms. If the degrees of cross-linking is increased, rigid regions increases with a decrease in the number of floppy modes. At a critical value, as the number and size of the rigid region grow, they begin to get interconnected to one another and a percolation transition occurs when $\rho_f = 0$, i.e. at $Z = 2.4$ as has already been discussed in the previous chapter. Simulations on a 3D network of two-fold, three-fold and four-fold coordinated atoms indicate that a distinct increase in the elastic constants C_{11} and C_{44} begin to

occur between $Z = 2.35$ and 2.45 [3], which is in good agreement with the mean field predictions [2]. Many physical properties such as optical band gap, thermal diffusivity, elastic constants etc. are found to show a threshold values at $Z = 2.4$.

In recent years there has been a great deal of interest in understanding the properties of semiconducting chalcogenide glasses because of their fundamental as well as technological importance. For application purposes, it is of particular significance to know the composition dependence of energy gap as well as other physical parameters of these materials like glass transition temperature, thermal diffusivity, conductivity etc. Since long range order is absent in non-crystalline solids, the electronic properties of these solids are determined primarily by the nature and range of short range order. Examining the amorphous structure of covalent glasses, the building elements can be classified into two components [5]. One is the normal building structure consisting of covalent bonds of density $\sim 10^{22}$ - 10^{23} cm^{-3} (which can be specified by chemical [6] and topological [7] nature) and the other is defects such as impurities, dangling bonds, valence alternation pairs and wrong bonds (homopolar bonds in stoichiometric alloys). The density of defects is in general less by $\sim 10^{-2}$ than that of covalent bonds. So the structural behaviour is determined mostly by the normal configurations, i.e. covalent bonds. Moreover, these covalent bonds are primarily responsible for the electronic properties such as optical bandgap in contrast to the gap states originating from defects.

Tanaka [7] and Zallen [8] considered the network dimension as unity for the two-fold coordinated glassy chalcogenide materials. Upon introducing higher coordinated atoms to a chalcogenide glass, the one dimensional molecules are cross-linked and a gradual structural transformation takes place in the material. At $Z = 2.67$ the layered structures are fully evolved [7,9-11]. Thus Tanaka modified the ideas of Phillips and Thorpe [12] by arguing that medium range order should also be considered in the constraint balancing condition as evidenced by characteristic signatures in the composition dependence of certain physical properties at $Z = 2.67$, which may be connected to the formation of stable layer structures in the network. If one assumes a hypothetical network having a plane lattice laid in a three

dimensional space, the angular term in the constraint balancing equation given by

$$N_d = (Z/2) + (2Z - 3) \quad (5.2)$$

gets modified. Including this feature, the bond bending term $(2Z-3)$ in equation (5.2) reduces to $(Z-1)$ and the constraint balancing equation gets modified to

$$N_d = (Z/2) + (Z - 1) \quad (5.3)$$

This predicts another composition driven phase transition at $Z = 2.67$. Two dimensional layered structures are fully evolved at this critical value and for higher values of Z , due to the increase in the number of cross-linked sites, there is a structural phase transition to a three dimensional network.

Chemical ordering existing in chalcogenide glasses is evidenced by features such as an extremum or change of slope at the stoichiometric composition of these glasses. The results are interpreted in terms of the chemically ordered covalent network (COCN) model according to which heteropolar bonding is maximized at the stoichiometric composition [13,14].

Like Ge-Ga-Se glasses, Ge-In-Se system also comes under the III-IV-VI group of chalcogenide glasses. These glasses also have the chemical threshold well resolved from the other two mechanical thresholds. This makes them an ideal system to investigate to test the validity of the above models. Moreover, they form bulk glasses in the entire range covering all the three predicted thresholds occurring at $Z = 2.4, 2.67$ and 2.73 .

We have carried out measurements on the optical band gap E_g and thermal diffusivity α of bulk $\text{Ge}_x\text{In}_5\text{Se}_{(95-x)}$ glasses using photoacoustic technique [15]. Photoacoustic technique has already been proved to be an effective method for the non-destructive characterization of semiconductors and many other materials [15]. The non-radiative absorption processes which are associated with the band structure, defect related energy loss

mechanism etc. can directly and very accurately be obtained from the analysis of photoacoustic spectra [16-19] which is very convenient for measuring optical properties of light absorbing glassy materials [20]. In this chapter, we present the results of our work on the composition dependence of optical band gap and thermal diffusivity of $\text{Ge}_x\text{In}_5\text{Se}_{(95-x)}$ ($12 \leq x \leq 32$) glassy alloys. The experimental procedures, the results obtained and their discussions are given in the following sections.

5.2 Preparation of samples

Bulk $\text{Ge}_x\text{In}_5\text{Se}_{(95-x)}$ ($12 \leq x \leq 32$) glasses have been prepared by melt quenching technique as outlined earlier. Appropriate amounts of highly pure (99.999%) Ge, In and Se elements are weighed and sealed in quartz ampoules under a vacuum of $\sim 10^{-5}$ Torr. The ampoules are heated to nearly 1000 °C for about 24 hrs with intermediate rotation for homogenization of the melt. The molten sample in the ampoules are then quenched in ice water to make the glass. The amorphous nature of the samples have been confirmed by X-ray method. The X-ray diffraction pattern of few typical samples are shown in Fig.(5.1). There is no observable sharp peak in the diffractograms which is characteristic of amorphous (glassy) materials. The average coordination numbers have been evaluated using the standard procedure [21] by adopting the (8-*N*) rule to arrive at the coordination of Ge, In and Se. However, it is known that the (8-*N*) rule is valid only for elements from the groups IV-VII, instead a formula of the type $Z = (8-n)$ has been suggested [22] to evaluate the *Z* values of compositions containing elements from groups I-VII. Based on this, for a composition with the general formula $\text{Ge}_x\text{In}_y\text{Se}_p$ ($x+y+p=1$), value of *Z* can be written as

$$Z = 8-(4x-3y-6p) \quad (5.4)$$

Referring to Ref [22] for further details, for Ge-In-Se system under consideration, it is seen to be tetrahedrally coordinated and the formal charge transfer would be from Se, leaving the

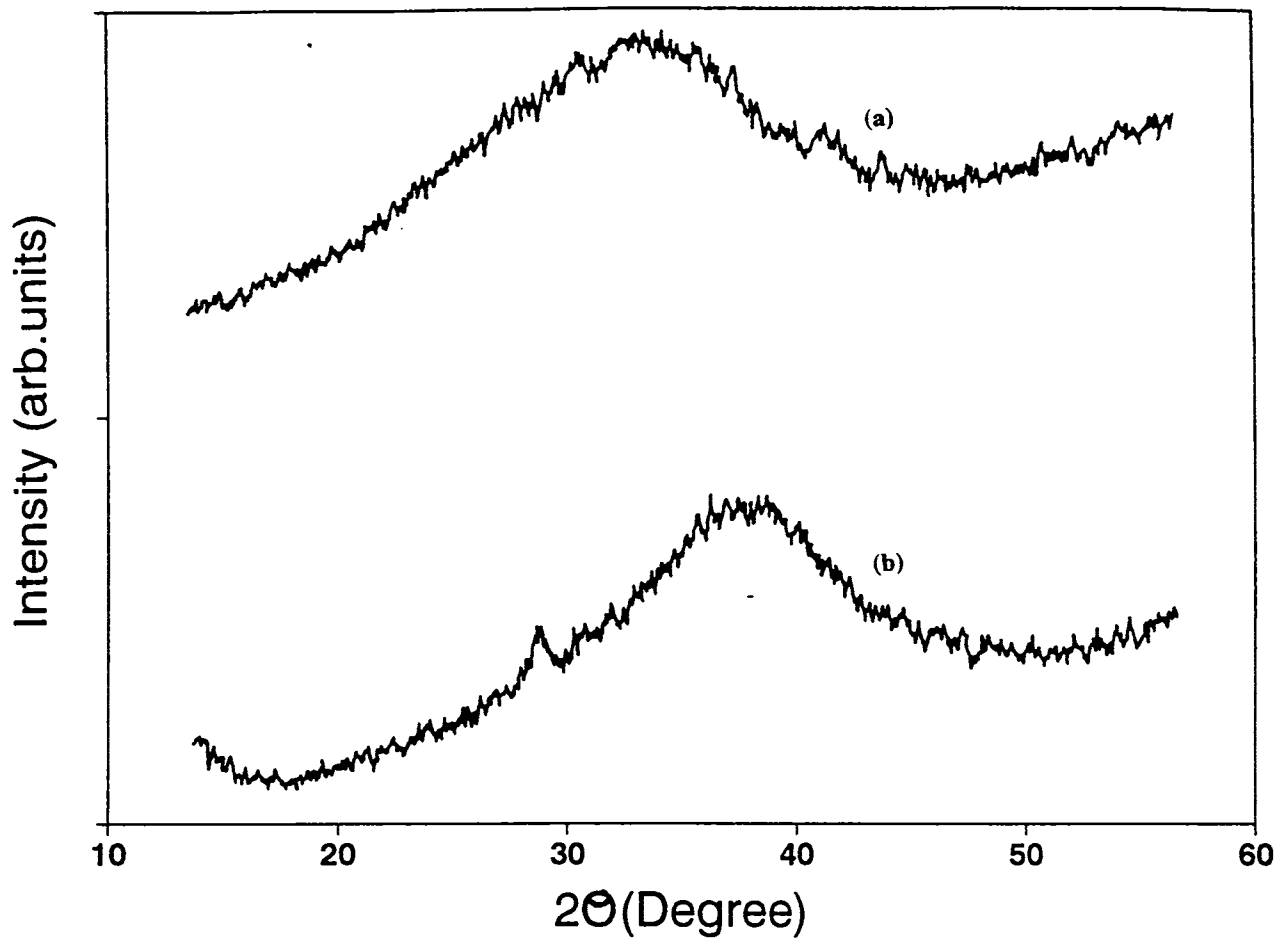


Fig. 5.1 X- ray diffraction pattern of (a) $\text{Ge}_{13}\text{In}_5\text{Se}_{82}$ and (b) $\text{Ge}_{26}\text{In}_5\text{Se}_{69}$ glasses.

normally four-fold coordinated Ge unchanged. For the evaluation of average coordination number of Se, $Z_{av}(\text{Se})$, this gives the formula

$$Z_{av}(\text{Se}) = (Z - 4x - 4y)/p \quad (5.5)$$

Also,

$$Z_{av}(\text{Se}) = (2p_2 + 3p_3 + 4p_4)/p \quad (5.6)$$

where p_2 , p_3 and p_4 are the number of two-, three- and four-fold coordinated Se atoms, respectively. Equation (5.4) to (5.6) yield

$$p_3 + 2p_4 = y$$

which shows that the number of extra chalcogen bonds relative to the normal two-fold coordination is uniquely determined by In concentration. Thus, equation (5.6) can be written as

$$Z_{av}(\text{Se}) = [2(p_2 + p_3 + p_4) + p_3 + 2p_4]/p \quad (5.7)$$

$$= (2p + y)/p \quad (5.8)$$

Equating (5.5) and (5.8) we get $Z = 4x + 5y + 2p$, a value already obtained in which a coordination of 5 was used for In, based on the (8- N) rule. A tetrahedral coordination has been indicated for In [23,24] in chalcogenide glasses. The glass forming regions of the system are shown in the phase diagram given in Fig.(5.2). For the $\text{Ge}_x\text{In}_5\text{Se}_{(95-x)}$ family, compositions with Z values from 2.39 to 2.85 could be prepared in the glass form.

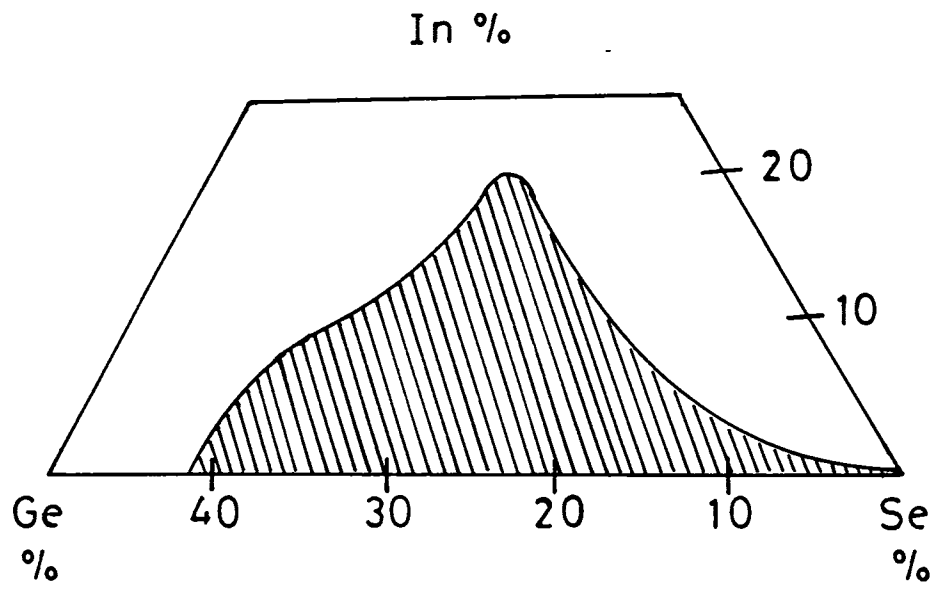


Fig. 5.2 Glass forming regions of Ge-In-Se system.

5.3 Experimental details

Optical band gap E_g is determined graphically by measuring the variation of the normalised PA signal as a function of incident wavelength. The PA spectrum for each sample has been normalized using the spectrum obtained with a highly absorbing carbon black sample. E_g has been determined as the energy at which the log PA amplitude versus energy plot deviates from the straight line region at higher absorption region as has already been described in chapter IV

The optical absorption spectra of all the samples have also been recorded with a UV-Vis-NIR spectrophotometer (Hitachi Model U-3410) for comparison. Powdered samples have been used for absorption studies.

Thermal diffusivity measurements have been carried out by the single beam PA phase lag method. Bulk samples of thickness approximately 0.5 mm and diameter 5 mm are used to carry out α measurements. The relative phase lag $\Delta\psi$ between the front and rear surfaces of illumination is measured at a single chopping frequency by rotating the PA cell about a vertical axis [25] by 180° . Thermal diffusivity is then calculated using the formula

$$\tan(\Delta\psi) = \tanh(a_s l_s) \tan(a_s l_s) \quad (5.9)$$

as has been explained in detail in chapter II.

5.4 Results and discussions

The variation of normalized PA signal as a function of wavelength in the samples investigated are shown in Figs.(5.3)and (5.4). Similarly, the optical absorption spectra obtained using UV-Vis-NIR spectrophotometer are shown in Figs. (5.5),(5.6) and (5.7). From each of the above the optical band gaps have been determined.

The variation of E_g with the average coordination number Z in these glasses using PA and UV-Vis-NIR absorption spectra are shown in Fig.(5.8). The E_g values determined from both the techniques are tabulated in Table 5.1 along with the Z values and the corresponding

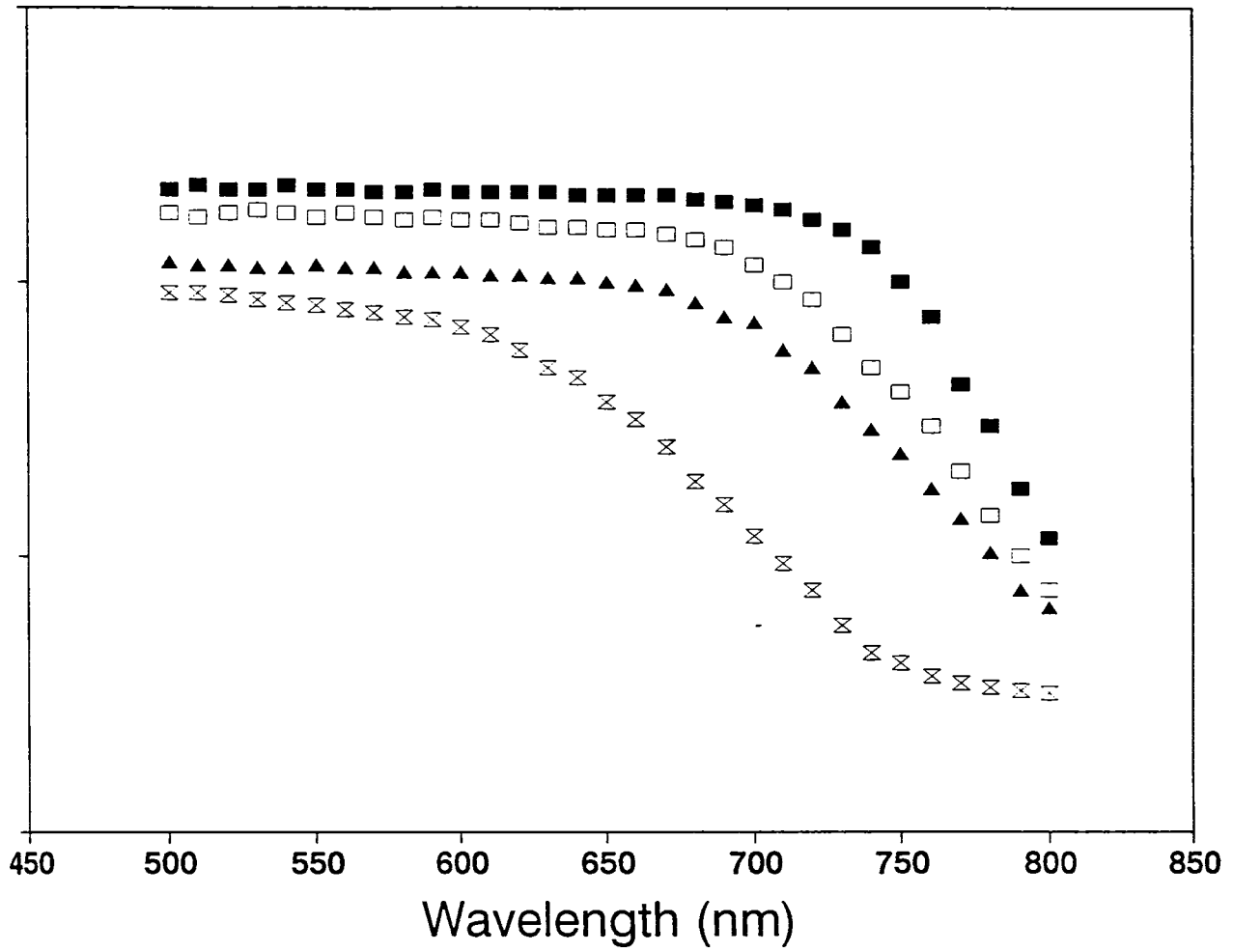


Fig. 5.3 PA spectra of $\text{Ge}_x\text{In}_5\text{Se}_{95-x}$ glasses.

(■) $\text{Ge}_{12}\text{In}_5\text{Se}_{83}$ (□) $\text{Ge}_{13}\text{In}_5\text{Se}_{82}$ (▲) $\text{Ge}_{16}\text{In}_5\text{Se}_{79}$ (X) $\text{Ge}_{18}\text{In}_5\text{Se}_{77}$.

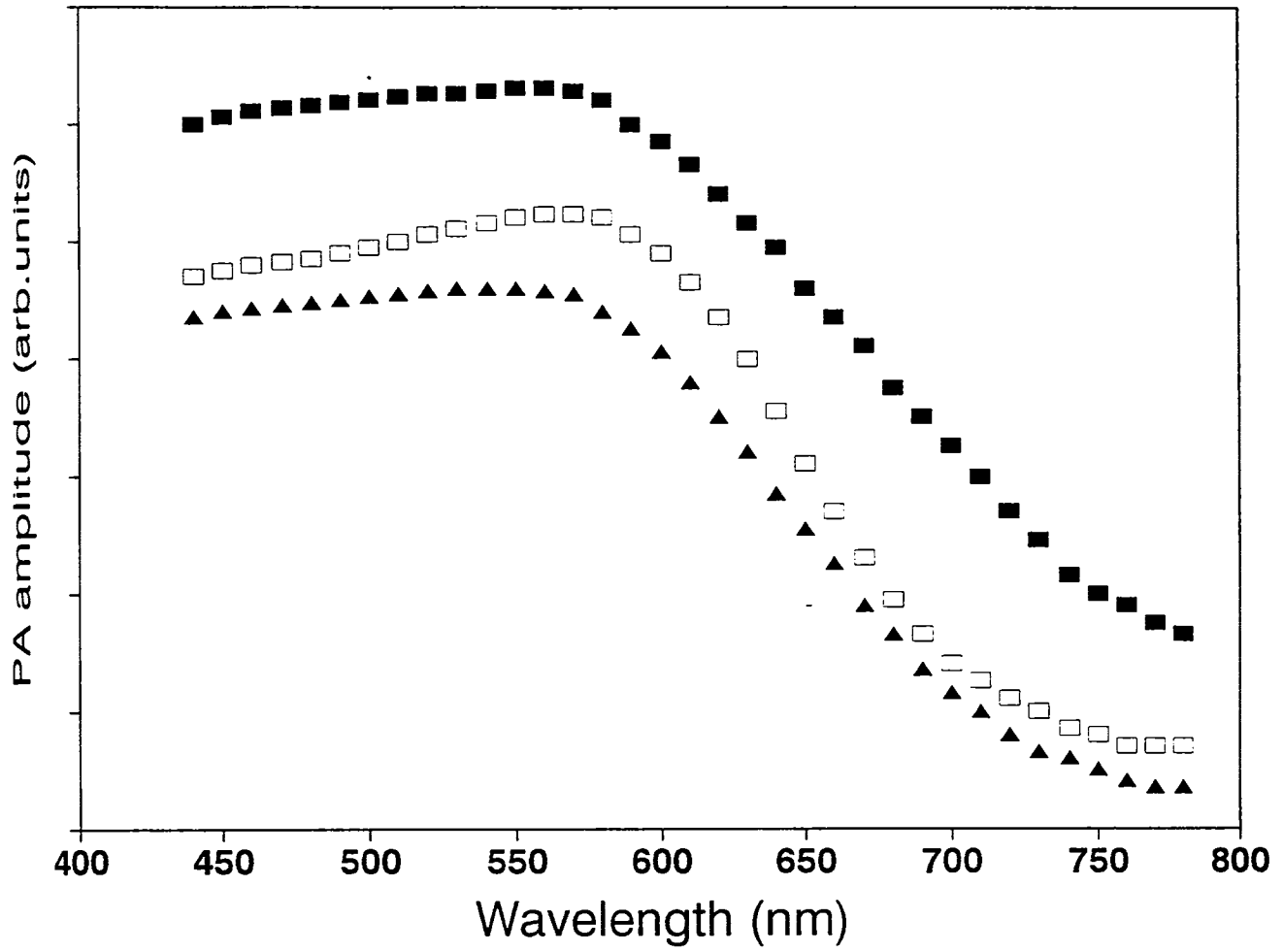


Fig. 5.4 PA spectra of $\text{Ge}_x\text{In}_5\text{Se}_{95-x}$ glasses.
(■) $\text{Ge}_{29.5}\text{In}_5\text{Se}_{65.83}$ (□) $\text{Ge}_{30}\text{In}_5\text{Se}_{65}$ (▲) $\text{Ge}_{32}\text{In}_5\text{Se}_{63}$.

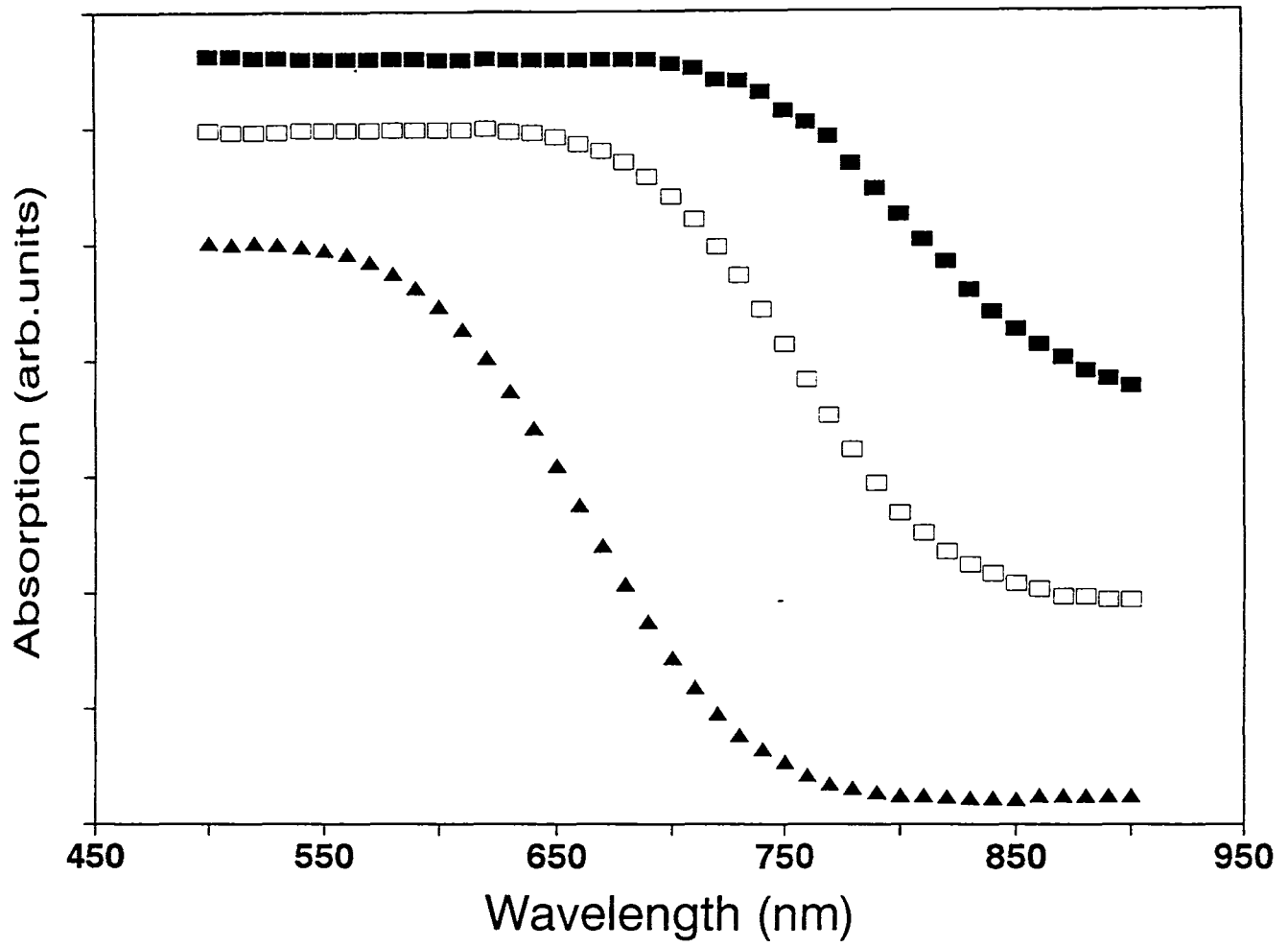


Fig. 5.5 UV-Vis - NIR spectra of $\text{Ge}_x\text{In}_5\text{Se}_{95-x}$ glasses.
 (■) $\text{Ge}_{12}\text{In}_5\text{Se}_{83}$ (□) $\text{Ge}_{16}\text{In}_5\text{Se}_{79}$ (▲) $\text{Ge}_{18}\text{In}_5\text{Se}_{77}$.

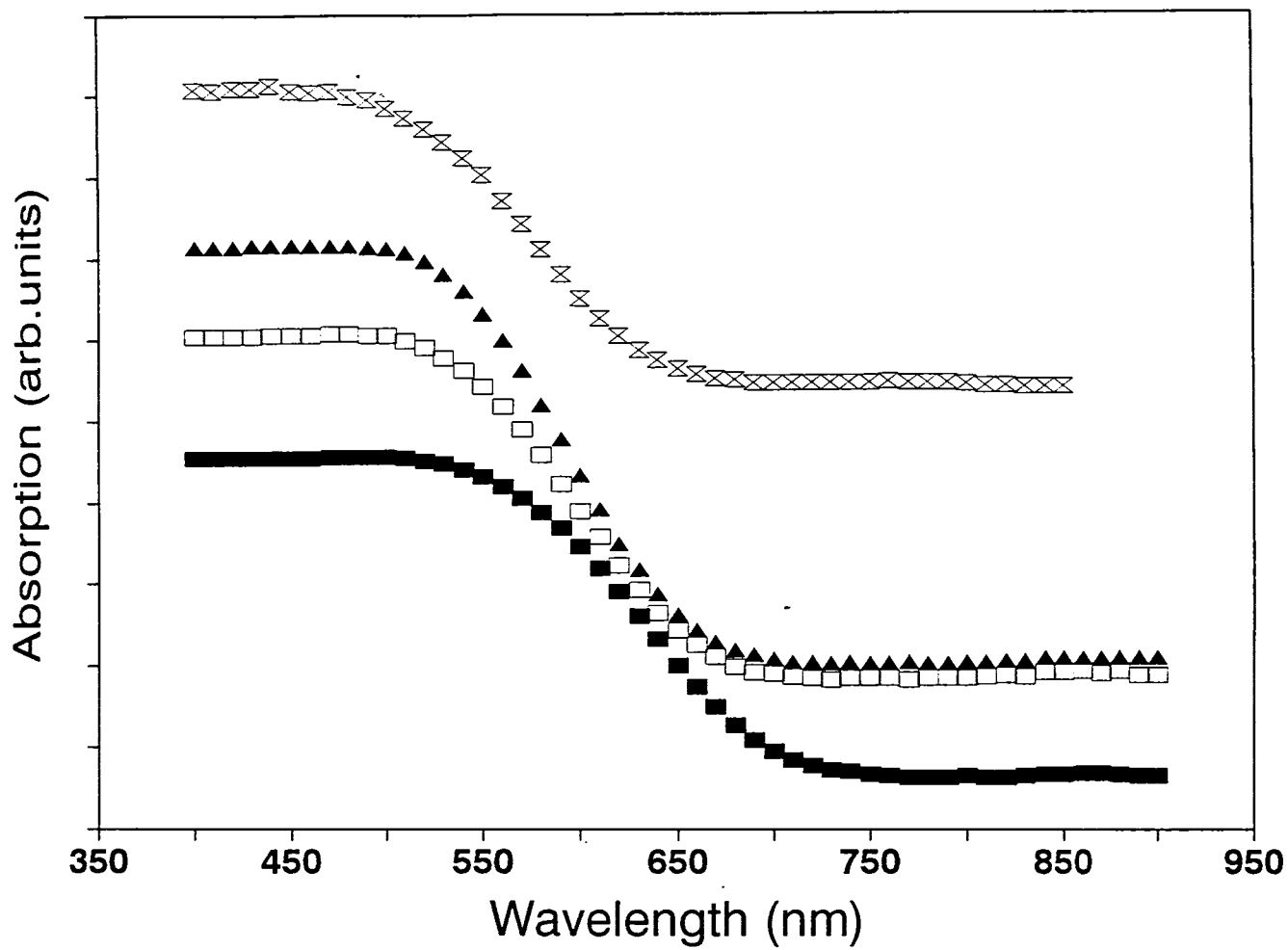


Fig. 5.6 UV-Vis - NIR spectra of $\text{Ge}_x\text{In}_5\text{Se}_{95-x}$ glasses.
 (■) $\text{Ge}_{22}\text{In}_5\text{Se}_{73}$ (□) $\text{Ge}_{25}\text{In}_5\text{Se}_{70}$ (▲) $\text{Ge}_{26}\text{In}_5\text{Se}_{69}$ (⊗) $\text{Ge}_{28}\text{In}_5\text{Se}_{67}$.

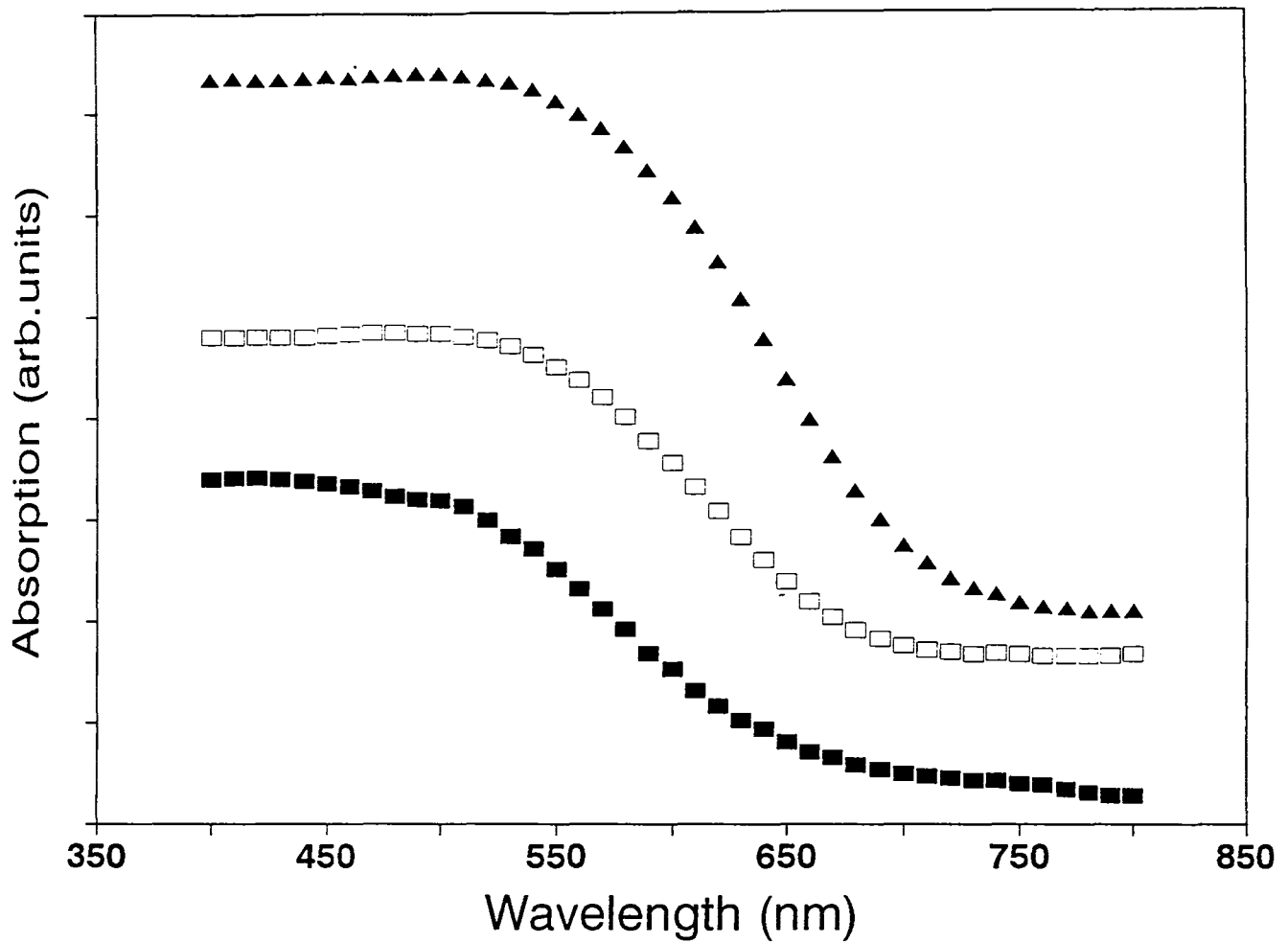


Fig. 5.7 UV - Vis - NIR spectra of $\text{Ge}_x\text{In}_5\text{Se}_{95-x}$ glasses.
 (■) $\text{Ge}_{29.17}\text{In}_5\text{Se}_{65.73}$ (□) $\text{Ge}_{30}\text{In}_5\text{Se}_{65}$ (▲) $\text{Ge}_{32}\text{In}_5\text{Se}_{63}$.

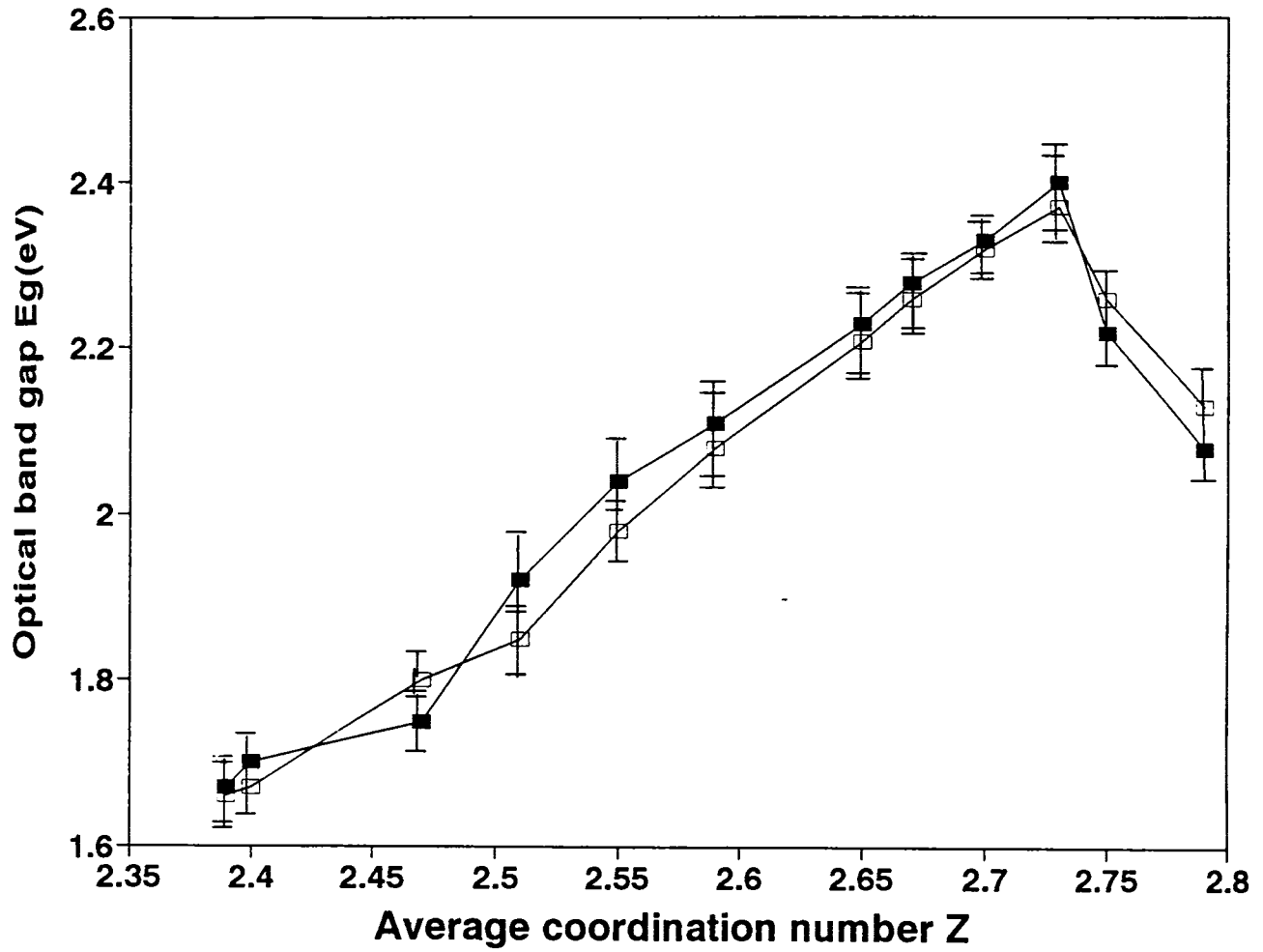


Fig. 5.8 Variation of the optical band gap E_g with average coordination number Z for the $\text{Ge}_x\text{In}_5\text{Se}_{95-x}$ glasses using PA technique (■) and UV-Vis-NIR absorption technique (□).

Table 5.1

Average co-ordination number Z , optical band gap E_g and thermal diffusivity α of
Ge - In - Se glasses.

| Composition | | | Z | E_g (eV) | | α $10^{-2} \text{ cm}^2 \text{ s}^{-1}$ |
|-------------|-----|-------|------|--------------|-------------------|---|
| Ge: | In: | Se: | | PA technique | UV-Vis-NIR method | |
| 12 | 5 | 83 | 2.39 | 1.67 | 1.66 | 0.76 |
| 13 | 5 | 82 | 2.41 | 1.70 | 1.67 | 1.41 |
| 16 | 5 | 79 | 2.47 | 1.75 | 1.80 | 1.21 |
| 18 | 5 | 77 | 2.51 | 1.92 | 1.85 | 0.99 |
| 20 | 5 | 75 | 2.55 | 2.04 | 1.98 | 0.88 |
| 22 | 5 | 73 | 2.59 | 2.11 | 2.08 | 0.95 |
| 25 | 5 | 70 | 2.65 | 2.23 | 2.21 | 1.48 |
| 26 | 5 | 69 | 2.67 | 2.28 | 2.26 | 1.63 |
| 28 | 5 | 67 | 2.70 | 2.33 | 2.32 | 1.48 |
| 29.17 | 5 | 65.83 | 2.73 | 2.40 | 2.37 | 1.18 |
| 30 | 5 | 65 | 2.75 | 2.22 | 2.26 | 0.95 |
| 32 | 5 | 63 | 2.79 | 2.08 | 2.13 | 0.69 |

compositions. The uncertainty in the values of E_g is of the order of 2%. It is found that E_g increases with increasing Ge content upto the tie-line composition corresponding to $Z = 2.73$ and decreases thereafter for Ge-rich glasses. The variation of thermal diffusivity with Z is shown in Fig.(5.9). These values are also tabulated in Table 5.1. The estimated error in thermal diffusivity values is lower than 4%.

The peak in the value of E_g occurring at the chemical threshold corresponding to $Z=2.73$ can be attributed to the chemical ordering taking place in these glasses. In the COCN model for atomic arrangement in glasses, the formation of heteropolar bonds is always favoured over the formation of homopolar bonds. In Se-rich glasses, the 2-fold coordination of Se causes the glassy network to be dominated by flexible chains of Se. The addition of elements of higher coordination results in the branching of chains. For a compound with the general formula A_xB_y , this model envisages only A-B type of bonds for the tie-line composition, A-B and A-A types of bonds for B-rich compositions. If we assume chemical ordering for the Ge-In-Se glasses, the glass structure can be pictured as being made up of cross-linked three-dimensional structural units of $GeSe_2$ and In_2Se_3 with excess of Ge or Se dispersed among these units. The composition $Ge_{29.17}In_5Se_{65.83}$ which shows a maximum in E_g can be considered to be made up of completely cross-linked three-dimensional structural units of $GeSe_2$ and In_2Se_3 only with neither Ge or Se present in excess. For the Ge-rich (or Se-rich) compositions, some of the original Ge-Se bonds on the $GeSe_2$ structural units in the tie-line composition are replaced by Ge-Ge bonds (or Se-Se bonds) and consequently result in the corresponding change in various properties. The decrease in E_g for Se-rich compositions can be attributed to the replacement of strong heteropolar Ge-Se bonds with bond energy 55.4 kcal/mole by weak homopolar Se-Se bonds with bond energy 44 kcal/mole. The bond energies have been calculated following Paulings relation [26], using the listed electronegativities of the elements [27]. Similarly the decrease in E_g for Ge-rich compositions is rationalised on the basis that Ge-Se bonds are replaced by weaker Ge-Ge bonds with bond energy 49.1 kcal/mole. This results in the decrease in the average bond energy of the system. According to Kastner [6], in tetrahedral semiconductors (like Ge) with

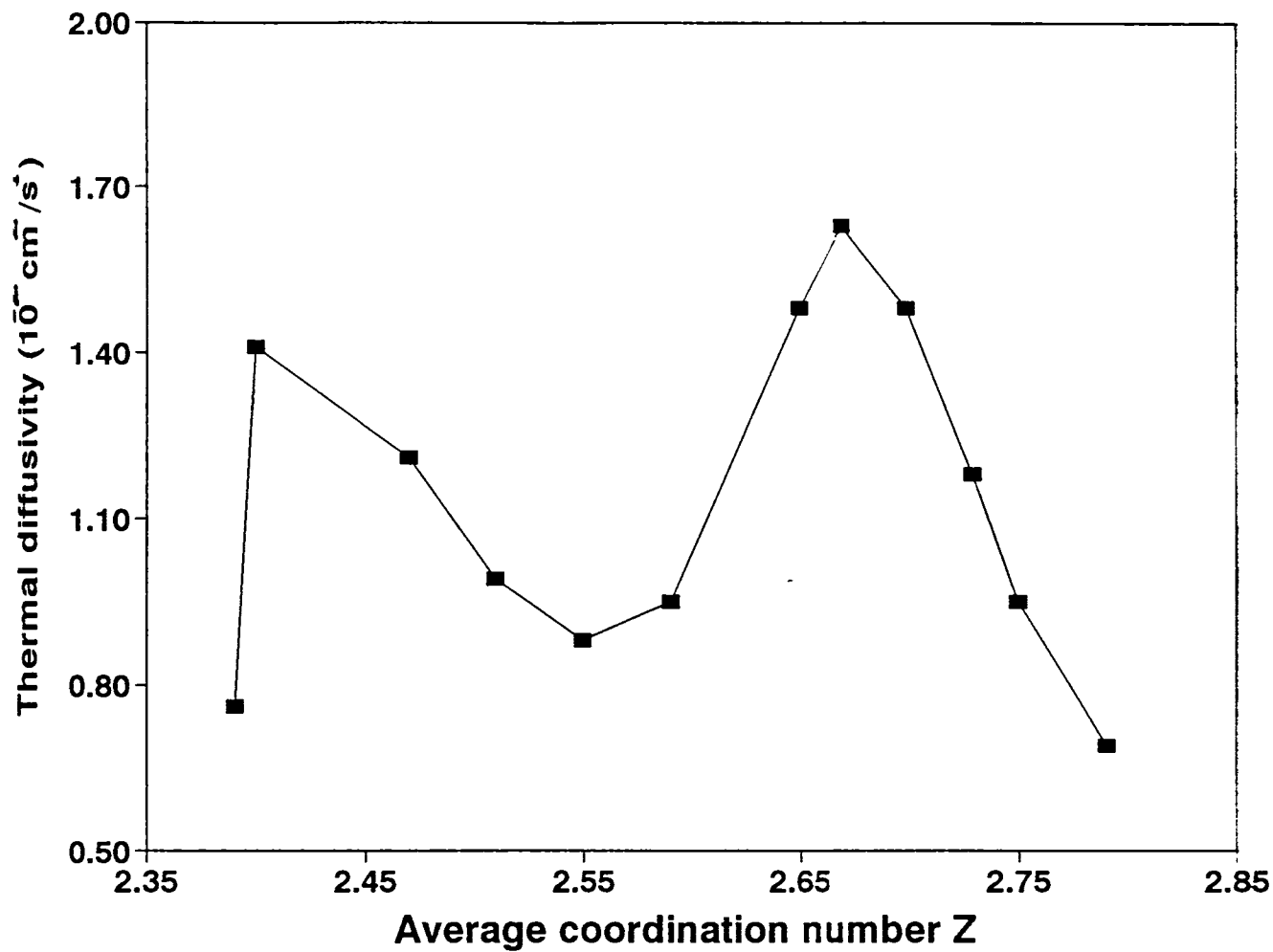


Fig. 5.9 Variation of thermal diffusivity α with average coordination number Z for $\text{Ge}_x\text{In}_5\text{Se}_{95-x}$ glasses.

its four-fold coordination, the hybridized sp^3 orbitals are split symmetrically into bonding (σ) and (σ^*) antibonding states. The bonding band forms the valence band and antibonding band form the conduction band. For Group VI elements, s-states lie much below the p-states and need not be considered. As only two of the 3p states are used for bonding, it is normally two-fold coordinated having one non-bonding electron pair which are called lone pair (LP) electrons. In solids these lone pair electrons form a band near the original p-state energy and σ and σ^* bands are split symmetrically with respect to this reference lone pair energy. Both the σ and L.P. bands are occupied so that the LP band becomes the valence band and σ^* band becomes the conduction band. The decrease in the average bond energy of the system tends to decrease the energy of the conduction band edge and thereby decrease E_g . The energy gap values of Ge-In-Se glasses reported from the data on activation energy for electrical conductivity also show an increase with Ge content upto the tie-line composition and thereafter it decreases for Ge-rich glasses [28]. The variation of glass transition temperature T_g with Z also report a maximum in T_g at $Z = 2.73$ [28]. The dependence of thermal diffusivity α on composition for these glasses show threshold maxima at $Z = 2.41$ and 2.67. No characteristic feature is observed at the chemical threshold corresponding to $Z = 2.73$ in these glasses. The peak at $Z = 2.41$ which lies very close to the critical average coordination number value predicted by Phillips and Thorpe can be explained on the basis of mechanical stiffening of the network at the critical composition due to threshold percolation of rigidity and the corresponding threshold in the internal stress of the system. When Z tends to 2.4, the network becomes more and more rigid and this correspondingly decreases the number of low frequency modes as explained in section 1 of this chapter. At $Z = 2.4$, the number of low frequency modes become zero offering minimum resistance to the propagating thermal waves due to reduced scattering by low frequency modes. This causes the observed maximum in α . Experimental results on elastic constants [29] and neutron scattering [30] support this argument. Scattering of the propagating thermal waves by low frequency modes for $Z < 2.4$ limits the value of α . Beyond $Z = 2.4$ the rigid regions get interconnected and

dominate the network giving rise to finite frequency modes such as the phonon modes characteristic of a rigid elastic network. Also the elastic forces are seen to build up fast giving rise to an increase in the values of elastic constants [3]. Normal phonon modes developed in the rigid network scatter the thermal waves which lead to a reduction in α for $Z > 2.4$.

The second maximum at the value of $Z = 2.67$ may be considered as due to the effect of topological change from two to three dimensional structure of the random network as predicted by Tanaka [9-11]. The change in dimensionality as Z increases reduces the flexibility of the network. The Ge-In-Se system can be considered to be made up of In-Se bonds dispersed in a three dimensional Ge-Se network. The Ge-Se bonds undergo mechanical stiffening at $Z = 2.4$. The In-Se structure prevalent in them form a layer like structure for $Z < 2.67$. So the material can be considered to be composed of a plane In-Se lattice laid in a three dimensional Ge-Se space. The layer structure of In-Se lattice is fully evolved at $Z = 2.67$ and the network undergoes a topological transition from 2D \rightarrow 3D structure at this composition. For $Z < 2.67$, the In-Se layers form a lattice misfit and act as scattering regions for the propagating thermal waves resulting in a reduced value for thermal diffusivity. As Z tends to 2.67 the lattice misfit decreases and a uniform three dimensional structure is evolved at $Z = 2.67$. This results in the observed maximum in α at 2.67. Beyond $Z = 2.67$, the elastic forces normally arising within a uniform three dimensional solid develops, giving rise to phonon modes which scatters the thermal waves causing further reduction in α for $Z > 2.67$. At the chemical threshold corresponding to $Z = 2.73$, the system as a whole forms a uniform stoichiometric glass.

5.5 Conclusion

The composition dependence of thermal diffusivity α of Ge-In-Se system investigated using the photoacoustic phase lag method have maxima at $Z = 2.41$ and 2.67, which are due to the floppy to rigid transition and a two to three dimensional structural transition

respectively occurring in these glasses. The optical band gap E_g versus Z data of these glasses show a maximum at the chemical threshold at $Z = 2.73$ of the system. The above results clearly shows the existence of effects due to topology and that due to chemical ordering in the system. Occurrence of a two dimensional network in a three dimensional lattice needs to be resolved with more experimentation. However, the results on Ge-In-Se glasses indicate that this is a model system in which a floppy to rigid transition associated with short range order, a two to three dimensional structural transition associated with medium range order and chemical order occur in the glass forming region at different average coordinations.

REFERENCES

1. J.C. Phillips, *J. Non-Cryst. Solids* **34**, 153 (1979).
2. M.F.Thorpe, *J. Non-Cryst. Solids* **57**, 355 (1983).
3. H.He and M.F.Thdorpe, *Phys. Rev. Lett.* **54**, 2107 (1985).
4. B.L.Halfpap and S.M.Lindsay, *Phys. Rev. Lett.* **57**, 847 (1986).
5. S.R.Ovshinsky, *Phys. Rev. Lett.* **36**, 1469 (1976).
6. M.Kastner, *Phys. Rev. Lett.* **28**, 355 (1972).
7. K.Tanaka, *Phys. Rev. B* **39**, 1270 (1990).
8. R.Zallen in *The Physics of Amorphous Solids* (Wiley, New York) (1983).
9. K.Tanaka, *Solid State Commun.* **60**, 295 (1986).
10. K.Tanaka, *J. Non-Cryst. Solids* **103**, 149 (1988).
11. K.Tanaka, *J. Non-Cryst. Solids* **97-98**, 391 (1987).
12. J.C.Phillips and M.F.Thorpe, *Solid State Commun.* **53**, 699 (1985).
13. P.Tronc, M.Bensoussan, A.Brenac and C.Sebenne, *Phys. Rev.B* **8**, 5947 (1973).
14. G. Lucovsky, F.L.Galeena, R.C.Keezer, R.H.Geils and H.A.Six, *Phys. Rev. B* **10**, 5134 (1974).
15. A.Rosencwaig in *Photoacoustics and Photoacoustic Spectroscopy*, (Wiley, New York) (1980).

16. A.C.Tam, *Rev. Mod. Phys.* **58**, 381 (1986).
17. V.P.Zharov and V.S.Letokhov in *Laser Optoacoustic Spectroscopy*, (Springer Series in Optical Sciences) Vol.37, (1986).
18. A.Zegadi, M.A.Slifkin, M.Djamin, A.E.Hill and R.P.Tomlinson, *Phys. Stat. Solidi(a)* **133**, 533 (1992).
19. D.Chen, *Appl. Phys. Lett.* **33**, 810 (1978).
20. A.K.Ghosh, K.K.Som, S.Chatterjee and B.K.Chaudhuri, *Phys. Rev.B* **51**, 4842 (1995).
21. S.R.Elliott in *Physics of Amorphous Materials* (Longman, London), chap.1 (1983).
22. J.Z.Liu and P.C.Taylor, *Solid State Commun.* **70**, 81 (1989).
23. F.Kosek, Z.Cimpl, M.P.Mikhailov and A.Karpova, *J.Non-Cryst. Solids* **86**, 265 (1986).
24. H.Fritzsche in *Proc. 7th Int. Conf. Amorphous and Liquid Semiconductors*, Edinburgh, 1977, ed. W.Spear 1977), p.3.
25. Sheenu Thomas, J. Isaac and J.Philip, *Rev. Sci. Instrum.* **66**, 3907 (1995).
26. L.Pauling in *The nature of Chemical Bond*, 3rd edn. (Cornell Univ. Press) (1960).
27. R.T.Sanderson in *Chemical Bonds and Bond Energy* . E.M.Loeb (Academic Press, New York) (1976).
28. S.Mahadevan and A.Giridhar, *J. Non-Cryst. Solids* **152**, 42 (1993).
29. S.S.Yun, H.Li, R.L.Cappelletti, P.Boalchand and R.N.Enzweiler, *Phys. Rev.B* **39**, 8702 (1989).
30. P.Boalchand, R.N.Enzweiler, R.L.Cappelletti, W.A.Kamitakahara, Y.Cai and M.F.Thorpe, *Solid State Ionics* **39**, 81 (1990).

CHAPTER VI

OPTICAL AND THERMAL PROPERTIES OF Bi-DOPED Ge-Se GLASSES

6.1 Introduction

The effect of impurities on the electronic properties of germanium chalcogenides have been a subject of great interest ever since their synthesis [1]. In recent years, a great deal of effort has been expended to understand the role of Bi or Pb in controlling the mechanism of electrical conduction in bulk chalcogenide glasses. It is known that bulk semiconducting glasses behave like intrinsic p-type semiconductors and are insensitive to impurity doping. Fermi level is considered to be pinned due to the equilibrium between the positively and negatively charged dangling bonds [2,3]. But Bi or Pb doped germanium chalcogenides show a carrier-type reversal (CTR) from p to n type at a certain doping level. This phenomenon of CTR was first observed in Ge-Bi-Se glasses [4,5] and subtle changes around the critical Bi concentration, which is seen to occur in the vicinity of $x = 7$ at % in $\text{Ge}_{20}\text{Bi}_x\text{Se}_{80-x}$ glasses, have been reported. Their projected technological applications are in the manufacture of new class of p - n junctions [6] based entirely on glasses which offer many manufacturing advantages [7]. Electrical resistivity, thermoelectric power and optical absorption coefficient measurements on Ge-Bi-Se system by Tohge et al [8] shows a gradual decrease in resistivity with increasing Bi content up to 9 at. % and decreased by about four orders of magnitude between $x = 9$ and 10% but remain almost constant for $x > 10$ at.%. Composition dependence of Seebeck coefficient shows that glass containing 7.5 at.% of Bi is p-type, similar to other melt quenched chalcogenide glasses, but incorporation of more than 9 at.% of Bi changes it to n-type. They also report from optical band gap measurements that incorporation of 2.5

at.% of Bi into $\text{Ge}_{20}\text{Se}_{80}$ glass results in decrease of E_g by as large as 0.65 eV, further addition of Bi causes only very small change in E_g and it is maintained constant for glasses containing more than 7.5 at.% of Bi. There are reports that heat capacity (C_p) measurements at 323K show a drastic change between $x = 6$ and 8 at.% [9]. δC_p , which is the difference between specific heats of glass and supercooled liquid, also show a maximum at 8 at.% of Bi. The d.c. electrical resistance measured on this sample shows an anomaly around $x = 8$ at.% of Bi [10]. In order to account for the observed variations in thermoelectric power, high pressure electrical resistivity etc. in Ge-Pb-Se glasses, which is another system exhibiting CTR and properties similar to the Ge-Bi-Se system, a structural model based on chemical nature of the constituents has been proposed [11] where the $p \rightarrow n$ transition has been attributed to the energetic disposition of the $sp^3 d^2$ band of Pb atoms, which is located closely above the lone pair band of Se. The CTR behaviour observed in Bi containing chalcogenide glasses has also been accounted for by this model by these authors. Several mechanisms have been proposed to account for the influence of Bi doping in Ge-Se system. Analysis based on network modelling led Phillips [12] and Nagels et al [13] to conclude that CTR occurs in the vicinity of the percolation threshold and is the result of transport anomalies in the system. Studies of electrical, thermoelectric and optical properties as a function of composition led Tohge et al [8] to explain the transport mechanism on the basis of chemical bonds. Based on EXAFS data, Elliot and Steel [14] have discussed the reason for this mechanism as due to the formation of partially ionic Bi-chalcogen bonds and subsequent unpinning of the Fermi level. An alternate discussion by Storiopoulous and Fuhs [15] leads to the explanation that a drastic decrease in band gap induces an increase of conductivity and a reversal of conduction type. In all these models a chemically ordered network model is assumed for the glass structure in which formation of heteropolar bonds is favoured over homopolar bonds. Investigations on composition dependence of resistivity, heat capacity etc. are in accordance with the Phillips model where the assumptions made are that these

glasses are inhomogeneous on the medium range scale and at a critical composition of the medium with p-type conduction, transition to n-type occurs. The purpose of the present work is to test whether any unusual feature is reflected in the composition dependence of optical and thermal properties of Bi doped Ge-Se glasses.

6.2 Experimental Method

Bulk semiconducting glasses with the general formula $\text{Ge}_{20}\text{Bi}_x\text{Se}_{80-x}$ ($0 \leq x \leq 12$) have been prepared in fused silica ampoules by the conventional melt-quenching technique, starting with appropriate quantities of 5N purity elements. The cooling rate required to obtain uniform glasses from the melt is ~ 200 K/s. The samples have been checked for vitreous nature by recording their X-ray powder diffraction spectra. The XRD patterns of typical samples prepared are shown in Fig.(6.1). The largest region of glass formation with bismuth was obtained for alloys with 20 to 30 at.% of Ge and 70 to 80 at.% of Se [8]. It is seen that for 20 at. % of Ge, the maximum bismuth content that can be incorporated into these glasses is 13 at.%, remaining being Se as shown in the phase diagram in Fig.(6.2). Since these glasses have high crystallising ability it is seen that further increase of bismuth gives partially crystallised glasses.

Measurement of the thermal diffusivity α of this system has been carried out using the PA technique. The basic principle and method of measuring thermal diffusivity employing PA phase lag technique are already discussed in the previous chapters. For measuring E_g values using UV-Vis-NIR absorption method powdered samples have been used. Bulk glasses of diameter ≈ 5 mm and thickness ≈ 0.5 mm are used to carry out thermal diffusivity measurements.

6.3 Results and Discussions

The optical absorption spectra recorded using UV-Vis-NIR absorption spectrophotometer [Hitachi Model U-3410] are shown in Figs.(6.3 and 6.4). The composition dependence of the optical band gap E_g is shown in Fig.(6.5). From this figure it is seen that

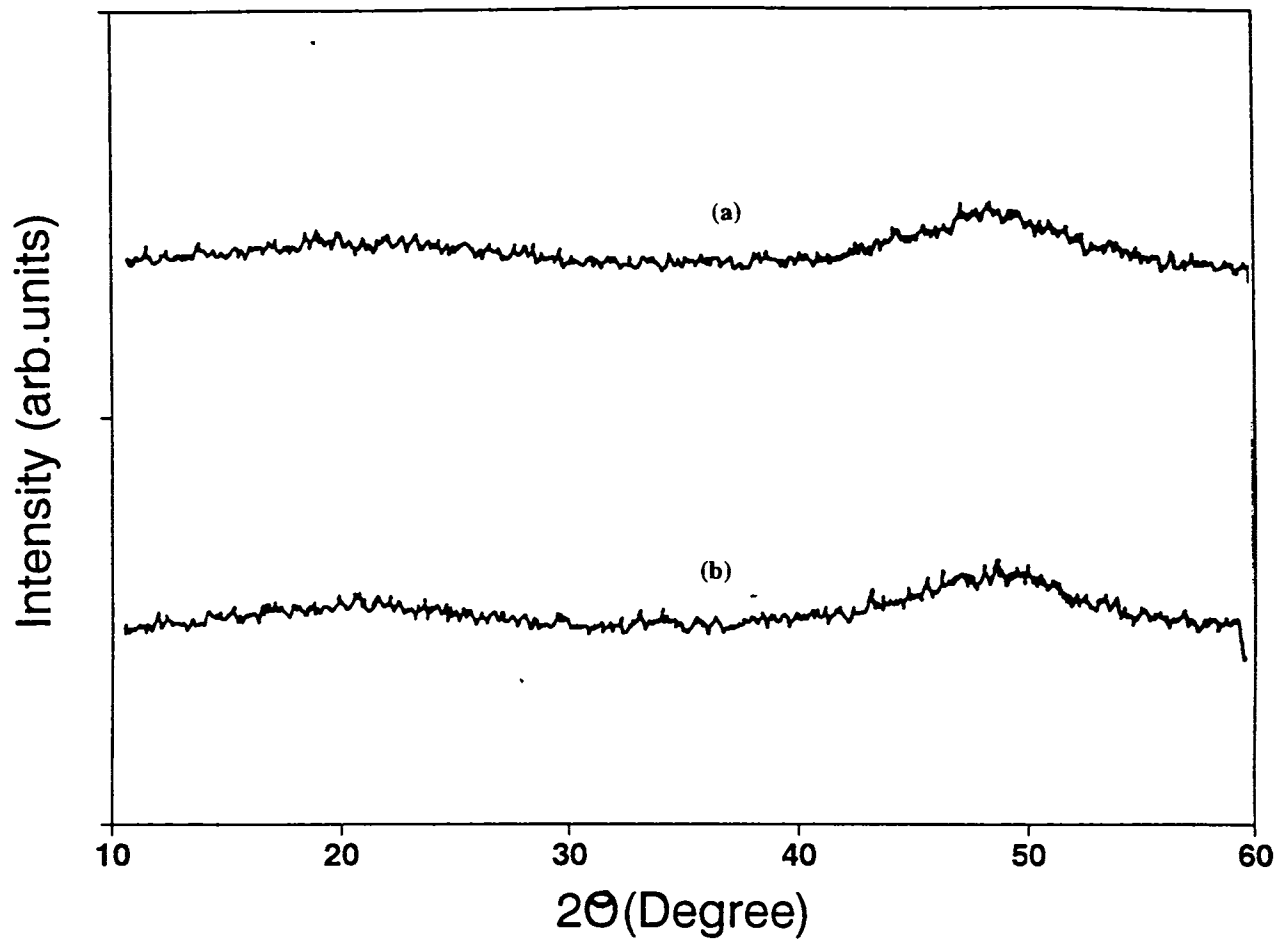


Fig. 6.1 X- ray diffraction pattern of (a) $\text{Ge}_{20}\text{Bi}_5\text{Se}_{75}$ and (b) $\text{Ge}_{20}\text{Bi}_{10}\text{Se}_{70}$ glasses.

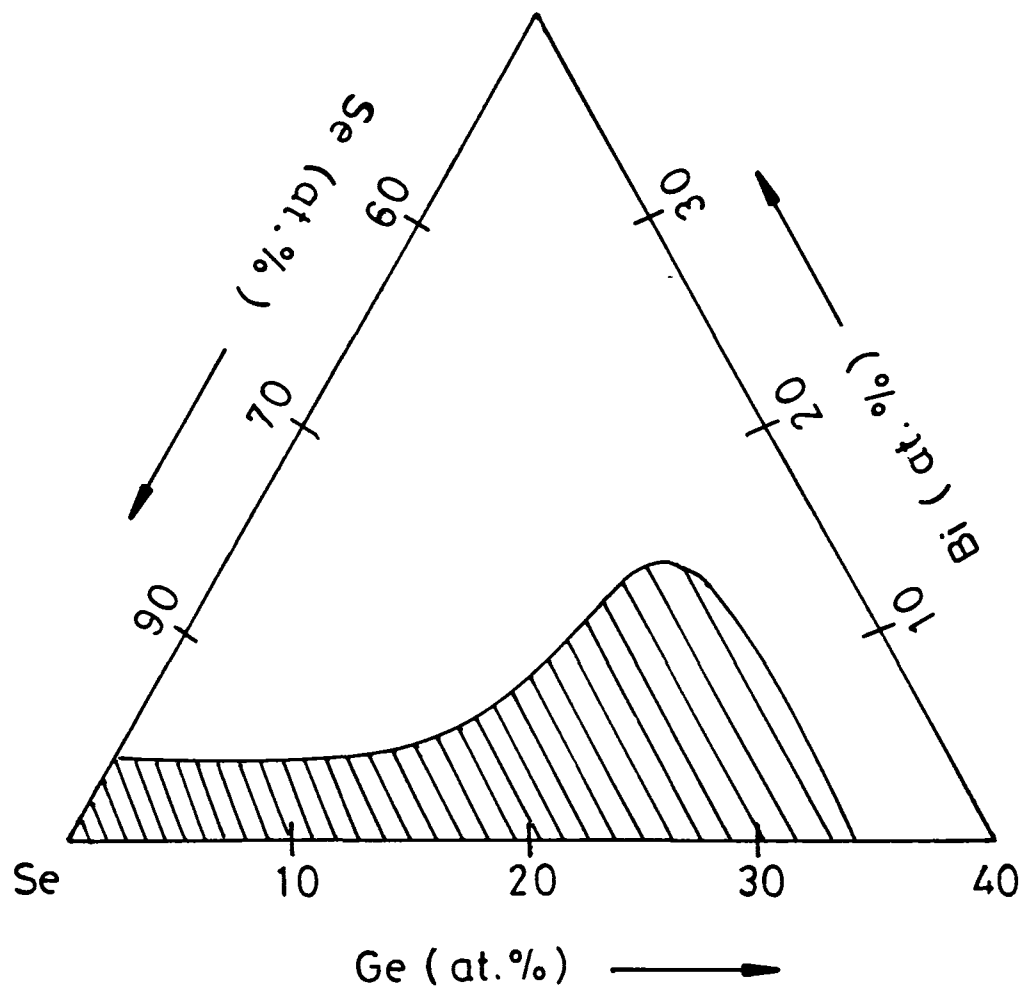


Fig. 6.2 Glass forming regions of Ge-Bi-Se system.

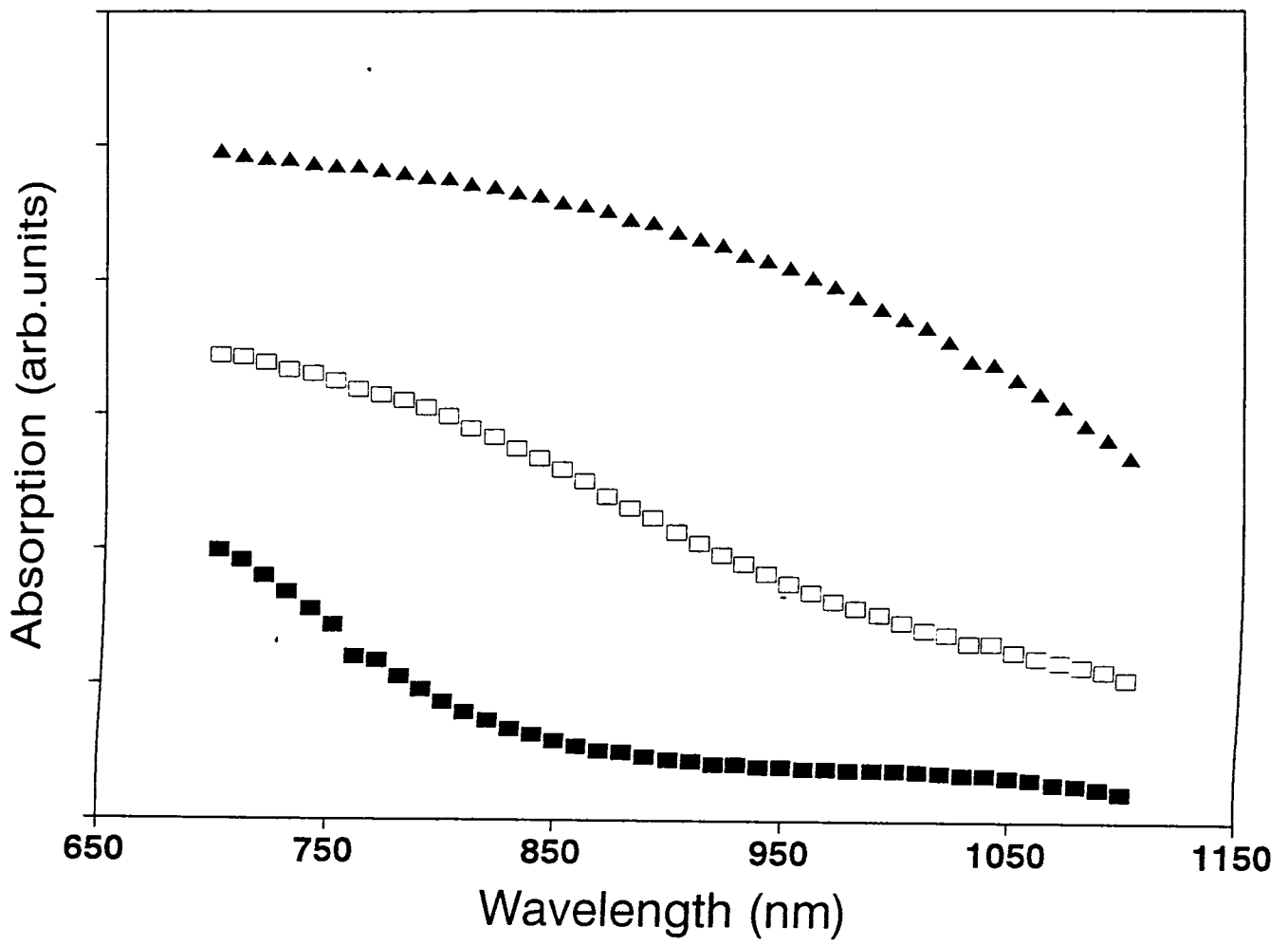


Fig. 6.3 UV-Vis - NIR spectra of $\text{Ge}_{20}\text{Bi}_x\text{Se}_{80-x}$ glasses.
 (■) $\text{Ge}_{20}\text{Bi}_2\text{Se}_{78}$ (□) $\text{Ge}_{20}\text{Bi}_4\text{Se}_{76}$ (▲) $\text{Ge}_{20}\text{Bi}_7\text{Se}_{73}$.

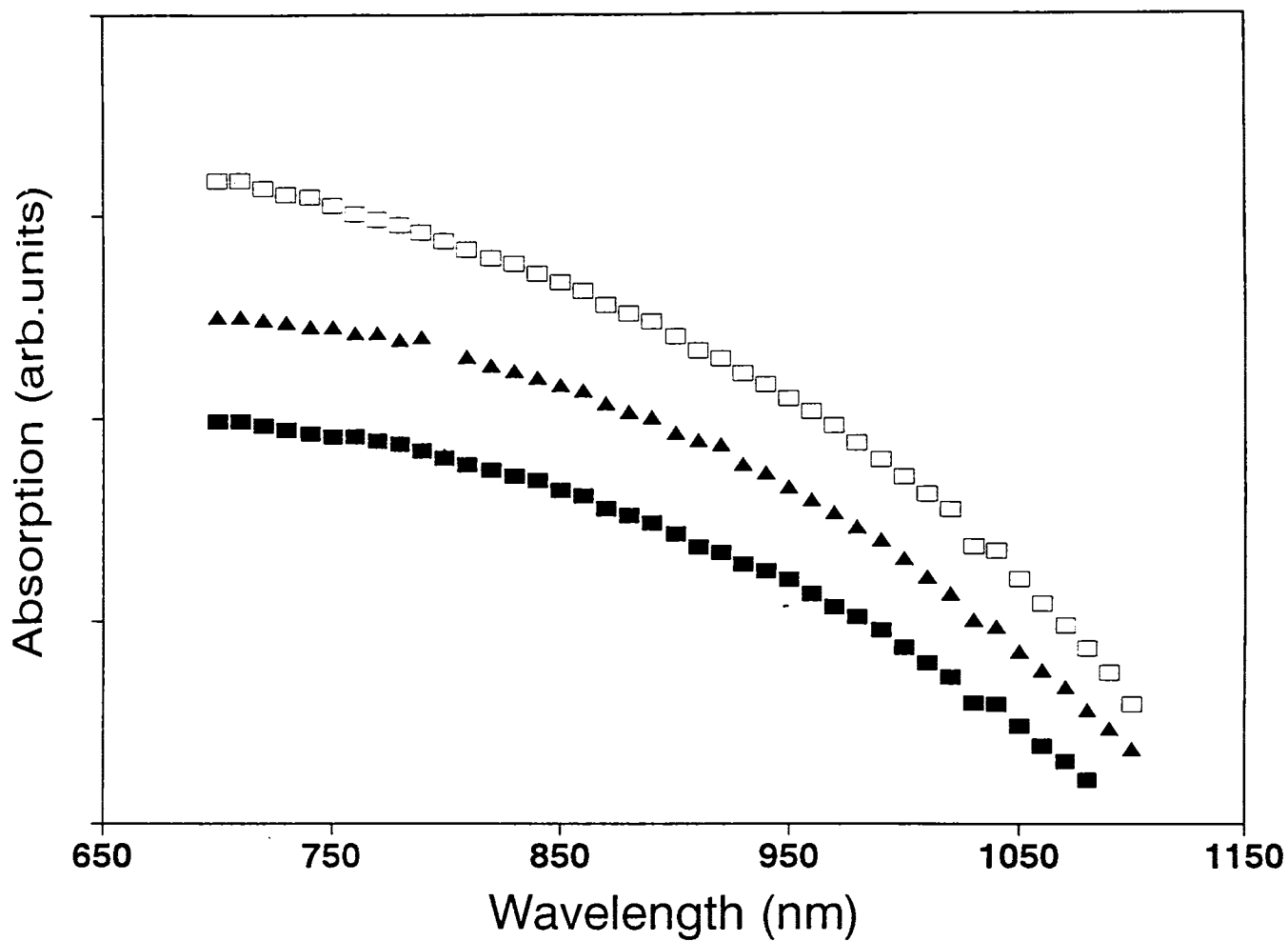


Fig. 6.4 UV-Vis - NIR spectra of $\text{Ge}_{20}\text{Bi}_x\text{Se}_{80-x}$ glasses.
(■) $\text{Ge}_{20}\text{Bi}_8\text{Se}_{72}$ (□) $\text{Ge}_{20}\text{Bi}_{10}\text{Se}_{70}$ (▲) $\text{Ge}_{20}\text{Bi}_{12}\text{Se}_{68}$.

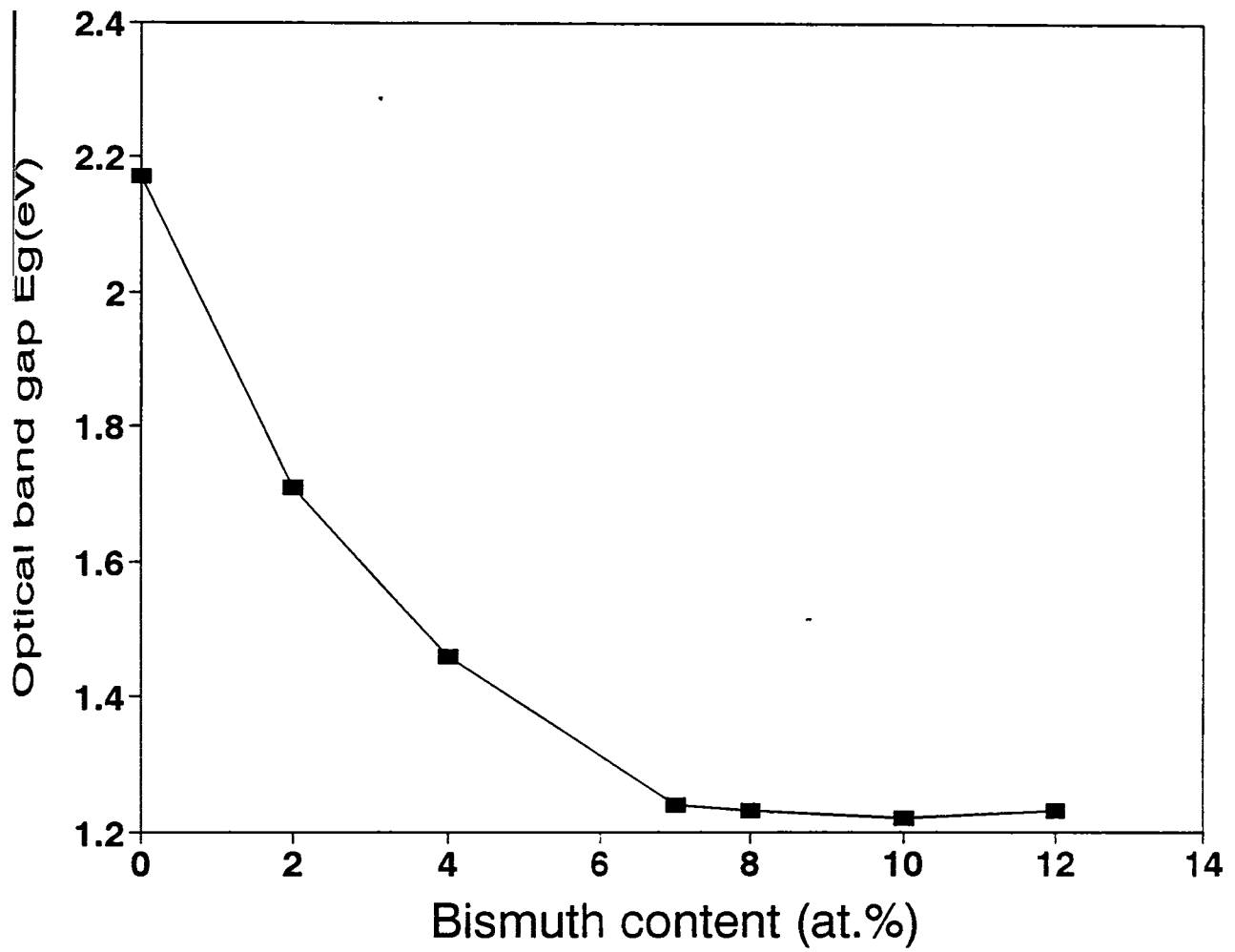


Fig. 6.5 Variation of the optical band gap E_g with average coordination number Z for the $\text{Ge}_{20}\text{Bi}_x\text{Se}_{80-x}$ glasses using UV-Vis-NIR absorption technique.

the variations of E_g with the incorporation of more than 2 at.% of bismuth is very small and it remains constant for glasses containing more than 7 at.% of Bi. The addition of approximately 2 at.% of Bi into $\text{Ge}_{20}\text{Se}_{80}$ glass results in the decrease of E_g by 0.56 eV. This is in good agreement with the corresponding values reported by Tohge et al [8] where the addition of 2.5 at.% of Bi into $\text{Ge}_{20}\text{Se}_{80}$ glass result in the decrease of E_g by 0.65 eV.

The measured composition dependence of thermal diffusivity of $\text{Ge}_{20}\text{Bi}_x\text{Se}_{80-x}$ ($0 \leq x \leq 12$) glasses is shown in Fig(6.6). It is seen that α increases gradually with bismuth content up to 7 at.% of Bi, beyond which it decreases at a faster rate.. The optical band gap and thermal diffusivity values determined using UV-Vis-NIR spectrophotometer and photoacoustic technique respectively are tabulated in Table 6.1 along with the corresponding compositions. The mechanisms responsible for carrier type reversal and the peculiar variation in thermal conduction in these glasses can be explained in terms of the electronic and structural inhomogeneity models respectively. In the electronic model, the various defect configuration of Bi are invoked which brings about the unpinning of the Fermi level due to the perturbation of valence alteration pairs [VAPS] [16]. Structural inhomogeneity model assumes the glass to be phase separated with n-type Bi_2Se_3 submicroscopic entities embedded in the Ge-Se glass matrix [10]. Measurements on double stage crystallisation give evidences for phase separation in these glasses [9].

Phillips and Thorpe have discussed in detail the features of the mechanical constraints theory in many of their papers [12,17]. For binary glasses belonging to $\text{IV}_x - \text{VI}_{(100-x)}$ group, they have predicted the critical composition to be around $x = 20$ at.% which corresponds to an average co-ordination number of $Z = 2.4$. Evaluation of Z for $\text{Ge}_{20}\text{Bi}_x\text{Se}_{80-x}$ glasses, treating this as a pseudobinary system, show that the value of x at which Z attains the critical value 2.4 is 7. However, for $\text{Ge}_x\text{Se}_{(100-x)}$ glasses, this value is found to be at a slightly higher composition of $x_c = 23$ at.%, which is attributed to the fact that not all bond bending constraints are effective in hindering intercluster motions [18]. There are reports that Bi_2Se_3 are n-type semiconductors [12,19] and in $\text{Ge}_{20}\text{Bi}_x\text{Se}_{(80-x)}$ glasses, the Bi_2Se_3 clusters are embedded in the Ge-Se glass matrix. The $\text{Ge}_{20}\text{Bi}_x\text{Se}_{80-x}$ glasses can be represented as

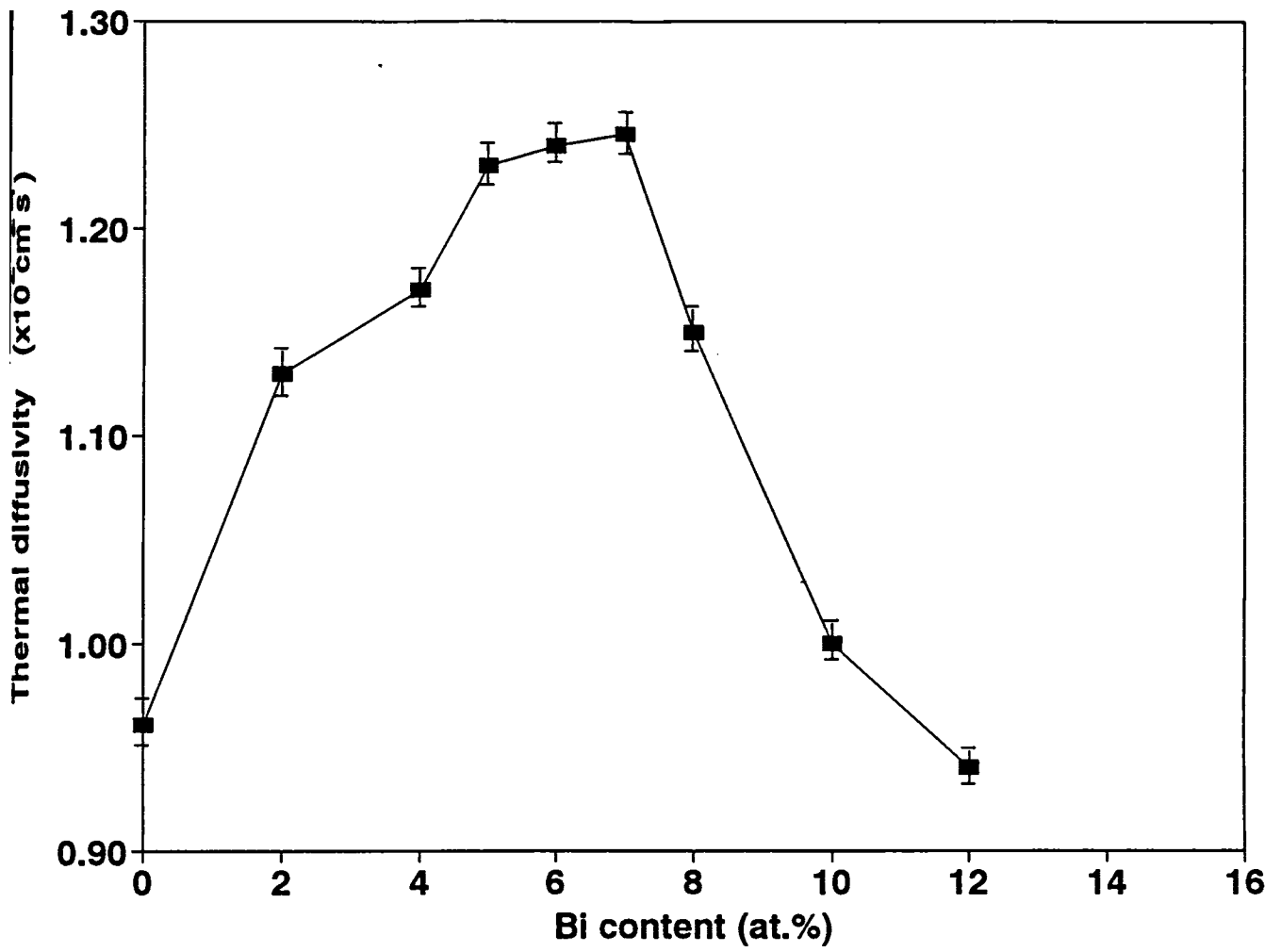


Fig. 6.6 Variation of thermal diffusivity α with average coordination number Z for $\text{Ge}_{20}\text{Bi}_x\text{Se}_{80-x}$ glasses.

Table 6.1

Composition dependence of thermal diffusivity α and energy gap E_g of Ge-Bi-Se glasses.

| Composition | | | Z | α | E_g (eV) |
|-------------|-----|----|------|---|---------------------|
| Ge: | Bi: | Se | | ($10^{-2} \text{ cm}^2 \text{ s}^{-1}$) | (UV-Vis-NIR method) |
| 20 | 0 | 80 | 2.40 | 0.93 | 2.17 |
| 20 | 2 | 78 | 2.42 | 1.13 | 1.71 |
| 20 | 4 | 76 | 2.44 | 1.17 | 1.46 |
| 20 | 5 | 75 | 2.45 | 1.23 | - |
| 20 | 6 | 74 | 2.46 | 1.24 | 1.32 |
| 20 | 7 | 73 | 2.47 | 1.25 | 1.24 |
| 20 | 8 | 72 | 2.48 | 1.15 | 1.23 |
| 20 | 10 | 70 | 2.50 | 1.00 | 1.22 |
| 20 | 12 | 68 | 2.52 | 0.94 | 1.23 |

$\text{Ge}_{20}\text{Se}_{80-5z} + \text{Bi}_{2z}\text{Se}_{3z}$. According to Phillips, when the Bi content is appreciably low, localised unconstructed Se^- defects are present in the Bi_2Se_3 tetradymite surfaces which are dispersed uniformly in the rest of GeSe_2 and Se flexible chains making them p-type semiconductors. At 6 at.% of Bi, the Bi_2Se_3 clusters retain in the melt. Also, $x = 6$ corresponds to $\text{Ge}_{20}\text{Se}_{65}\text{-Bi}_6\text{Se}_9$ and $\text{Ge}_{20}\text{Se}_{65} = \text{Ge}_{20}\text{Se}_{(100-y)}$ with $y = 24$ which agrees with the elastic stiffness threshold composition $y_c = 23$ of the glasses found in other experiments [18]. At $x \geq 6$ at.%, the Bi_2Se_3 tetradymite clusters find themselves in a matrix of increased mechanical rigidity and the mechanical misfit between the clusters become high which lead to a plastic deformation of these clusters. This give rise to an increase in Se^- defects which evolve in a percolative manner at the mechanical threshold and produce n-type conduction in these glasses. In terms of chemical bond formation, the carrier-type reversal from p-type to n-type is related to the formation of fairly large number of Bi-Se bonds and the disappearance of Se-Se bonds at this critical composition. According to the charged dangling bond model, the equilibrium between the positively and negatively charged dangling bonds which pins the Fermi level is affected maximum at this critical composition by charged impurities [4]. Vaidyanathan et al [11] have considered these glasses as a pseudobinary system with Bi acting as modifiers to the basic $\text{Ge}_{20}\text{Se}_{80}$ network. The modification of the host network makes the Fermi level move towards the conduction band edge and alters the conduction mechanism from p-type to n-type. They have also proposed a structural model to explain the phenomenon of CTR.

The dependence of thermal diffusivity α on Bi content of these glasses shows a threshold maximum around 7 at.% of Bi which lies very close to the value predicted by the constraints model. In the light of the earlier reports on phase separation in these glasses, the increase in α up to $x = 7$ can be attributed to the mechanical stiffening of Ge-Se network with the Bi_2Se_3 clusters dispersed in it. The elastic misfit between the Bi_2Se_3 cluster and GeSe_2

network is relieved by distortions of the Se atom chains for $x < 7$. When $x \geq 7$, the grown up Bi_2Se_3 cluster find themselves embedded in a matrix of increased mechanical rigidity. This enhanced elastic misfit leads to plastic deformation of Bi_2Se_3 clusters resulting in an increased density of Se^- defects. The finite frequency defect modes show up as fluctuations and internal surface modes in the rigid cluster regions. These cause a rapid decrease in thermal diffusion through the rigid network. Obviously, CTR being a purely electronic property should not get manifested in the thermal transport properties of the medium. However, the threshold maximum in α occurring at around 7 at.% of Bi content in $\text{Ge}_{20}\text{Bi}_x\text{Se}_{80-x}$ glasses can only be attributed to the effects due to the existence of a mechanical threshold at this composition. It so happens that the two occur at the same composition in Ge-Bi-Se glasses.

Bismuth impurity induced structural modifications in the parent Ge-Se glass which is responsible for $p \rightarrow n$ transition in these semiconductors is reflected in the optical absorption spectra [20]. Elliot and Steel [14] have suggested that the $p \rightarrow n$ transition in these glasses is accompanied by a significant change in the local structural order surrounding the Bi impurity atoms. At low Bi concentrations, the Bi-Se bond remains covalent in character and at higher Bi concentrations it becomes partially ionic with slight increase in bond lengths [14]. It has further been proposed that the process of the dissolution of the Bi impurity in the selenium rich regions at lower concentrations produce Se^- centres making the Bi impurities positively charged. Further addition of Bi in larger concentrations do not produce appreciable additional defects as it enters in a modified network [14]. Consequently, the absorption edges are not appreciably affected. From the activation energy versus composition parameter data reported by Bhatia et al [21], at lower Bi concentrations there is little change in activation energy E_{av} whereas at higher concentrations a considerable decrease in E_{av} is observed which is explained as due to the shift in the Fermi level towards the conduction band. At present the origin of n-type conduction in Bi doped chalcogenide glasses is not fully understood. According to Nagels et al [13] the appearance of this conduction type in $\text{Ge}_{20}\text{Bi}_x\text{Se}_{80-x}$ glasses

is assumed to be connected with the perturbation of the equilibrium of the negatively and positively charged dangling bonds induced by Bi as a charged Bi^- impurity. The transition from p to n type with increasing Bi content is then related to the disappearance of Se-Se bonds.

According to Tohge et al [8], in $\text{Ge}_{20}\text{Se}_{80}$ glasses only Ge-Se and Se-Se bonds are supposed to be present. When Bi is incorporated into this glass, Bi is expected to combine freely with Se, followed by the decrease in the concentration of Se-Se bonds because the bond energy of Bi-Se bond is larger than that of the Bi-Ge bond (40.7 and 31 kcal/mole respectively) [22]. The concentration of Ge-Se bonds is almost constant over the whole composition range, whereas that of Bi-Se bond increases and that of Se-Se bond decreases monotonically with increasing Bi content up to 10 at.% after which the Se-Se bond vanishes. A further increase of the Bi content results in the formation of Bi-Bi or Bi-Ge bonds provided Bi is still six-fold co-ordinated with Se. Co-ordination numbers of four and two for Ge and Se respectively are assumed and the number of covalent bonds per Bi atom is reported to be six in these glasses [23]. Investigations on electrical properties on these glasses show an abrupt decrease in resistivity and the appearance of n-type conduction which is again related to the formation of fairly large number of Bi-Se bonds and the disappearance of Se-Se bonds. For six-fold co-ordinated Bi in crystalline Bi_2Se_3 , the occurrence of p^3d^3 or sp^3d^2 hybridisation have been suggested. If this is the situation with Bi in chalcogenide glasses, the Bi-Se bond becomes electron deficient in the former case (or in the latter case) and Bi atom gets negatively charged which is compensated by the positive charge on the Se atom. Thus the equilibrium between the positively and negatively charged bonds which pins Fermi level is affected by the charged impurities which is described in the charged dangling bond model.

Vaidyanathan et al [11] have proposed a structural model to explain the phenomenon of carrier type reversal in Pb doped germanium chalcogenides, which has then been extended to explain similar behaviour in Bi doped Ge-Se glasses. Spectroscopic investigations such as diffuse reflectance spectra and variation of optical energy gap obtained from peak maximum energies in DRS as a function of Pb concentration also show similar behaviour. FTIR spectra

and Raman spectra together confirm that Ge and Pb or Bi in this type of glass system are present in tetrahedral and octahedral co-ordinations only using the above spectroscopic features. A structural model has been proposed on the basis of vibrational spectra and XANES. Thus Pb is assumed to be in a sp^3d^2 state of hybridisation. The Se atoms are in sp^n ($n=1,2$ and 3) hybridisation. Germanium utilises its sp^3 hybridised orbitals for bond formation. The lowest energy levels result from the overlap of the bonding orbitals. The Ge-Se and Ge-Ge bonds constitute the lowest energy levels. The next higher energy level is constituted of sp^n lone pair originating from Se. The sp^3d^2 orbitals of Pb ions are likely to occupy a slightly higher level and just above Se lone-pair levels. Similarly increase in Bi concentration in Ge-Bi-Se glasses leads to rapid growth of sp^3d^2 band and the top of sp band which results in the rapid increase of electron contribution to conductivity, which exceeds the contribution from holes. As a consequence p to n transition occurs as a function of Bi concentration. This overlap of orbitals with increasing Bi concentration brings about the decrease in E_g values. Only Pb and Bi containing Ge-Se glasses are known to exhibit such a p to n transition. This unique behaviour can be associated with the unique tendency of Pb or Bi towards octahedral co-ordination and more importantly with the energetic disposition of their d-bands which can overlap in energy with those of lone pair bonds of Se in particular. The closeness of the sp^3d^2 band with those of the lone pairs of chalcogen is suggested to be responsible in bringing about the carrier type reversal.

6.4 Conclusion

Thermal diffusivity and optical band gap measurements on Bi doped germanium chalcogenides using photoacoustic technique and UV-Vis-NIR absorption method respectively exhibit significant changes across the p \rightarrow n transition as a function of composition. The carrier type reversal, which is purely an electronic property should not, in principle, get manifested in thermal transport properties. The threshold maximum in thermal diffusivity which occur around 7 at.% of Bi content in $Ge_{20}Bi_xSe_{80-x}$ glasses can only be attributed to the effects due to the existence of a mechanical threshold in these glasses. The

E_g data is in good agreement with the structural model proposed by Vaidyanathan et al[11]. It so happens that the two effects occur at the same composition. Whether any further correlation exists between mechanical rigidity and $p \rightarrow n$ type electronic transition need to be investigated with more experimentation and modelling.

REFERENCES

1. D.Lathrop, H.Eckert, *J. Phys. Chem.* **93**, 7895 (1989).
2. N.F.Mott, E.A.Davis, R.A.Street, *Phil. Mag. B* **32**, 96 (1975).
3. M.Kastner, D.Adler and H.Fritzsche, *Phys. Rev. Lett.* **37**, 1504 (1976).
4. N.Tohge, Y.Yamamoto, T.Minami and M.Tanaka, *Appl. Phys. Lett.* **34**, 640 (1979).
5. N.Tohge, T.Minami and M.Tanaka, *J. Non-Cryst. Solids* **38-39**, 283 (1980).
6. N.Tohge, K.Kanda, T.Minami, *Appl. Phys. Lett.* **48**, 1739 (1986).
7. P.Kounavis, E.Mytilineou, M.Roilos, *J. Appl. Phys.* **66**, 708 (1989).
8. N.Toghe, T.Minami, Y.Yoshitaka and M.Tanaka, *J. Appl. Phys.* **51**, 1048 (1980).
9. M.K.Rabinal, K.S.Sangunni, E.S.R.Gopal and S.V.Subramanyam, *Solid State Commun.* **88**, 251 (1993).
10. L.Tichy, H.Ticha and A.Triska, *Solid State Commun.* **53**, 399 (1985).
11. B.Vaidhyathan, S.Murugavel, S.Asokan and K.J.Rao, *J. Phys. Chem. B* **101**, 9717 (1997).
12. J.C.Phillips, *Phys. Rev.B* **36**, 4265 (1987).
13. P.Nagels, L.Tichy, A.Triska and H.Ticha, *J. Non-Cryst. Solids* **59**, 1015 (1989).
14. S.R.Elliot and A.T.Steel, *Phys. Rev. Lett.* **57**, 1316 (1986).
15. J.Storiopoulous and W.Fuhs, *J. Non-Cryst. Solids* **114**, 97 (1989).
16. S.R.Elliot and A.T.Steel, *J. Phys. C: Solid State Phys.* **20**, 4335 (1987).
17. J.C.Phillips and M.F.Thorpe, *Solid State Commun.* **53**, 699 (1985).
18. W.Bresser, P.Boalchand and P.Suranyi, *Phys. Rev. Lett.* **56**, 2493 (1986).
19. A.Feltz in *Physical and Chemical Properties of Semiconducting Compounds*, (Nauka,

- Moscow) 97 (1979).
20. K.L.Bhatia and V.K.Bhatnagar, *J. Non-Cryst. Solids* **104**, 17 (1988).
 21. K.L.Bhatia, G.Parthasarathy and E.S.R.Gopal, *J.Non-Cryst. Solids* **69**, 189 (1985).
 22. L.Pauling, in *The Nature of the Chemical Bond*, 3rd ed. (Cornell Univ., New York) 62 (1960).
 23. E.Mooser and W.B.Pearson, *J. Phys. Chem. Solids* **7**, 68 (1958).

CHAPTER VII

SUMMARY AND CONCLUSION

The work presented in this thesis is centred around the investigations on the optical and thermal properties of selected semiconducting chalcogenide glasses. The aim of the present work was to test the validity of various models proposed by different authors. The advantage of amorphous semiconductors is that it offers composition dependent tunability over wide ranges of compositions of various physical properties making them ideal systems for technological applications such as optoelectronic detectors, switching devices, charge storage materials etc. Moreover a new class of p-n junctions may get emerged as a result of the discovery of carrier type reversal in Bi or Pb doped germanium chalcogenides which could offer many manufacturing advantages over its crystalline counterparts. The photoacoustic technique, which is based on the detection of the acoustic signal generated when a sample placed inside an enclosed cell containing a gas is irradiated by an intensity modulated beam of light, is the main experimental tool used to carry out the measurements. The PA signal detected by a sensitive microphone depends on the optical as well as thermal properties of the sample. The modules of the PA spectrometer for the present study consists of a high power Xe arc lamp, a monochromator, a mechanical chopper, a variable temperature PA cell and a lock-in amplifier. The optical band gap has been determined from the photoacoustic spectra being recorded by measuring the PA signal amplitude as a function of incident wavelength. The PA spectrum has been normalized with the power spectrum of the source using highly absorbing carbon black sample acting as a reference. The thermal diffusivity measurements have been carried out using a novel technique in which the phase difference between the front and rear surfaces of illumination is measured at a single chopping frequency. This is achieved by rotating the PA cell freely about a vertical axis through 180°. The advantage of this phase lag measurement technique is that it can be used

with both thermally thick and thin samples and moreover, measurements can be carried out at a single chopping frequency. The complexities involved in optics while using beam splitters in order to obtain the front and rear surface signals can be avoided using this phase lag technique. A low temperature PA cell has been fabricated for this purpose which can be used to measure optical and thermal properties of the samples from liquid nitrogen temperature to ~ 450 °C. The cell has been calibrated using standard samples and the accuracy of the technique is found to be better than 5%.

An accurate temperature controller has also been designed and fabricated to control the furnace temperature while preparing the samples. This proportional plus integral temperature controller can be used over a wide range of temperatures ranging from 50 to 1200°C with a control stability of 0.5 °C over a wide range.

Semiconducting chalcogenide glasses belonging to IV-III-VI and IV-V-VI groups have been selected for the present investigations. $\text{Ge}_x\text{Ga}_5\text{Se}_{(95-x)}$ [$10 \leq x \leq 31$], $\text{Ge}_x\text{In}_5\text{Se}_{(95-x)}$ [$12 \leq x \leq 32$] and $\text{Ge}_{20}\text{Bi}_x\text{Se}_{(80-x)}$ [$0 \leq x \leq 12$] have been prepared by the conventional melt quenching technique at a quenching rate of $\sim 10^2$ K/sec. Appropriate quantities of selected materials are sealed in quartz ampoules and heated to a temperature of the order of 1000 °C. Initial characterization of the samples have been done by recording their X-ray powder diffractograms.

Both the samples belonging to the IV-III-VI group of elements are found to be easy glass formers in the entire glass forming range and also they cover the threshold values predicted by Phillips, Thorpe and Tanaka making them ideal candidates for investigating threshold properties of such samples. Moreover, the three predicted threshold values of coordination numbers are well resolved in Ge-Ga-Se and Ge-In-Se systems, unlike other semiconducting glasses in which the chemical threshold is found to coincide with one of the topological thresholds. The optical band gap of Ge-Ga-Se and Ge-In-Se glasses measured using PA as well as UV-Vis-NIR absorption method show a maximum at the stoichiometric composition or at the chemical threshold corresponding to average coordination number

$Z = 2.73$ in these glasses. Results are attributed to the existence of chemical ordering in these glasses. This is explained using the COCN model according to which heteropolar bonding is favoured over homopolar bonding at the stoichiometric composition. The decrease in E_g above and below the chemical threshold is explained as due to the replacement of the stronger Ge-Se bonds by weaker Ge-Ge or Se-Se bonds. The decrease in E_g is thus due to the decrease in the average bond energy of the system.

The thermal diffusivity measurements on these glasses measured as a function of average coordination number shows threshold maxima at 2.42 and 2.67 in Ge-Ga-Se system and 2.41 and 2.67 in Ge-In-Se system respectively. This corresponds to the topological thresholds predicted by Phillips et al and Tanaka. The threshold maxima observed near $Z=2.4$ is attributed as due to a threshold in mechanical rigidity occurring in these glasses. At this composition, the system goes from a floppy type to a rigid type. The peak at 2.67 is attributed to a structural transition taking place at this composition where the system goes from a two dimensional network to a three dimensional one as proposed by Tanaka. Thus investigation of optical band gap and thermal diffusivity in IV-III-VI glasses with average coordination number using photoacoustic technique establishes the coexistence of effects due to chemical ordering and topological thresholds.

The third system which we have investigated is the Ge-Bi-Se system, which is reported to exhibit carrier type reversal from p-type to n-type at a particular Bi doping level. A number of structural and electronic models have been proposed but no conclusive explanation has been put forward so far. $\text{Ge}_{20}\text{Bi}_x\text{Se}_{(80-x)}$ glasses prepared by the melt quenching technique is reported to exhibit a CTR at 7 at.% of Bi. The threshold observed in thermal diffusivity value measured using PA technique is in good agreement with the Phillips constraints balancing theory. He has predicted a mechanical threshold occurring at the same Bi doping level of 7 at.%. The E_g versus Z data shows a steep decrease in E_g when Bi content is varied from 0 to 7 at.% and remains constant thereafter. This is explained with the help of structural models and electronic models proposed by Vaidyanathan et al., Tohge et al and Nagels et al. More investigations are required on similar systems which exhibit carrier type

reversal in order to get a clear idea of this phenomenon. Ge-Pb-Se glasses form an interesting candidate for further studies since they also are reported to exhibit a carrier type reversal from p-n type as Bi doped Ge-Se glasses. Also this forms an ideal system because the composition at which this $p \rightarrow n$ switching is observed is found to be different from the mechanical threshold in these glasses. Hence the two effects remain well resolved at two different coordination values. Thermal diffusivity on this system can throw more light in to the physics of Bi or Pb doped germanium chalcogenides.

Neutron scattering measurements on the above systems can provide valuable information about the variation in bonding structure with average coordination number. Investigations on elastic properties also can prove the occurrence of the mechanical thresholds in these glasses.

In summary, we have carried out investigations of the topological and chemical thresholds associated with amorphous semiconductors using PA technique. The results obtained are important not only in understanding the physics of amorphous solids in a better way but also in establishing the potentiality of PA technique as a calorimetric and spectroscopic tool. There is plenty of scope for doing very interesting further work in this area, in view of the fact that several questions still remain unanswered. It is not clear why a property such as carrier type reversal, which is of purely electronic in origin, get manifested in thermal transport behaviour in Bi doped Ge-Se glasses. More experimental results are required to test the validity of different models proposed to explain the effect. It is necessary to extend the investigations to other systems which exhibit / are likely to exhibit this property.